ELECTRICAL SCIENCE

A Series of Monographs and Texts

Edited by

Henry G. Booker
UNIVERSITY OF CALIFORNIA AT SAN DIEGO
LA JOLLA, CALIFORNIA

Nicholas DeClaris
CORNELL UNIVERSITY
ITHACA, NEW YORK

JOSEPH E. ROWE. Nonlinear Electron-Wave Interaction Phenomena. 1965

MAX J. O. STRUTT. Semiconductor Devices: Volume I. Semiconductors and Semiconductor Diodes. 1966

AUSTIN BLAQUIERE. Nonlinear System Analysis. 1966

VICTOR RUMSEY. Frequency Independent Antennas. 1966

CHARLES BIRDSALL AND WILLIAM BRIDGES. Electron Dynamics of Diode Regions. 1966

In preparation:

CHARLES COOK AND MARVIN BERNFELD. Radar Signals: An Introduction to Theory and Application.

A. D. KUZ'MIN AND A. E. SALOMONOVICH. Radioastronomical Methods of Antenna Measurements

Frequency Independent Antennas

by VICTOR H. RUMSEY

Department of Electrical Engineering
University of California
Berkeley, California

ACADEMIC PRESS New York and London **1966**

COPYRIGHT © 1966, BY ACADEMIC PRESS INC.
ALL RIGHTS RESERVED.
NO PART OF THIS BOOK MAY BE REPRODUCED IN ANY FORM,
BY PHOTOSTAT, MICROFILM, OR ANY OTHER MEANS, WITHOUT
WRITTEN PERMISSION FROM THE PUBLISHERS.

ACADEMIC PRESS INC.
111 Fifth Avenue, New York, New York 10003

United Kingdom Edition published by
ACADEMIC PRESS INC. (LONDON) LTD.
Berkeley Square House, London W.1

LIBRARY OF CONGRESS CATALOG CARD NUMBER: 66-17290

PRINTED IN THE UNITED STATES OF AMERICA

PREFACE

Until quite recently, experience showed that all antennas were selective to frequency. For example, the change in radiation pattern with frequency seemed to have a universal character: invariably, the main beam became sharper and the minor beams more numerous as frequency was raised. The discovery of frequency independent antennas overturned these empirical laws and produced a radical improvement in the technology of radiating systems. It started from a simple theory, and theory was often ahead of observation in the sequel. Research in this area has uncovered many striking phenomena which remain unexplained, and has generated solutions of Maxwell's equations which have yet to be observed. In short, the subject is a fascinating combination of theory and observation which will interest mathematicians and physicists, as well as engineers.

The book is a reasonably complete coverage of the subject from its inception until the middle of 1965. Most of the contents have not previously been published, except in scattered journal articles, and some are original. The first six chapters are written at a fairly easy level—about the level of a beginning graduate student or the more advanced undergraduate. The last two chapters, which deal with solutions of Maxwell's equations, are at a somewhat higher level.

In writing this preface it would be a pity not to support the custom of expressing gratitude to those who have helped the author. But one hardly knows where to stop, for on reflection, one is struck by how completely indebted he is not only to his teachers, colleagues and students, but to the previous generation who taught them, and so on. The author would simply like to express his gratitude to many

friends at Ohio State University, the University of Illinois, and the University of California (in historical order), with whom he worked in the 1950's.

VICTOR H. RUMSEY

August, 1966

1

ELEMENTARY PRINCIPLES

To open the subject we shall discuss a few fundamental ideas about antennas. Doubtless this is not the most enticing introduction, nor is it necessary for the reader who wants to go straight to the heart of the matter. Chapter 2 would be the place for him to start. But a careful discussion of fundamentals will finally be needed, and Chapter 1 is the logical place for it. Our aim here is, then, to show how typical measurements can be understood in terms of classical electromagnetic theory: in other words, how to make sense of measured data, how to set up apparatus to get meaningful data, and how to test their significance.

1.1 Dipole Antennas

The dipole has been chosen for the sake of illustration because it is probably the most familiar type of antenna. It consists of two colinear wires each about a quarter of a wavelength long, the gap between them forming the terminal region. There are two ways of understanding how it works.

(1) In the conventional way it is pictured as a resonator. Current is thought of as traveling along the wire with the velocity of light, being reflected from the end with phase reversal, and so coming back to the terminals exactly in resonance with the outgoing wave. The distribution of current is consequently sinusoidal, being zero at the ends and maximum at the center. Thus far the picture is clear, but now it is difficult to see how this causes a signal to be picked up on some receiving antenna

far away, although there are straightforward formulas for calculating the result.

(2) Alternatively, we can think of the current as continuously leaking out of the wire into the surrounding medium so that none is left at the end. This explains in quite a different way why the current changes with distance along the wire. It also shows directly how current passes into the surrounding medium and so flows out to the distant receiving antenna.

Method (1) is approximate, because there is an infinite number of modes for propagation of current along a wire. What spectrum of this infinite set will actually be set up depends on the physical details of the terminal region. But if the wire is thin compared to the wavelength, all except the mode that travels with the velocity of light are rapidly attenuated. So, for sufficiently thin wires, the approximation is good except in the immediate vicinity of the terminals.

Method (2) is exact but is of little value for quantitative purposes: its value is conceptual. It is justified by the Maxwell equation

$$\oint_C \mathbf{H} \cdot dl = \int_S (\sigma + j\omega\epsilon)\mathbf{E} \cdot \mathbf{n}\, dS$$

using the $e^{j\omega t}$ time convention, C being the edge of surface S and $\mathbf{n}$ being the unit vector normal to S. The symbols $\mathbf{E}$, $\mathbf{H}$, σ, ϵ, and ω have their usual significance. The expression $(\sigma + j\omega\epsilon)\mathbf{E}$ represents the total current $\mathbf{J}$, the combination of conduction and displacement currents. When S is a closed surface, the perimeter of C shrinks to zero. So

$$\oint_S \mathbf{J} \cdot \mathbf{n}\, dS = 0$$

This means the total current $\mathbf{J}$ is continuous everywhere: in particular it is continuous in crossing a metal surface. Hence the reduction in conduction current with distance along the wire must equal the flow of displacement current out of its surface [hence method (2)].

If we accept the fact that the velocity of light is independent of frequency, method (1), although approximate, correctly expresses the scaling principle. It shows that the current distribution remains fixed if the size of the antenna and the wavelength are changed by the same fraction. Because this is the key to frequency-independent-antenna design, it is important that we establish it rigorously. The proof depends on Maxwell's equations and a theorem derived from them which says that the field

radiated from some antenna is uniquely determined by tangential **E** on any surface that encloses the generator. We take the surface so that it follows the surface of the antenna and runs across the gap between the terminals. If the gap is small enough and if the antenna is perfectly conducting, tangential **E** will be zero on S except at the gap, where it will represent the applied voltage.

Turning now to Maxwell's equations, we express them in the form

$$\nabla \times \mathbf{E} = -j\omega\mu\mathbf{H}$$

$$\nabla \times \mathbf{H} = j\omega\epsilon\mathbf{E}$$

We are therefore considering a perfectly lossless medium with μ and ϵ independent of frequency. Let

$$k = \omega(\mu\epsilon)^{1/2} = 2\pi/\lambda$$

$$Z_0 = (\mu/\epsilon)^{1/2}$$

We transform the equations so that the unit of length is the wavelength λ, the new equations being indicated by a prime. Thus $x = \lambda x'$, $y = \lambda y'$, and $z = \lambda z'$. The result is

$$\nabla' \times \mathbf{E} = -Z_0\mathbf{H}$$

$$\nabla' \times \mathbf{H} = Z_0^{-1}\mathbf{E}$$

Now Z_0 is independent of ω. Therefore the field is independent of ω if tangential **E** on S, and S itself, are fixed in the primed system; that is, *S must scale with λ*. Note that the antenna must be perfectly conducting and the surrounding medium must be perfectly lossless. In practice, a copper antenna surrounded by air easily fits these requirements. Note also that the surrounding medium does not have to be uniform: μ and ϵ can be functions of position but, to fit the scaling principle, when expressed as functions of $x'y'z'$ they must be independent of λ. Thus any lossless system composed of a mixture of dielectrics and metals fits the geometric scaling principle; that is, the entire electrical performance is frequency-independent if *all* length dimensions are scaled in inverse proportion to frequency.

1.2 Characteristic Impedance

A major step toward an understanding of antennas was made in 1941 by Schelkunoff in his analysis of biconical structures.[4] Its effectiveness is largely due to the fact that the principal mode for two metal cones with a common apex fits the simple formulas for propagation along a uniform transmission line. This holds for cones of arbitrary cross section[5], but for the sake of simplicity let us take up the special case of circular cones with a common axis (as well as common apex). Imagine that the apices are separated by an infinitesimal gap so that they form the input terminals—see Fig. 1.1. Then Maxwell's equations are satisfied by

$$\mathbf{E} = \frac{E_0 e^{-jkr}\hat{\boldsymbol{\theta}}}{r \sin \theta}, \qquad \mathbf{H} = \frac{H_0 e^{-jkr}\hat{\boldsymbol{\phi}}}{r \sin \theta} \tag{1.1}$$

$$E_0 = Z_0 H_0 \tag{1.2}$$

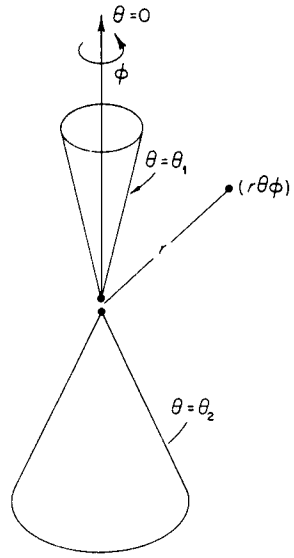

FIG. 1.1. Coaxial biconical structure.

$r\theta\phi$ being a standard set of spherical coordinates and $\hat{\boldsymbol{\theta}}$ and $\hat{\boldsymbol{\phi}}$ the corresponding unit vectors. The symbols k and Z_0 are the intrinsic propagation factor and impedance for the medium between the cones, as used in Section 1.1. It should be noted that this is not a general solution. It

is only one of an infinite number of possible solutions which make **E** normal to the metal cones. To proceed, we define V and I by

$$V = \int_{\theta_1}^{\theta_2} E_\theta r \, d\theta = E_0 e^{-jkr} \ln \frac{\tan(\theta_2/2)}{\tan(\theta_1/2)} \tag{1.3}$$

$$I = H_\phi 2\pi r \sin\theta = H_0 e^{-jkr} 2\pi \tag{1.4}$$

$$Z_{00} = \frac{V}{I} = \frac{Z_0}{2\pi} \ln \frac{\tan(\theta_2/2)}{\tan(\theta_1/2)} \qquad [Z_0 = (\mu/\epsilon)^{1/2}] \tag{1.5}$$

Evidently when $r \to 0$, V and I represent the input voltage and current. Thus for this solution (or mode) the input impedance is independent of frequency and is a pure resistance. If the cones extended to infinity, only this mode would be excited by a generator at the input, and so the input impedance would be Z_{00}. For a finite biconical antenna the input impedance converges to Z_{00} with increasing frequency.

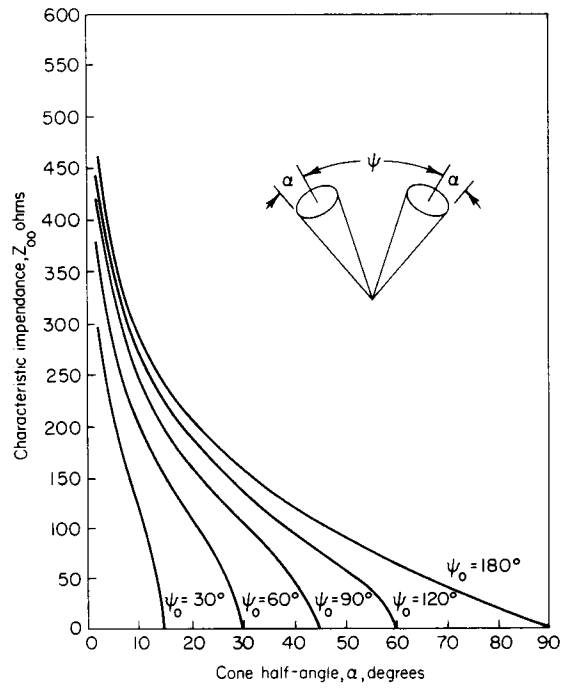

FIG. 1.2. Characteristic impedance for inclined circular cones [after Ref. 1].

To deal with the case where the cross section of the cones is arbitrary, we use the following solution of Maxwell's equations:

$$\mathbf{H} = \nabla \times \hat{\mathbf{r}}g \qquad \text{and} \qquad \mathbf{E} = \nabla \times \mathbf{H}/j\omega\epsilon \tag{1.6}$$

where

$$g = e^{-jkr}T(\theta\phi) \tag{1.7}$$

and

$$\nabla^2 T = 0 \tag{1.8}$$

The solution (1.1) is the special case of this when T is independent of ϕ. Like (1.1) this gives a wave with no radial components of $\mathbf{E}$ or $\mathbf{H}$: $\mathbf{E}$ is the gradient of T apart from a constant. Thus the solution is fixed by making T constant on the cross section of the cones with a sphere. We shall work out an example in Chapter 3, but for the present we can proceed to the final result for a specific practical case, two circular cones of half-angles α_1 and α_2 with axes inclined at angle ψ:

$$Z_{00} = \frac{Z_0}{2\pi} \cosh^{-1} \frac{\cos \alpha_1 \cos \alpha_2 - \cos \psi}{\sin \alpha_1 \sin \alpha_2} \tag{1.9}$$

Figure 1.2 shows a graph of this formula for the case $\alpha_1 = \alpha_2$.[1]

1.3 Antenna Measurements

In subsequent chapters we shall see that the research on frequency-independent antennas shows up surprising errors in all types of antenna measurements. For example, most of the reported impedance variation is spurious, and so is much of the pattern variation. That is why this section on antenna measurements has been included.

Let us begin with impedance measurement. The elementary idea of impedance refers to a pair of terminals which are an infinitesimal distance apart compared to the wavelength. In practice, of course, the terminals have to be a finite distance apart. Thus a rational approach to impedance measurement would be to make a series of measurements for decreasing spacing of the terminals until there is convincing evidence that this series tends to a definite limit. Such an approach is, of course, very difficult to carry out, but essential if one is to measure circuit-theory impedance.

A more practical definition refers to a specific mode in a specific

waveguide. For example, most measuring equipment gives the impedance seen by the lowest mode in a specific coaxial line. This also is the impedance that counts in actual systems, because the antenna has to be fed by a specific transmission line. Thus if we measure a biconical antenna that is big enough to be effectively infinite, we do not get the characteristic impedance of Section 1.2, because that is the circuit-theory definition of impedance. We shall approach that impedance as the cross section of the measuring line is reduced.

It follows that error is introduced by connecting wires between the impedance being measured and the measuring equipment. The magnitude of the error can be estimated by considering the wires as forming a nonuniform transmission line of either the biaxial or biconical forms, whichever represents the closer approximation to their physical disposition. In this way it will be found that, if a piece of wire about a quarter of an inch long is used to connect to a 50-Ω load, the error is about $100\,j\Omega$ in series at 3000 Mc/s. Thus it will be seen that the precise theoretical dimensions must be modelled within at least 0.01 inch for frequencies above 1000 Mc/s; reasonably accurate measurements require a precision of 0.001 inch.

In pattern measurements the fundamental point is that both the distribution of radiated power *and its polarization* are required to describe the radiation field. The distribution is usually described in terms of the spherical angles θ and ϕ, the latitude and longitude. Conventionally the magnitudes of E_θ and E_ϕ are measured, but this is not sufficient, because their phase difference is necessary to fix the polarization. Since the phase is difficult to get directly, it is more practical to supplement $|E_\theta|$ and $|E_\phi|$ with $|E_\theta + E_\phi|$ and $|E_\theta - E_\phi|$, the 45° linearly polarized components. It will be seen that one of these four measurements is redundant in principle, but in practice the extra one gives a useful estimate of the error. Even these four do not fix the polarization, because they do not give the sense of rotation of an elliptically polarized vector (which is the nature of the field being measured). For this reason, and others too, it is better to measure the circularly polarized components $|E_\theta + jE_\phi|$ and $|E_\theta - jE_\phi|$. They can be picked out by an array of two identical orthogonal dipoles spaced $\lambda/4$ apart along the direction of propagation and connected by identical transmission lines to the input. There are other ways of selecting the circularly polarized components, but this one has the advantage that it depends only on measurement of length and angle and does not depend on dipole impedance or mutual impedance.

It is of course essential that transmission lines and other apparatus be disposed so as not to disturb the field being measured. There is only one convincing way of demonstrating that what is being measured is independent of the measuring apparatus—to repeat the measurement for various dispositions of the apparatus. In this way it is found that the typical error in reasonably good pattern measurements is about 5% of the maximum $|E|$.

On the subject of measurement error, it is worth noting that frequency-independent antennas provide a valuable standard for all types of antenna measurements, because they give a predictable variation with frequency. This is particularly significant in the case of pattern measurements, because there is no other kind of antenna whose pattern behavior is known accurately.

1.4 Balanced and Unbalanced Modes

Consider the amateur antenna adjuster, precariously perched on the roof while his wife below watches the results on the TV set. "That's much better," says she, unaware that the antenna has just fallen to the ground, leaving behind the disconnected transmission line. This experiment illustrates the significance of balanced and unbalanced modes. Obviously if the transmission line is correctly excited, it should receive zero when disconnected from the antenna: if it does not, it is evidently acting as an antenna, as well as a transmission line, and any analysis that assumes it to be simply a transmission line is plainly false.

A thorough analysis of any transmission line involves an infinite number of modes. However, at sufficiently low frequencies, all but a finite number of them are so rapidly attenuated as to be insignificant. In this frequency range the circuit-theory approach is valid. Thus for a pair of parallel wires there are only two modes, because in circuit theory the electrical state is entirely represented by I_1 and I_2, the two current distributions on them. Now we can express I_1 and I_2 in terms of the u and b modes by the formulas (which define what we mean by u and b modes)

$$I_1 = I_u + I_b \qquad 2I_u = I_1 + I_2$$
$$I_2 = I_u - I_b \qquad 2I_b = I_1 - I_2$$

These modes are usually called the "unbalanced" and "balanced,"

but as shown in Fig. 1.3, "unaxial" and "biaxial" fit just as nicely, and describe the H field more clearly. The propagation factor for both is the intrinsic value for the surrounding medium and both are excited in the typical practical system. The problem is, of course, to eliminate the u mode.

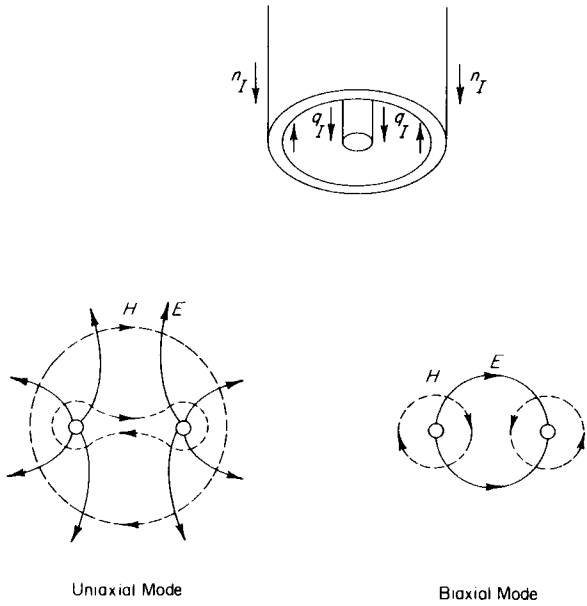

FIG. 1.3. Unbalanced and balanced modes on biaxial line.

The problem is vastly easier to solve with a coaxial type of transmission line than with the biaxial type. Basically, the reason is that the balanced mode is entirely confined to the interior region, and the unbalanced mode to the exterior region, as illustrated in Fig. 1.4. (This readily follows from Maxwell's equations, assuming perfect conductivity. At

FIG. 1.4. Balanced and unbalanced modes on coaxial line.

very low frequencies this assumption will fail but it is quite satisfactory above, say, 1 Mc/s for a solid outer conductor.) Thus any generator that is completely encased in copper except for a coaxial output must launch only the balanced mode in a coaxial line. The unbalanced mode may, however, be set up by the "load" connected to the other end of the coaxial line. For example, if the load is a dipole antenna, a very strong unbalanced component will be generated by reflection.

Antennas made out of metal sheet can sometimes be fed successfully by a coaxial line, as shown in Fig. 1.5. Here the coaxial line is embedded

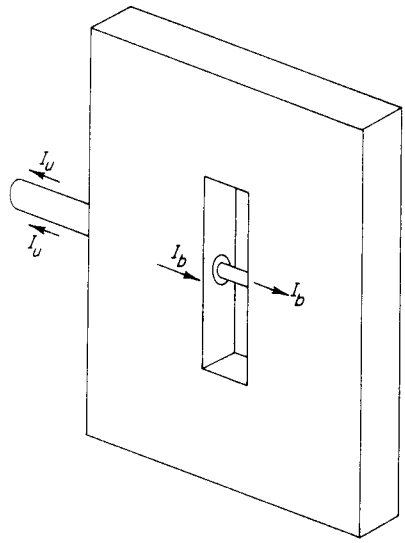

FIG 1.5. Coaxial line excitation of slot antenna.

in the metal sheet, so that the only place where unbalanced current I_u could arise is at the edge of the sheet. If the sheet is large enough, the density of current at the edge will be low enough to make I_u insignificant. In practice, the coaxial line is bonded to the outside of the sheet instead of being embedded inside. Evidently this is equivalent if the diameter of the coaxial line is sufficiently small. Most of the frequency-independent antennas to be described were fed in this manner.

In some cases this method is impractical, and then a mode converter from the coaxial to biaxial geometry is needed (more commonly known as a *balun*). Many different baluns have been invented, only some of which are in fact true mode converters, and only one of which is frequen-

cy-independent. The last is simply a gradual transition from coaxial to biaxial cross section, which clearly must accomplish the mode conversion if the transition is spread out over a sufficient number of wavelengths.[2] Thus the outer conductor of the coaxial line is gradually cut away, so that after some distance less than half of it remains. At this point the resemblance to a pair of wires is clear, and a smooth deformation to the biaxial geometry easily follows. However, at microwave frequencies the cross section becomes so small that the necessary precision of construction becomes very hard to attain. In that case a different version, which can be fabricated by etching copper from both sides of a thin dielectric sheet, is eminently practical.

The form of this balun is shown in Fig. 1.6. The outer conductor

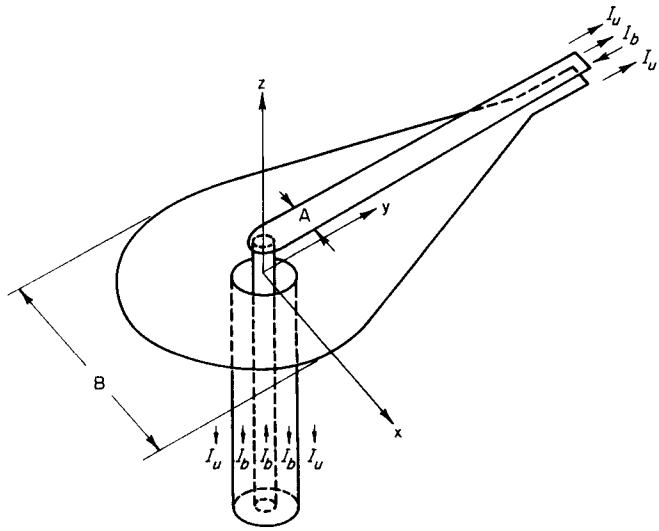

FIG. 1.6. Frequency-independent balun constructed of flat sheet.

of the coaxial line fits into a hole in the lower plate, and the inner conductor is connected to the upper plate. To analyze the mode conversion, suppose the lower plate had constant width B, which means the taper is infinitely gradual. Note that I_u on the coaxial line arises from leakage of the field around the edge of the lower plate, as in Fig. 1.7; I_u would be zero if $B = \infty$. Thus we can say that I_u relative to I_b is of the order of this leakage flux relative to the flux from upper to lower plate. This ratio can obviously be made arbitrarily small by making

$B \gg A \gg C$. Note that this requirement depends on the electrostatic field configuration, so B can be as small a fraction of wavelength as desired. Typical dimensions for 50-Ω characteristic impedance are $B = 685$ mils, $A = 43$ mils, $C = 10$ mils, with Teflon sheeting separating the upper and lower plates. Microwave measurements on this structure showed practically perfect mode conversion.[3]

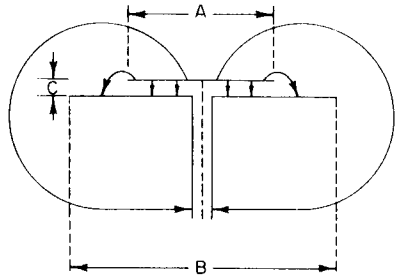

FIG. 1.7. Typical field configuration at the junction.

REFERENCES

1. Carrel, R. L., *IRE Trans.* **AP-6**, 197–201 (1958).
2. Duncan, J. W., and V. P. Minerva, *Proc. IRE* **48**, 156–164 (1960).
3. Gans, M. J., D. Kajfez, and V. H. Rumsey, *Proc. IEEE* **53**, 647 (1965).
4. Schelkunoff, S. A., "Electromagnetic Waves." Van Nostrand, Princeton, New Jersey, 1943.
5. Schelkunoff, S. A., "Advanced Antenna Theory." Wiley, New York, 1952.

2

BASIC FEATURES OF FREQUENCY-INDEPENDENT ANTENNAS

2.1 Basic Principles

We have seen in Chapter 1 that if we double all the dimensions of an antenna and at the same time double the wavelength, the performance of the antenna remains the same. Putting it more specifically, the impedance, polarization, pattern, etc., are invariant to a change of scale that is in proportion to the change in wavelength, provided the antenna is made of practically perfect conductors and dielectrics. This shows that if the shape of the antenna were entirely determined by angles, the performance would have to be independent of frequency, for such a shape would be invariant to a change of scale. The infinite biconical antenna, discussed in Chapter 1, is one example of the unlimited variety of such shapes. However, because it is infinite, it is obviously not a practical antenna. It would lead to a practical antenna if truncation of the cones still gave the same results as the infinite case. Thus in addition to the "angle principle" it is necessary that the shape also fit this "truncation principle."

The biconical antenna does not in fact fit the truncation principle. One proof is that the total current I on the infinite structure does not decrease with distance from the terminals—see (1.4). Consequently, truncation, no matter how far from the terminals, has a radical effect on the pattern. Putting it another way, no matter how high the frequency, the pattern of the finite structure never approaches the pattern of the infinite structure. Thus we see that the truncation principle implies that I approaches zero with distance away from the terminals, and that

the pattern of the finite structure approaches a limiting form with increasing frequency. The latter is the clearest indication of frequency-independent operation in practice.

Of course, frequency-independent operation is actually observed only over a limited band. The low-frequency limit is evidently set by the maximum dimension, and the high-frequency limit is set by how precisely the input terminal region can be constructed. Thus if the outside dimension of the antenna were about 10 ft and the outside dimension of the transmission line were about $\frac{1}{10}$ inch, the bandwidth would be very roughly 1000:1. In practice such bandwidths far exceed the development of transmitters and receivers, so that 40:1 is about the highest that has actually been obtained.

The equiangular spiral antenna shown in Fig. 2.1 is an example of a

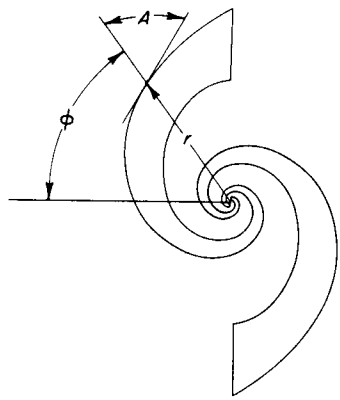

FIG. 2.1. Planar-sheet spiral antenna.

shape which fits both the angle and truncation principles. It is discussed fully in Chapter 4, and appears in this chapter only for the sake of illustration. The formula for the spiral curve in polar coordinates is

$$\phi = \phi_0 + (\tan A) \ln r \tag{2.1}$$

which shows it to be determined entirely by the two angles ϕ_0 and A. The latter is the angle between the radius and the tangent, shown in Fig. 2.1. If we put

$$r' = Kr$$

and

$$\phi' = \phi + (\tan A) \ln K$$

ϕ' is the same function of r' as ϕ is of r. Thus an expansion by the factor K is equivalent to a rotation through the angle $(\tan A)(\ln K)$, so that $K = \exp(2\pi \cot A)$ brings the structure back onto itself.

A different type of structure, which is determined by angles, is shown in Fig. 2.2. (The angles that determine it can be picked out by examina-

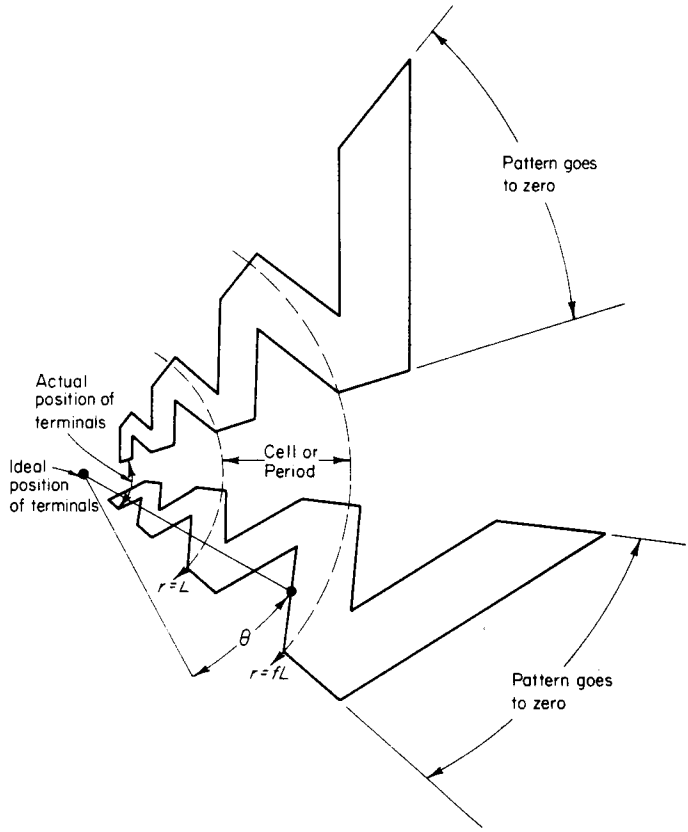

FIG. 2.2. Log-periodic structure.

tion of the illustration.) It consists of a geometric progression of "cells," such that each cell is identical to its neighbor except for a constant expansion factor f. Thus an expansion by the factor f brings the structure back onto itself. Consequently, the performance remains unchanged when the frequency is increased by the factor f, but, of course, this does not make it independent of frequency. This is reflected by the fact

that the (infinite) structure is not *entirely* specified by angles, for it will be seen that one characteristic length, such as that labeled L, has to be specified in addition. Such structures are called *log-periodic* because the typical outline in the $r\theta$ plane is represented by $\theta =$ a periodic function of $\ln r$, with period $\ln f$.[1,2] Because the performance (of the infinite structure) repeats when the frequency is increased by factor f, all electrical characteristics are periodic in the logarithm of frequency, with period $\ln f$. Many examples of these structures are discussed in Chapter 5.

It will be seen that the equiangular spiral antenna is also a log-periodic structure with $f = \exp(2\pi \cot A)$. Its radiation pattern is frequency-independent only in a coordinate system which rotates with the logarithm of frequency, making one rotation for an increased of f in frequency. When measured in a frame fixed to the antenna, the pattern is evidently log-periodic. However, it happens for many spiral and many log-periodic structures that the variation within a period is slight, so that both are practically frequency-independent in a fixed frame. Thus we may say that the third principle needed for a practical antenna is negligible variation within a period (although there are some cases where rotation of a fixed pattern with logarithm of frequency can be turned to advantage). Evidently a clear indication that all three principles are satisfied is a constant pattern over a range of frequencies covering several periods.

2.2 General Formulas for Shapes Determined by Angles[1]

To illustrate the general approach, let us consider all plane curves which remain essentially the same when scaled to a different unit of length. Such curves can be used to determine the shape of a plane-sheet antenna, by taking the input terminals at the common point of intersection of four curves, as illustrated in Fig. 2.1. It follows, then, that the antenna is unchanged when scaled to a different wavelength, provided we add the condition that the terminals stay fixed when the scale is changed. Now the fact that a typical curve remains essentially unchanged by a change of scale implies that the new curve can be made to coincide with the old one by translation and rotation. Since a translation is eliminated by the requirement that the common point remain fixed, the problem is to determine all curves such that a change of scale is equivalent to a rotation. This can be stated symbolically in the form

$$Kr(\varphi) = r(\varphi + C) \tag{2.1}$$

where $r(\varphi)$ denotes the radius r as a function of the polar angle φ, K is the scale change, and C is the angle of rotation to which it is equivalent. Thus K depends on C, but K and C are independent of φ (and r). Therefore,

$$r(\varphi)\frac{dK}{dC} = \frac{\partial r(\varphi + C)}{\partial C} \tag{2.2}$$

$$K\frac{dr(\varphi)}{d\varphi} = \frac{\partial r(\varphi + C)}{\partial \varphi} \tag{2.3}$$

But

$$\frac{\partial r(\varphi + C)}{\partial C} = \frac{dr(\varphi + C)}{d(\varphi + C)} = \frac{\partial r(\varphi + C)}{\partial \varphi} \tag{2.4}$$

Therefore,

$$r(\varphi)\frac{dK}{dC} = K\frac{dr(\varphi)}{\partial \varphi} \tag{2.5}$$

or

$$\frac{dr}{d\varphi} = ar \tag{2.6}$$

where a is independent of φ:

$$a = \frac{1}{K}\frac{dK}{dC} \tag{2.7}$$

It follows from (2.6) that

$$r = r_0 e^{a\varphi} \qquad (r_0 \text{ a constant}) \tag{2.8}$$

Let

$$r_0 = e^{a\varphi_0} \qquad (\varphi_0 \text{ a constant}) \tag{2.9}$$

Then

$$r = \exp[a(\varphi + \varphi_0)] \tag{2.10}$$

or

$$\varphi + \varphi_0 = \frac{1}{a}\ln r \tag{2.11}$$

We recognize this as the formula for an equiangular spiral. Thus the shape of all plane-sheet frequency-independent antennas must be defined by equiangular spirals. Theoretically it might appear that we could obtain four curves by selecting four different combinations of a

and φ_0, but it is easily verified that unless a is the same for all, such curves overlap at infinitesimal values of r, thus placing a short circuit across the terminals. It is therefore necessary to choose four different φ_0 with the same a.

The general problem is to find the class of all surfaces which have the property that a change in the unit of length is equivalent to a certain rotation. Then if we construct a metal antenna whose surface is one of this class, its performance will be the same at all wavelengths except for a rotation of the coordinate system. This problem is much more difficult to analyze than the plane case we have just considered, so we shall simply state the result. It is expressed by

$$\phi - b \ln r = f(\theta) \tag{2.12}$$

where $r\theta\phi$ are a standard set of spherical coordinates and $f(\theta)$ is any function of θ. This is far too general to be practical, however. We still get an infinite variety of possibilities from the special case expressed by

$$\theta - \theta_0 = \text{periodic function of } (\phi - b \ln r) \tag{2.13}$$

For example,

$$\theta - \theta_0 = \sin(\phi - b \ln r) \tag{2.14}$$

Formula (2.13) is sufficiently general to cover all cases we shall encounter. Putting $\theta = \theta_0$ evidently gives the spiral (on the surface of a cone $\theta = \theta_0$). Putting $\phi =$ constant gives a log-periodic shape (in the plane $\phi =$ constant).

2.3 A Fundamental Characteristic of the Pattern

We have seen that a frequency-independent antenna must be a truncated version of some infinite structure which is entirely specified by angles. We now prove that the pattern must go to zero in all directions that would be occupied by the infinite structure.

The "pattern" is understood to mean the component of the field which varies as $1/r$. For this component the distributions of E and H are the same (but their polarizations are different), so the "pattern" refers equally to E and H. Now we have seen that the total current I must go to zero as $r \to \infty$, to fit the truncation principle. Also I varies as rJ, where J is the surface density of current moment on the metal,

and J is tangential H turned through 90°. Thus rH must go to zero as $r \to \infty$. Now rH as $r \to \infty$ is the pattern, by definition. It must therefore be zero at all points on the infinite metal structure. Hence the principle previously stated. It is illustrated in Fig. 2.2.

One obvious application of this principle is as a means of pattern synthesis: it shows how to design to force the pattern to zero in specified directions. However, attempts along this line have so far proved rather discouraging. The other obvious application is as a test of the significance of measured patterns. If the measured patterns do not conform to the principle, either the frequency is too low or the structure does not satisfy the truncation principle. This latter application has proved to be quite important in practice.

2.4 General Effect of Curvature

When frequency-independent designs were first proposed, it was suggested that curvature of the structure was necessary to ensure attenuation of the current.[2] Putting it another way, the shape should be such as to direct the current flow out of the radial direction, for we know from the biconical solution that there is no attenuation of the radial type of flow. In fact, all the subsequent theoretical and empirical evidence supports this idea, as we shall see in Chapters 4–8. There are several approaches to an understanding of this point, but perhaps it should be remarked that attenuation by radiation is not one of them (because the biconical antenna radiates!). The periodic-structure-theory approach given in Chapter 6 is reasonably convincing for log-periodically loaded transmission lines. It suggests that any such structure will fit the truncation principle. The rigorous field-theory solutions described in Chapters 7 and 8 represent quite a different point of view. Although limited to highly idealized cases, they show most clearly that the attenuation of current increases with curvature.

In view of all the data pointing to the significance of curvature, it is perhaps worthwhile to indicate how the effect might be understood in a general way. This can be done in terms of the waveguide modes for a single wire. Here "mode" means a wave traveling along the wire with the same field distribution in all transverse planes. For example, the lowest mode for a straight wire travels with the velocity of light, and E and H vary inversely as distance from the axis. To launch that mode by itself requires an infinite source distributed over a transverse

plane in conformity with the mode distribution; for example, a sheet of electric and magnetic current proportional to H and $(-E)$ turned through 90° is such a mode source. A similar mode source could be used to terminate the wave with no reflection. In this way it is seen how the pure mode can be generated over a finite length of straight wire.

A curved wire can be tackled in the same way by dealing with it as part of a torus. Solutions to Maxwell's equations in toroidal coordinates are available,[3] but it is very difficult to extract simple concepts from them. There are modes that vary exponentially with the angle measured about the axis of the torus, but because these are usually chosen to be periodic over 2π, they show no attenuation. However, by limiting the field to a segment of the torus, in the manner just described, the usual physical requirement for periodic solutions is removed, and it seems reasonably clear that then even the lowest mode must have a complex exponential factor.

Alternatively, a satisfactory picture is revealed in terms of more familiar ideas by thinking of a curved wire as a perturbation of a straight one. If the wire is thin compared to a, its radius of curvature, Maxwell's equations in toroidal coordinates can be arranged to show that the "free" mode on a curved wire is equivalent to a "forced" mode on the straight wire. The forced mode is generated by the electric and magnetic densities of current moment

$$\mathbf{J} = j\omega\epsilon\mathbf{E}\frac{\rho}{a}\cos\phi \qquad \text{and} \qquad \mathbf{K} = j\omega\mu\mathbf{H}\frac{\rho}{a}\cos\phi$$

to the order $(\rho_0/a)^2$, where $\rho\phi z$ are the usual cylindrical coordinates, and ρ_0 is the radius of the wire. Thus it is a matter of solving Maxwell's equations for a straight wire excited by this source (in addition to the launching and terminating transverse sources). The effect of this source is to couple the lowest mode to the higher modes; e.g., the first harmonic or $\cos\phi$ mode in $\mathbf{E}$ gives $\cos^2\phi = \frac{1}{2}(1 + \cos 2\phi)$ when put in $\mathbf{E}\cos\phi$, and so couples to both fundamental and second harmonic. Now the fundamental mode is unattenuated, as we have already seen, but all higher modes are rapidly attenuated. For example, the typical TM mode is expressed by

$$\mathbf{H} = \nabla \times \hat{\mathbf{z}}\, g e^{\gamma z}$$

with

$$g = H_n^{(2)}(T\rho)\sin(n\phi + A) \qquad T^2 = k^2 + \gamma^2$$

and the Hankel function has to vanish at ρ_0. This means T is complex and hence γ also. Thus curvature couples these highly attenuated modes to the fundamental mode, and so causes attenuation of the current.

The same conclusion comes more simply by considering the static current distribution on a curved wire: evidently, current is more concentrated on the inside of the curve. Such a nonuniform distribution is obviously represented by a combination of the fundamental uniform density (independent of ϕ) with harmonics in ϕ, and this must therefore be characteristic of the wave mode. Thus again, curvature couples the fundamental to the harmonics, which are highly attenuated.

REFERENCES

1. DuHamel, R. H., and D. E. Isbell, *IRE Intern. Conv. Record* **1957**, Pt. I, 119–128.
2. Rumsey, V. H., *IRE Intern. Conv. Record* **1957**, Pt. I, 114–118.
3. Weston, V. H., *J. Math. and Phys.* **39**, 64–71 (1960).

3

PLANE-SHEET ANTENNAS

From the practical point of view, plane-sheet antennas are obviously attractive, because they can easily be cut out. They are attractive also from the theoretical point of view because a number of beautiful theorems can be established which have a fundamental influence on our understanding of antennas. The purpose of this chapter is to bring out the ideas behind these theorems.

3.1 Dual Solutions of Maxwell's Equations

As a preliminary, we consider a simple property of Maxwell's equations concerned with the interchange of electric and magnetic quantities. We write Maxwell's equations in the form

$$\nabla \times \mathbf{H} = \mathbf{J} + \mathscr{Y}\mathbf{E} \tag{3.1}$$

$$\nabla \times \mathbf{E} = -\mathbf{K} - \mathscr{Z}\mathbf{H} \tag{3.2}$$

in which $\mathbf{J}$ and $\mathbf{K}$ represent the densities of electric and magnetic current moment and $\mathscr{Y}$ and $\mathscr{Z}$ the passive characteristics of the medium. Then the dual solution, represented by the primed quantities, is obtained by the simple conversions

$$\mathbf{E}' = Z_0\mathbf{H} \qquad \mathbf{H}' = -Y_0\mathbf{E} \tag{3.3}$$

$$\mathbf{K}' = -Z_0\mathbf{J} \qquad \mathbf{J}' = Y_0\mathbf{K} \tag{3.4}$$

with $Z_0 = (\mathscr{Z}/\mathscr{Y})^{1/2} = 1/Y_0$. In free space Z_0 is constant, so the dual solution is obtained by interchanging **E** and **H** (apart from a constant).

When applied to an antenna, **J** and **K** represent the generator at the terminals. The former represents a constant current source and hardly calls for comment, but **K** may require some explanation. Consider, then, the source illustrated in Fig. 3.1. It consists of a square metal plate

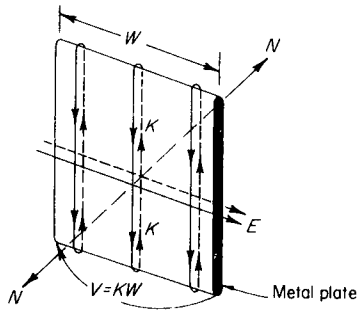

FIG. 3.1. Constant voltage source formed by magnetic current sheet K enveloping a metal plate.

having a sheet of magnetic current flowing upward on the back and the same flowing downward on the front. Now it follows from the Maxwell equation that a sheet of magnetic current with surface density **K** Volts/meter produces a discontinuity in tangential **E** according to the rule

$$\mathbf{K} = \mathbf{N} \times (\mathbf{E}_2 - \mathbf{E}_1)$$

where **N** is the unit normal to the sheet pointing from side 1 to side 2. Note that both the upward and downward **K**'s are backed on one side by the metal plate, where tangential **E** is zero. Consequently, the external **E**'s are the same on front and back, and equal to **K** turned through a right angle, as shown. This arrangement therefore produces a voltage

$$EW = KW = V \qquad \text{(the total magnetic current)}$$

between the edges of the metal plate. In other words, if $W \ll \lambda$, this is a constant voltage source because its internal impedance is zero, and its voltage is independent of what the edges of the plate are connected to.

3.2 Complementary Antennas

In this section we consider antennas whose shapes may be arbitrary, but they must be entirely on a single plane surface so that there is free space on both sides of this plane. Now we can apply the previous section to the region on one side of the plane if, in addition to interchanging electric and magnetic sources, we also interchange the conditions on **E** and **H** at the boundary of the region. The point here is that the field is determined uniquely by tangential **E** or **H** over the infinite plane (plus the radiation condition at infinity). Tangential **E** is easily specified over the part of the plane occupied by the antenna—there it is zero. We can get tangential **H** over the rest of the plane as follows. The field obviously comes from electric currents, all of which flow in the plane. Any element of this current sheet therefore produces a magnetic field which passes through the plane at right angles. Therefore, tangential **H** is zero over the portion of the plane not occupied by the antenna, except for the region occupied by the generator.

The generator region is shown in Fig. 3.2. The source is a constant-current generator consisting of a square sheet of electric current **J** amp/m. Thus the input current to the antenna is JW amperes, where W is the width of the square, half of which appears on the front and the other half on the back of the metal surface. From symmetry, tangential

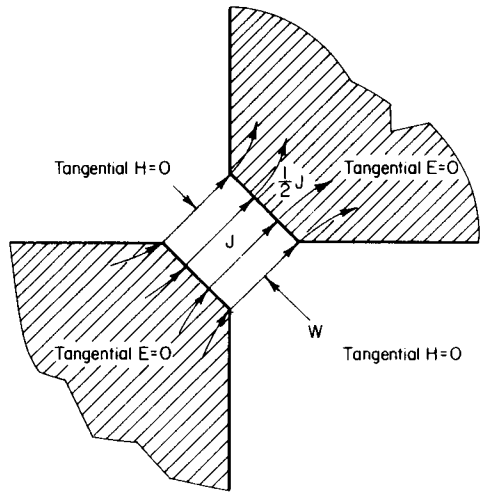

FIG. 3.2. Terminal region fed by constant current source.

H is evidently $\frac{1}{2}$**J** (turned through a right angle) over the region occupied by **J**. Thus the field on one side is now specified uniquely because tangential **E** or **H** has been specified over the whole plane.

Now we look at the complementary antenna, which is shown in Fig. 3.3. The shaded region in Fig. 3.2 is now unshaded and vice versa.

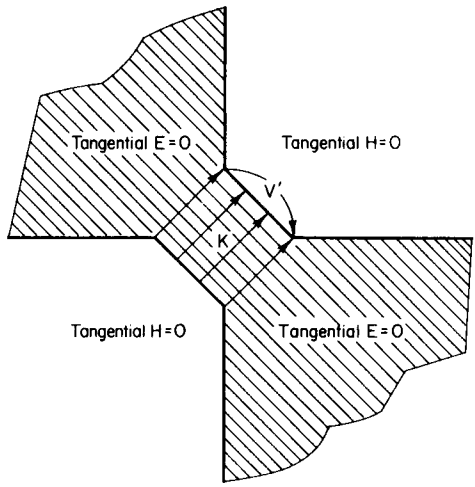

FIG. 3.3. Complement fed by constant voltage source.

Here tangential **E** vanishes where tangential **H** vanished before, and vice versa. To see how to construct the complementary source, we note in Fig. 3.1 that nothing would be changed by the introduction of a magnetic conductor in the unshaded region, with half of **J** on one side of it and half on the other side. In this way, the two sides of Fig. 3.2 are perfectly isolated from each other. It is now clear that the complement of $\frac{1}{2}$**J** backed by a magnetic conductor is **K** backed by metal as shown in Fig. 3.3, **K** and $\frac{1}{2}$**J** being related by (3.4). Thus, using a prime to indicate the complement,

$$V' = KW = Z_0 \tfrac{1}{2} JW = \tfrac{1}{2} Z_0 I$$

and $\frac{1}{2}I'$ = input current on one side of Fig. 3.1 equals $WH' = WY_0E = Y_0V$. Therefore,

$$\frac{4V'}{I'} = Z_0^2 \frac{I}{V}$$

or

$$ZZ' = \frac{Z_0^2}{4} \simeq (189)^2 \tag{3.5}$$

This is Booker's relation for complementary antennas.[1] Mushiake pointed out that as a result self-complementary antennas have a constant impedance of 189 Ω at all frequencies.[4,7] This is a very surprising result, considering the infinite variety of self-complementary shapes, a few of which are illustrated in Fig. 3.4.

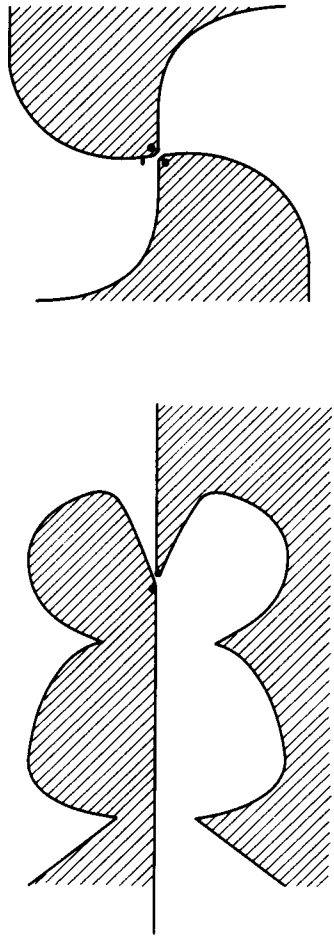

FIG. 3.4. Two examples of self-complementary shapes.

One class of self-complementary shapes is obtained by drawing four identical curves through the origin and placing them around it at 90° intervals. There is an important feature of the radiation from such structures when they function as antennas, namely, that the same power is radiated in directions which differ by a rotation of 90° around the normal to the plane. To see this we note that the complement is produced by a rotation of 90° in ϕ. Because E for the complement is the same as H for the original (apart from a constant),

$$E(\phi) = Z_0 H(\phi + \pi/2)$$

The power density in the radiation field is given either by $Y_0 \mid E \mid^2$ or $Z_0 \mid H \mid^2$, so the power densities in directions ϕ and $\phi + \pi/2$ are the same. Evidently this is a further advantage of self-complementary structures—they tend to give a constant power pattern with respect to ϕ.

3.3 Plane-Sheet Antennas with Many Terminals

As we have seen in Chapter 2, a frequency independent array must have all its terminals located at a common point. We therefore consider an array made of coplanar metal sheets with input terminals labeled 1, 2, ..., n, all within an infinitesimal distance of the origin. The input currents $I_1, I_2, \ldots, I_n$ must fit Kirchhoff's law:

$$\sum_{k=1}^{n} I_k = 0 \tag{3.6}$$

The input voltages $V_1, V_2, \ldots, V_k$ may be referred to an arbitrary reference if

$$\sum_{k=1}^{n} V_k = 0$$

The impedance matrix Z is defined as usual by

$$V = ZI \quad \text{or} \quad V_i = \sum_{k=1}^{n} Z_{ik} I_k \tag{3.7}$$

As in Section 3.2, we use the prime to denote the characteristics of the complementary structure, that is, that with metal and open space interchanged. By using the result of Section 3.1, the relation between

matrices Z and Z' can be derived, as Booker's relation was derived in Section 3.2. This has been done by Deschamps,[3] and the result can be expressed as follows:

$$\Delta Z' \Delta^T Z I \simeq (189)^2 I \tag{3.8}$$

for all I subject to (3.6). Here Δ^T is the transpose of matrix Δ and

$$\Delta = \begin{pmatrix} 1 & 0 & 0 & \cdot & \cdots & -1 \\ -1 & 1 & 0 & \cdot & \cdots & 0 \\ 0 & -1 & 1 & 0 & \cdots & 0 \\ \vdots & & & & & \\ 0 & \cdot & \cdot & \cdot & -1 & 1 \end{pmatrix} \tag{3.9}$$

To get the extension of Mushiake's relation, consider first a structure with n-fold symmetry; that is, rotation of $2\pi/n$ leaves the structure unchanged. Then the matrix Z evidently simplifies to the form

$$Z = \begin{pmatrix} Z_0 & Z_1 & Z_2 & \cdots & Z_{n-1} \\ Z_{n-1} & Z_0 & Z_1 & \cdots & Z_{n-2} \\ \vdots & & & & \\ Z_1 & Z_2 & \cdot & \cdots & Z_0 \end{pmatrix} \tag{3.10}$$

and, moreover, by the reciprocity theorem,

$$Z_k = Z_{n-k} \tag{3.11}$$

It is also apparent that any excitation $I_k V_k$ can be expressed as a combination of the harmonic forms represented by

$$I_{km} = I_0 e^{jk2\pi m/n} \qquad V_{km} = V_0 e^{jk2\pi m/n} \tag{3.12}$$

For example, for $n = 4$, we would have

I_{km}/I_0 for $n = 4$

m \ k	0	1	2	3
0	1	1	1	1
1	1	j	-1	$-j$
2	1	-1	1	-1
3	1	$-j$	-1	j

(3.13)

Then for the mth harmonic the currents and voltages effectively reduce to the single quantities I_0 and V_0 by (3.12), and the impedance matrix is effectively a scalar denoted by $\mathscr{Z}_m$:

$$\mathscr{Z}_m I_0 = V_0 \tag{3.14}$$

In this way (3.8) reduces to

$$\mathscr{Z}_m \mathscr{Z}_m' \sin^2 \frac{m\pi}{n} \simeq (94)^2 \tag{3.15}$$

[Obviously, this is not to be applied to $m = 0$, which has to have $I_0 = 0$, since $\sum I_k = 0$; see (3.13), for example.] For the self-complementary case it follows that

$$\mathscr{Z}_m \simeq 94 \csc \frac{\pi m}{n} \simeq \frac{1}{\mathscr{Y}_m} \tag{3.16}$$

(A representative self-complementary structure is shown in Fig. 3.5.) Now it follows from (3.12) and (3.14) that

$$\mathscr{Y}_m = \sum Y_k e^{jk2\pi m/n} \tag{3.17}$$

and so it is found that the extension of Mushiake's relation takes the form

$$Y_m \simeq \frac{1}{94n} \sin \frac{\pi}{n} \left(\cos \frac{2m\pi}{n} - \cos \frac{\pi}{n} \right)^{-1} \tag{3.18}$$

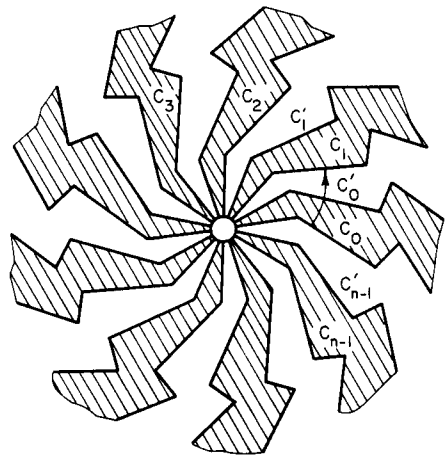

FIG. 3.5. Self-complementary symmetric structure [after Ref. 3].

The easiest way of putting this to practical application is to reduce the n terminals to two, for example, by connecting all even terminals together to form one terminal and all odd to form the other. Thus we are led to consider grouping the n terminals into p sets of connected terminals (p would be 2 in the preceding example). The admittance matrix for the p terminals so formed is represented by

$$Y_c = C^T Y C \tag{3.19}$$

where

$$\begin{aligned} C_{ij} &= 1 \quad \text{if terminal } i \text{ is one of group } j \\ &= 0 \quad \text{if not} \end{aligned} \tag{3.20}$$

Y_c has p rows and columns, that is, $p \times p$, C is $n \times p$ and Y is $n \times n$. The impedance between group j and group k is then obtained by putting all I's zero except $I_j = -I_k$. Typical results are illustrated in Fig. 3.6. For example, when alternate terminals are connected together the impedance is $377/n$. It is thus possible to get a lower input impedance by using many elements.

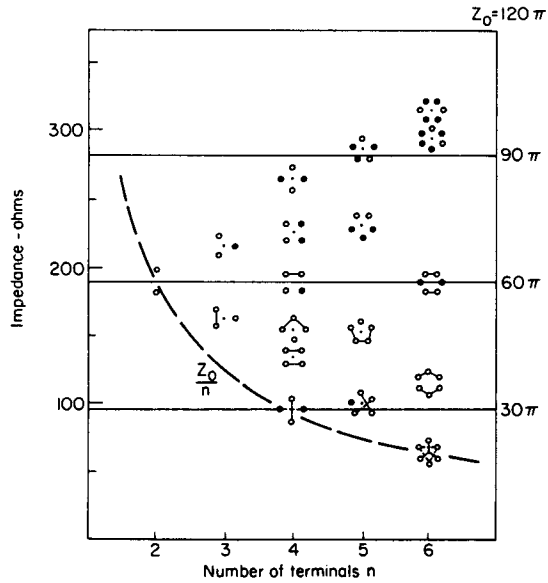

FIG. 3.6. Table of impedance levels obtained for various configurations of terminals. For each configuration, the two groups of terminals connected to the source are represented by circles. The floating terminals are represented by dots [after Ref. 3].

Deschamps points out an interesting feature of self-complementary two-port structures—the characteristic impedance of the two port is 189 Ω—that is, when one port is terminated in 189 Ω, the input impedance at the other is 189 Ω. An example of a self-complementary two port is shown in Fig. 3.7.

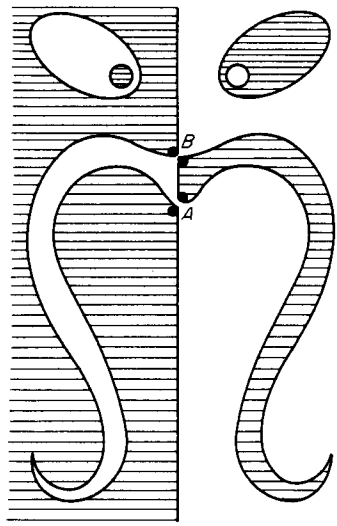

FIG. 3.7. For all frequencies the impedance seen at A is 189 Ω when B is terminated in 189 Ω.

3.4 Characteristic Impedance for Flat Cones

Here we consider two flat metal cones with arbitrary angles between their planes and between their center lines. The appropriate solution of Maxwell's equations is given in Chapter 1 by Eqs. (1.6) to (1.8). It amounts to finding the solution of $\nabla^2 T = 0$ on the surface of the sphere, such that T is constant on the two lines C_1 and C_2, where the cones pass through the sphere. This is simplified by introducing a change of coordinates from θ, ϕ to ρ, ϕ, where

$$\rho = \tan \theta/2 \tag{3.21}$$

When $\nabla^2 T = 0$ is expressed in terms of ρ and ϕ, the result is the same as if ρ and ϕ were the familiar cylindrical coordinates.[2] Consequently, the problem is transformed to solving $\nabla^2 T = 0$ in the $\rho\phi$ plane for the

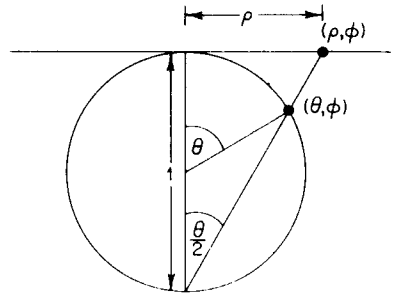

FIG. 3.8. Projection of sphere onto plane.

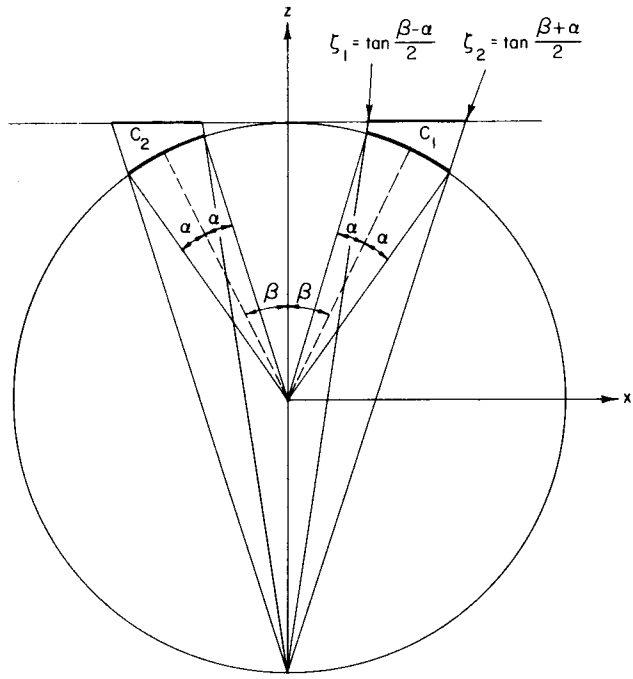

FIG. 3.9. Projection of two coplanar flat cones onto $\rho\phi$ plane.

pair of electrodes formed by the projection of C_1 and C_2 onto the plane. The projection has a simple geometric interpretation, which is evident from Eq. (3.21). If the sphere is of unit diameter, the $\rho\phi$ plane is the tangent plane at the pole $\theta = 0$, as in Fig. 3.8. The sphere is mapped onto the plane by projecting a line from the opposite pole $\theta = \pi$ through a point on the sphere to the corresponding point on the plane.

The well-known method of conformal transformations can be applied by introduction of the complex variable $\zeta = \rho e^{j\phi}$. It will be recalled that the basis of this method is the fact that any analytic function of ζ satisfies Laplace's equation. Thus the solution is given by that function whose real part is constant on C_1 and on C_2. It will be illustrated by the case of two equal coplanar cones of half-angles α, with angle 2β between their center lines, as in Fig. 3.9.

The coordinates are chosen so that the cones lie in the zx plane, the z axis lying along the bisector of angle between them. The projections of C_1 and C_2 on the ζ plane are therefore the two straight-line segments shown in Figs. 3.9 and 3.10. Their end points are (ζ_1, ζ_2) and $(-\zeta_1,$

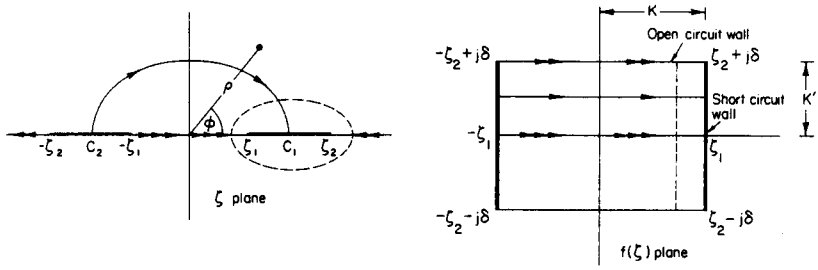

FIG. 3.10. Mapping of the ζ plane onto the f plane.

$-\zeta_2)$, where $\zeta_1 = \tan[(\beta - \alpha)/2]$ and $\zeta_2 = \tan[(\beta + \alpha)/2]$. Thus in the ζ plane, the problem is to find the characteristic impedance of two equal coplanar strips. The transformation that accomplishes this can be derived by the Schwartz–Christoffel method.[2,6] It is expressed by

$$f(\zeta) = \int_0^{\zeta/\zeta_1} \frac{dw}{\{(1 - w^2)[1 - (\zeta_2^2 w^2/\zeta_1^2)]\}^{1/2}}$$

Evidently this maps the real axis from $\zeta = 0$ to $\zeta = \pm\zeta_1$ into the real axis from $f = 0$ to $f = \pm K$, where

$$K = \int_0^1 \frac{dt}{[(1 - t^2)(1 - k^2 t^2)]^{1/2}}$$

with

$$k = \frac{\zeta_2}{\zeta_1} = \frac{\tan[(\beta + \alpha)/2]}{\tan[(\beta - \alpha)/2]}$$

The electrode between ζ_1 and ζ_2 has to be considered the limit of a closed curve such as the dashed curve in Fig. 3.10. Evidently, as ζ is increased beyond ζ_1, the real part of $f(\zeta)$ remains constant until ζ reaches ζ_2. Proceeding thus, we shall find that the positive imaginary side of the electrode between ζ_1 and ζ_2 maps into the straight line between $f = f(\zeta_1) = K$ and $f = f(\zeta_2 + j\delta) = K + jK'$, where $\delta \gtrless 0$ and

$$K' = \int_0^1 \frac{dt}{[(1 - t^2)(1 - k'^2t^2)]^{1/2}}$$
$$k' = (1 - k^2)^{1/2}$$

The negative imaginary side maps into the straight line between $f = K$ and $f = -K'$. So it is found that the $f(\zeta)$ map takes the form shown in

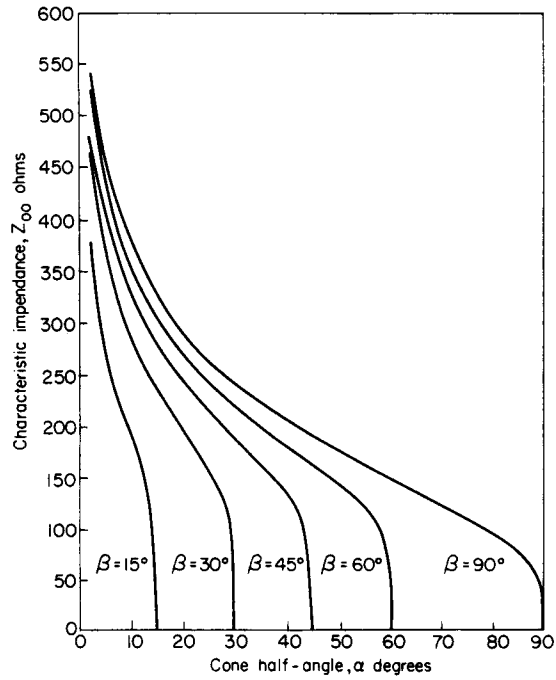

FIG. 3.11. Characteristic impedance of two coplanar flat cones [after Ref. 2].

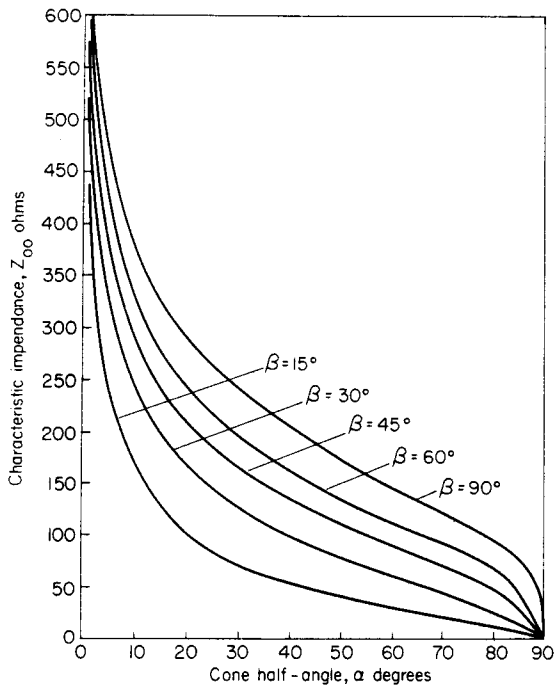

FIG. 3.12. Characteristic impedance of two flat cones oriented orthogonal to the plane of their center lines [after Ref. 2].

Fig. 3.10. The entire region outside of C_1 and C_2 in the ζ plane, that is, the entire ζ plane, maps into the region inside of the rectangle represented by $\pm K$ $\pm jK'$ in the f plane. The map of three typical field lines, distinguished by single, double, and triple arrows, shows how all field lines become straight in the f map. The boundary between $f = \pm K + jK'$ is thus an open circuit wall. Now the characteristic impedance for such a configuration is evidently $Z_0 K/K'$, with $Z_0 = (\mu/\epsilon)^{1/2}$, and this remains invariant under the transformation from the original pair of cones. The characteristic impedance is thus expressed in terms of K and K', which are complete elliptic integrals of the first kind. Typical results are plotted in Fig. 3.11.

Another interesting case is the symmetric configuration that would result from turning each of the cones in Fig. 3.9 about its center line

through 90°. The result here is expressed by the same ratio of elliptic integrals with

$$k = \left(\frac{1 - \sin \alpha}{1 + \sin \alpha}\right)^{\pi/2\beta}$$

It is plotted in Fig. 3.12.

REFERENCES

1. Booker, H. G. *J. I. E. E.* (*London*) **IIIA**, No. 4, 620–627 (1946).
2. Carrel, R. L., *IRE Trans.* **AP-6**, 197–201 (1958).
3. Deschamps, G. A., *IRE Trans. Spec. Suppl.* **AP-7**, S271–S378 (1959).
4. Mushiake, Y., *J. Inst. Elec. Engrs. Japan* **69** (1949), in Japanese.
5. Schelkunoff, S. A., "Advanced Antenna Theory." Wiley, New York, 1952.
6. Smythe, W. R., "Static and Dynamic Electricity." McGraw-Hill, New York, 1950.
7. Uda, S., and Y. Mushiake, *Tech. Rept. Tohoku Univ.* **14** (1949).

4

SPIRAL ANTENNAS

The first practical frequency-independent antennas were discovered by Dyson while working for his Ph.D. at the University of Illinois.[1,2] He measured hundreds of patterns on equiangular spiral antennas, but for some time the frequency-independent mode was obscured by a variety of spurious effects (which, incidentally, are always present in such measurements but they usually go undetected). When it became clear that the pattern did not change over a 20:1 band as it would for a conventional antenna, the measurement technique was refined to bring out the frequency-independent mode as strongly as possible. In the end, many designs were found that clearly showed frequency-independent performance, so that now it is hard to understand what a great number of things were tried before the fact was established. This may help to explain why some of the early measurements discussed in this chapter are not very convincing. They are included not for historical interest, however, but because they are the only evidence we have for certain effects which, in view of what we now know, appear to be significant in understanding frequency-independent operation.

4.1 Plane Spiral Antennas

The plane equiangular spiral antenna has been illustrated in Fig. 2.1, and the question of feeding it has been discussed in Section 1.4. In the present case a fine coaxial line is embedded in one arm. A dummy line is similarly disposed on the other arm to preserve symmetry, and is connected to the inner conductor of the coaxial line at the center.

As we saw in Chapter 3, the theoretical input impedance is about 189 Ω for the infinite self-complementary structure. In practice the measured values are apt to be lower than this because of the feed line: measurements of the arms by themselves fed from a balanced biaxial line do, of course, tend to the theoretical value. As frequency is raised, the impedance converges more rapidly to the frequency-independent condition than does the pattern. Consequently, the radiation field has always been the feature of greatest interest.

The convergence of the pattern is itself remarkably rapid for designs near the self-complementary shape. Typically, when the wavelength is shorter than the arm length, the performance is practically frequency-independent. The minimum radius needed is thus a surprisingly small fraction of a wavelength; for example, for an expansion factor f of 4 per turn the minimum radius is only about $\lambda/4$. The self-complementary shape shows up definitely as optimum from the point of view of pattern measurements; that is, the pattern is then most nearly symmetric around the axis. Even for $f = 7$, this symmetry is practically perfect: more gradual expansion tends to improve symmetry, of course. However, it should be noted that measured patterns usually show sundry imperfections, of the order of 5% of the maximum for average conditions of measurement. These can be reduced by meticulous care in the design of the antenna and equally careful attention to the method of measurement. When free of these imperfections, the measured field-strength patterns for $f < 7$ closely approximate two equal osculating spheres touching the plane of the antenna at the feed point. In other words, the field-strength amplitude varies approximately as $\cos\theta$, where θ is the angle between the normal to the plane of the antenna and the direction of observation. Note that this does conform to the general principle of Section 2.3; that is, the pattern goes to zero in all directions that would be occupied by the infinite antenna. More rapid expansion does show a degradation: the pattern is not symmetric and eventually breaks up into many lobes.

The polarization appears to be circular within the accuracy of measurement, not only on the axis, but even at 70° off the axis for the self-complementary case with $f < 7$. The direction of rotation of E is that corresponding to expansion of the spiral. Thus with respect to fixed axes, it is the same on both sides, but with respect to the direction of propagation it is opposite on the two sides. Circular polarization in practically all directions is an amazing result, which is as significant as the frequency-independent operation. It is tied in with the symmetry

of the pattern. To see this we first note that the variation of field with angle ϕ around the axis can be expressed generally as a Fourier series:

$$\mathbf{E} = \sum_{n=-\infty}^{\infty} \mathbf{E}_n e^{jn\phi} \tag{4.1}$$

Now all terms except $n = \pm 1$ must give zero field on the axis $\theta = 0$, otherwise E would not be defined there (see Fig. 4.1). Therefore, if the

FIG. 4.1. Field configuration at $\theta = 0$ for various harmonics.

amplitude of E_ϕ (or E_θ) is constant with respect to ϕ and not zero on $\theta = 0$, only one term is not zero, and that must be either $n = \pm 1$. Therefore, in terms of the θ and ϕ components,

$$E_{\theta \text{ or } \phi}(\phi) = e^{\pm j\phi} E_{\theta \text{ or } \phi}(0) \tag{4.2}$$

For a self-complementary shape, a rotation of $\pi/2$ produces the complement. As we saw in Chapter 3, $\mathbf{H}$ for the complement is the same as $\mathbf{E}$ for the original apart from a constant. Specifically then,

$$\begin{aligned} E_\theta(\phi) &= Z_0 H_\theta\left(\phi + \frac{\pi}{2}\right) && \text{(because it is self-complementary)} \\ &= -E_\phi\left(\phi + \frac{\pi}{2}\right) && \text{(in the radiation field)} \\ &= \mp j E_\phi(\phi) && \text{[by Eq. (4.2)]} \end{aligned} \tag{4.3}$$

This says that $\mathbf{E}$ is circularly polarized. We can determine which sign is right from the known sense of the polarization. Introducing the instantaneous field $\mathscr{E}$ we have

$$\mathscr{E} = \mathrm{Re}(e^{j\omega t}\mathbf{E}) \tag{4.4}$$

and, by Eq. (4.1),

$$\begin{aligned} \mathbf{E} &= \hat{\boldsymbol{\theta}} E_\theta + \hat{\boldsymbol{\theta}} E_\phi \\ &= (\mp j\hat{\boldsymbol{\theta}} + \hat{\boldsymbol{\theta}}) E_\phi \end{aligned} \tag{4.5}$$

where $\hat{\theta}$ and $\hat{\theta}$ are the unit base vectors. Therefore,

$$\mathscr{E} \sim \pm\hat{\theta} \sin \omega t + \hat{\theta} \cos \omega t \tag{4.6}$$

Thus the upper sign represents left-handed rotation around the outward radial direction. Now, considering the field on the side $z > 0$ as a particular case, we can take the outward radial direction as the z axis. A left-handed expansion means $a < 0$ in $e^{a\phi}$, and this gives left-handed circular polarization with respect to the positive z axis. Thus $a < 0$ gives $e^{j\phi}$ and $a > 0$ gives $e^{-j\phi}$. Hence a self-complementary antenna with $|E_\theta|$ and $|E_\phi|$ independent of ϕ implies circular polarization everywhere in the radiation field. In fact, Dyson found that circular polarization was the best indication of a good frequency-independent pattern. The equiangular spiral is thus an excellent standard for circular polarization over wide ranges of frequency and direction.

4.2 Conical Spiral Antennas

The conical spiral antenna consists of two metal strips on the surface of a cone $\theta = \theta_0$, whose shapes are defined by the equiangular spiral

$$r = e^{a\phi \sin\theta_0} \tag{4.7}$$

It is illustrated in Fig. 4.2. The angle α between the radius and the tangent to the spiral is $\cot^{-1}a$ as before. The planar spiral is thus the special case represented by $\theta_0 = 90°$. We can speak of a self-complementary structure in the conical case, meaning that the region of the cone covered by the metal arms is the same as that not covered except for a rotation of 90°; that is, the arm width δ in Fig. 4.2 is 90°. (The properties of self-complementary structures worked out in Chapter 3 will not apply, of course, to this extension of the idea.) It does turn out, however, that the self-complementary shape gives the best radiation patterns.[3,4]

The effect of changing from the planar to conical shape is roughly to give more radiation from the nose of the cone, that is, in the direction $\theta = 180°$, and less in the direction $\theta = 0$. Typical patterns for $\theta_0 \leqslant 15°$ are shown in Fig. 4.3. Larger values of θ_0 give a lobe in the direction $\theta = 0$: larger expansion factors give a more ragged pattern. The conical form brings out an important feature, which cannot be distinguished in the planar form—that the radiation comes from a wave traveling inward toward the apex.

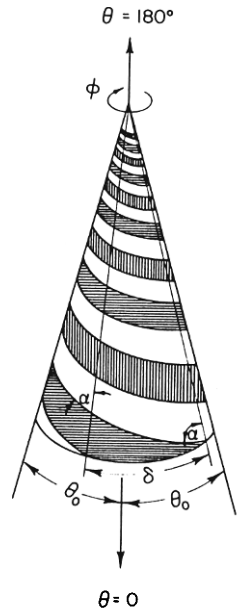

FIG. 4.2. Conical spiral antenna.

The ragged patterns observed with rapid expansion factors should not be summarily ignored. Although they are not much use in practical applications, they are significant if we wish to understand the frequency-independent mode. One conclusion stands out right away if we express the pattern as a Fourier series in ϕ, as in Section 4.1—a ragged pattern implies many harmonics in the series. Consider then the current distribution $e^{jn\phi}$ on a circle of radius $r \sin \theta_0$. Its phase reverses $2n$ times in the circumference $2\pi r \sin \theta_0$, a reversal every $\pi r \sin \theta_0/n$ meters. If this distance is much less than half a wavelength, the contributions from adjacent pieces $\pi r \sin \theta_0/n$ long are nearly self-canceling. Thus the current relative to the radiation field is large unless $2\pi r \sin \theta_0 > n\lambda$, or, in other words, unless the phase velocity is faster than the velocity of light. Consequently, when high harmonics show up strongly in the radiation pattern, the region where the current on the spiral becomes negligible must be far from the center. A ragged pattern in a plane $\phi =$ constant points with equal certainty to the same conclusion, the argument now being based on the phase velocity along radial lines. (This will be worked out thoroughly in Chapter 7, but here a rudimentary approach suffices.)

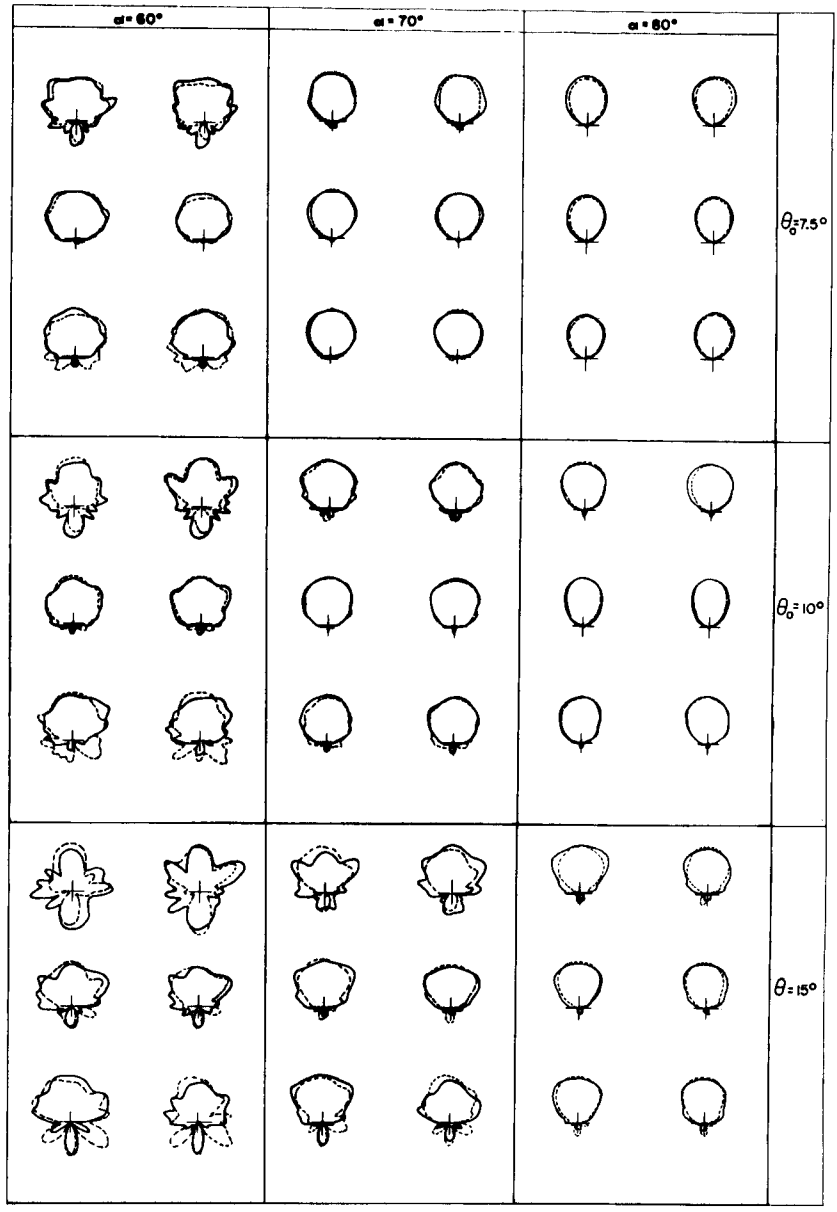

FIG. 4.3. Radiation patterns of conical spiral antennas [after Ref. 4].

The polarization of the radiated field is remarkably close to circular in all directions, as it was also in the planar case. There is, however, a consistent increase in ellipticity with θ, the direction of the radiated field. The best case quoted by Dyson is self-complementary with $\theta_0 = 10°$ and $\alpha = 70°$. It gives axial ratios of unity at $\theta = 0$ and about 1.4 at $\theta = 60°$. Note, however, that the radiated power at $\theta = 60°$ is only about one-tenth of that at $\theta = 0°$. In fact, over a wide range of θ_0 and α, the polarization is practically circular in all directions where the radiated power is significant.

The characteristic impedance Z_0 for typical cone angles θ_0 is shown in Fig. 4.4. It is interesting to see that Z_0 for the self-complementary

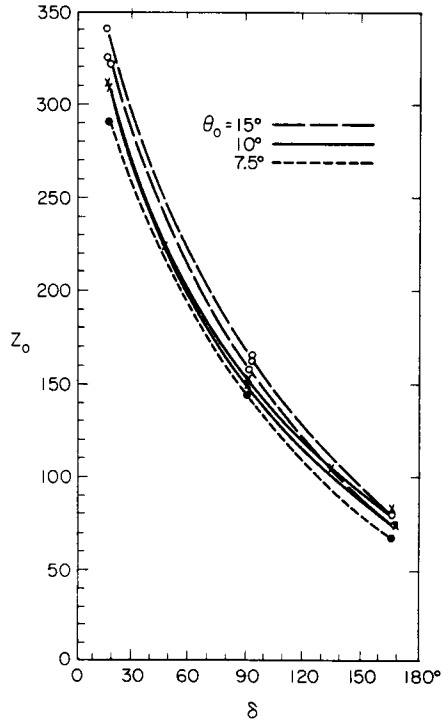

FIG. 4.4. Characteristic impedance of the conical spiral [after Ref. 4].

case is not much different from the planar value of 189 Ω. The effect of the expansion factor is indicated for two typical values by the double curves for $\theta_0 = 15$ and 10°: It is practically negligible.

4.3 Current Distribution and Near Field

The current on a metal surface is represented by the vector **H** turned through a right angle. For a planar antenna it can therefore be found by measuring the corresponding **E** on the complementary structure. This has some practical advantages over measurement of H, and so the first measurements were made in this way. A rather unexpected effect immediately showed up—the surface current was decidedly not linearly polarized.[1] Although it has not been thoroughly investigated, this effect is sufficiently striking to justify the inclusion of a typical plot, as shown in Fig. 4.5. It shows the orientation of the major axis of the tangential

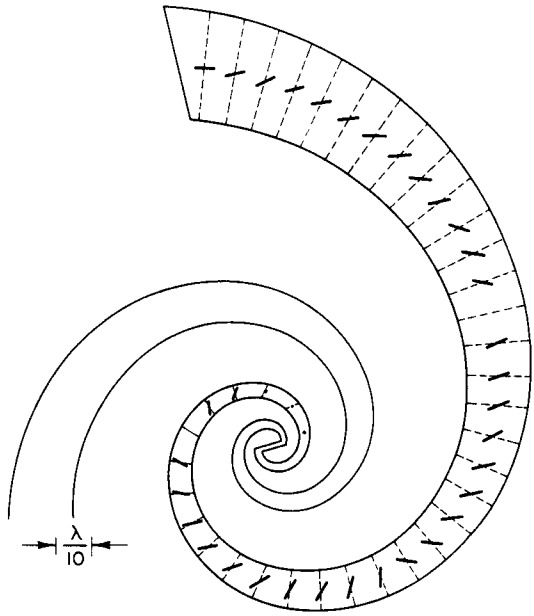

FIG. 4.5. Orientation of polarization ellipse of E in the slot [after Ref. 1].

E polarization ellipse in the middle of the slot. The current on the center of the complement would be oriented at right angles. Note that even when the arm width is much less than $\lambda/10$, the direction of current flow is definitely not along the arm. Now, it cannot be emphasized too often that such results are spurious (from the point of view of the characteristic mode) unless they prove to be independent of frequency.

Measurements were made at other frequencies and they do not agree closely with Fig. 4.5. But there is a significant agreement in the general character, for example, in the point where the inclination of the major axis passes through the symmetrical orientation.

For the planar antennas, the distribution of surface current density J (or tangential H) along the arm is approximately exponential over the first one or two wavelengths. It decreases by 15–20 db in one wavelength measured along the arm, for a variety of expansion factors and arm widths. Note that the total current I is represented by rJ, where r is distance from the center. Obviously then the exponential cannot hold near $r = 0$, since dc conditions are valid there, and therefore $|I|$ must be constant. Also, it is obviously not valid for rapid expansion, because this approaches the biconical case, which gives constant $|I|$ at all r. For the range of practical interest, however, it is a good empirical approximation and shows that $|I|$ decreases with increasing r more rapidly as the expansion is made more gradual.

Before going into the case of the conical spiral, we need to consider rather carefully the significance of measured current distributions. Ideally, to measure tangential H we move an infinitesimal loop antenna at an infinitesimal separation from the surface current. Actually, of course, we have to replace "infinitesimal" by "as small as possible." Then the results are significant only if changing these nominal infinitesimals by, say, a factor of 2 makes no observable difference. It turns out for typical conical spirals that a change of only 0.01 λ in the separation makes an essential difference to the observed distribution. The explanation of this follows. Very close to the apex, the distribution along a generator of the cone consists of $\mathbf{J}$ over one arm, followed by a gap, followed by $-\mathbf{J}$ over the other arm, followed by a gap, and so on. Thus the current reverses every 0.01 λ, let us say, and so the phase changes very rapidly with r. In other words, if we think of the distribution along r in terms of a Fourier integral or a spectrum of phase velocities, as in Section 4.2, we see that the strongest components in the spectrum are very slow waves. We can represent any such wave locally by the function $e^{-j\beta r-\alpha d}$, where d represents distance from the surface of the cone and $\beta^2 = k^2 + \alpha^2$. For very slow waves, $\beta \gg k$, so $\alpha \simeq \beta$. Thus the strength of the wave decreases very rapidly with d; for example, if $\beta = 100k$, the decrease in 0.01λ is $e^{2\pi} > 500$. Farther away from the apex, the spacing between arms is larger, and the phase delay in passing round the cone becomes significant, so that the predominant component in the spectrum eventually is a fast wave ($\beta < k$). Thus we expect the

distribution measured parallel to the surface to be nearly the same as the surface distribution at points far from the apex, but very much less near the apex. The effect is greater the closer the arms, so the more gradual the expansion, the more it shows up at a given radius. That is why it is more noticeable with the typical conical structures.

Although it is common practice to measure along a line parallel to the surface under test, it would evidently be better to take a line passing through the apex. Then the measured distribution should at least be independent of frequency, which is a telling mark of its significance. It would also be less influenced by the slow-wave effect.

Coming now to the results, let us take the planar case first. For small distances from the apex, the phase distribution corresponds, as it must, to a wave traveling with the velocity of light c along the arm. About half a wavelength from the apex, the phase velocity begins to exceed c: it averages between $1.3c$ and $2c$ for the next wavelength, by which time the amplitude is practically insignificant.

The results for the conical spiral are shown in Fig. 4.6.[4] The term

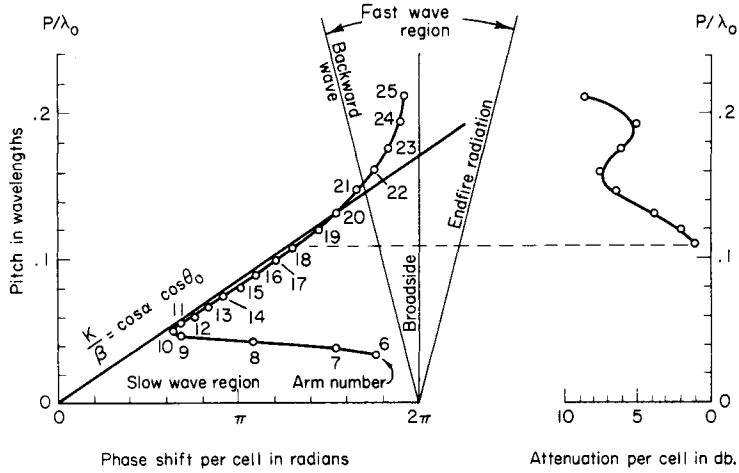

FIG. 4.6. Phase and amplitude distribution for the conical spiral [after Ref. 4].

cell in the abscissa means the distance p along the axis corresponding to one turn of the spiral (that is, p = pitch). Note that β now means the phase factor measured along the z axis. The numbered dots represent the arm positions, or the turns. From turn 11 to turn 21, the phase distribution corresponds closely to an outward wave traveling

along the arms with the velocity of light, which is represented by the straight line $k = \beta \cos \alpha \cos \theta_0$. (Owing to the influence of the slow-wave effect on the measurements, there may be some question about the significance of the data for the turns nearer the apex.) The attenuation becomes noticeable just after the phase shift per cell exceeds π. The other straight line, $p(\beta + k) = 2\pi$, represents the condition that the phase shift per cell βp should be such as to put the direction of maximum radiation along $\theta = 180°$ (Fig. 4.2)—that is, apart from the addition of 2π, which makes no difference to the physical phase, βp exactly compensates kp, the delay per cell of a radiating wave traveling toward the apex. Note that the attenuation per cell is locally a maximum just about where this condition is attained. Remember also that the region near the apex does not radiate much, because of the self-canceling nature of the slow wave that exists there. We see then that both phase and amplitude measurements point to the region between the cell with phase shift π and that with $2\pi - kp$ as the "active" region. Therefore, the active region lies roughly between the turns whose lengths are $\lambda/2$ and $\lambda - p$, at least for gradual expansion and small θ_0. For more rapid expansion the active region is more extensive and tends to lose its significance. The idea of an active region is confirmed by the phase of the radiation pattern, which shows that the main portion of the beam consists of approximately spherical waves emanating from a "phase center" in this region, usually closer to the cell with phase shift π. (It should be noted that, as a whole, the near field is essentially like that of certain log-periodic structures, which will be described in Chapter 5. Since most of the effects discussed in this section have been beautifully demonstrated in this other connection, the reader may wish to refer to Section 5.5 for further evidence.)

4.4 Multielement Spiral Antennas

As an illustration of a multielement spiral antenna, consider four self-complementary elements on the surface of a cone. In this case a rotation in ϕ of 45° is equivalent to the interchange of the regions occupied by metal and the rest of the conical surface. There are four input terminals and any excitation of them can be expressed as a combination of the harmonics $\exp j(0, \phi, 2\phi,$ and $3\phi)$—see Section 3.3. The first is physically impossible, because it does not fit Kirchhoff's current law. The second and fourth are difficult to get in practice because they

require 90° phase difference between consecutive terminals. That leaves $e^{j2\phi}$, which is easily set up, because it requires 180° difference. It is illustrated in Fig. 4.7. Clearly, the resulting field on the axis is

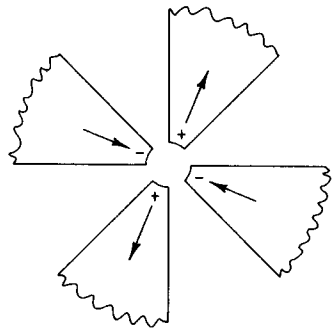

FIG. 4.7. Current distribution at the input of a four-element antenna.

zero, whereas for a two-element spiral it is maximum. As to other details, probably the best indication of the patterns of planar multi-element antennas is given by the theoretical solution described in Chapter 7.

Measurements on the conical case were aimed at getting maximum power in the plane $\theta = 90°$ with uniform distribution in ϕ.[5] It is instructive to consider typical results shown in Fig. 4.8. We note immediately that they are only crudely frequency-independent, yet the frequency-independent mode is unmistakably in operation. The crude appearance of the results is due mainly to two factors: (1) having four input terminals to connect makes it more difficult to model the input region, and (2) aiming to get maximum radiation in $\theta = 90°$ requires a comparatively rapid expansion ($\alpha = 45°$), which means a more extensive active region, as we have seen. Smoother patterns are in fact obtained for larger α, but they have a maximum where $\theta < 90°$. Perhaps it should be emphasized again that the messy shapes of the patterns are caused by inaccuracies in antenna construction. For example, if the construction is accurate and the feeding is symmetric, the variation with ϕ must be periodic over 90°. The deviation from this condition therefore indicates the error of measurement.

The fact that maximum radiation can be obtained in the plane $\theta = 90°$ is quite significant from the theoretical viewpoint. It implies that the principal component in the current distribution along a generator of

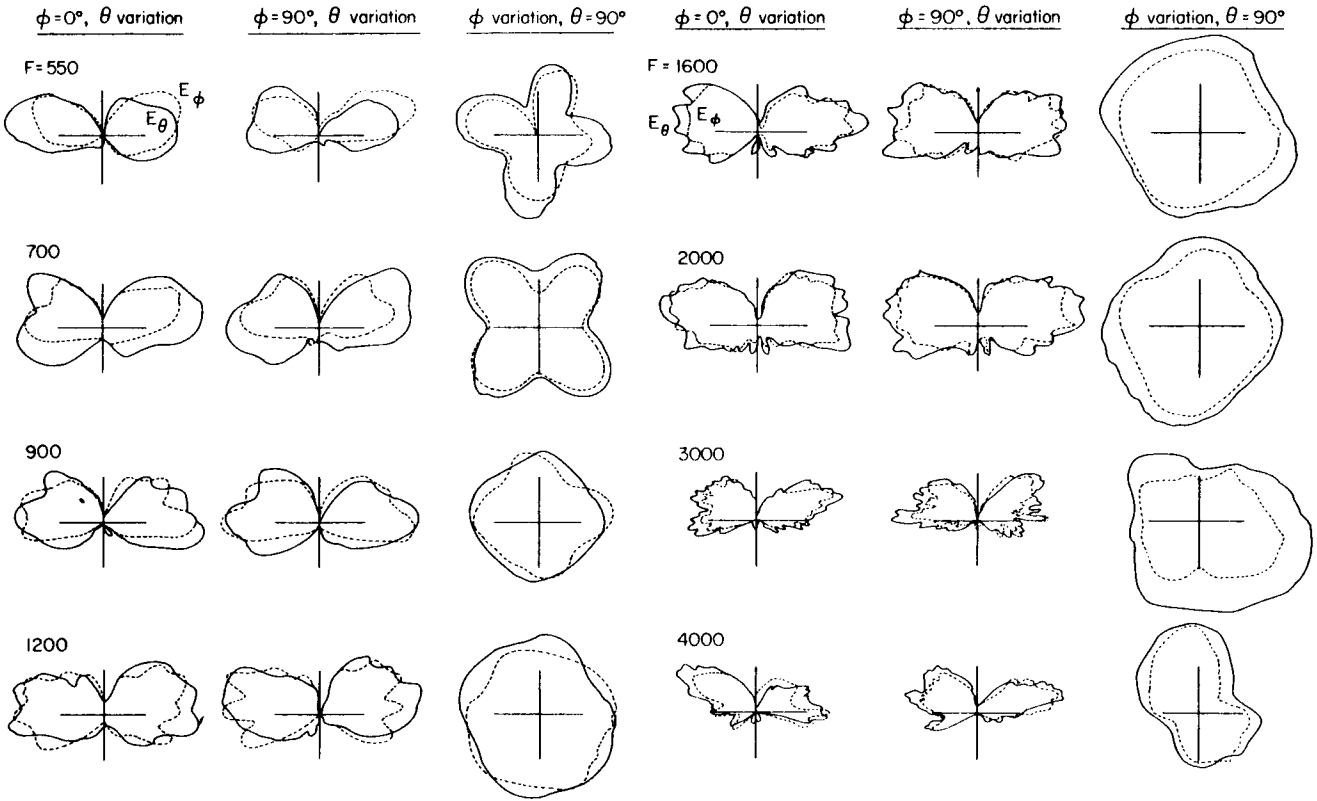

FIG. 4.8. Patterns of a four-arm conical antenna with $\theta_0 = 7.5°$, $\alpha = 45°$ [after Ref. 5].

the cone is an *outward*-traveling fast wave. The polarization is again circular, as closely as one can tell from the measurements. It may also be worth noting that the antenna which gave Fig. 4.8 was not self-complementary, although it was not far from it. Presumably the self-complementary design would give some improvement.

Some very interesting effects were observed when the antenna was excited to produce the $e^{j\phi}$ and $e^{3j\phi}$ modes.[5,6] As a preliminary, note that $e^{3j\phi}$ is physically the same at the input as $e^{-j\phi}$, because the difference is $2\pi n$ at every terminal, n being an integer. However, $e^{3j\phi}$ and $e^{-j\phi}$ are of course quite distinct, if we measure the continuous variation of phase with ϕ. Indeed, the infinite spectrum of harmonics will in principle be set up by the antenna, as in Section 4.1. In the present case the structure and the input currents are such that a rotation of 90° leaves the field unchanged, so the only harmonics arising from $e^{\pm j\phi}$ excitation must be $e^{jn\phi}$ with $n = \pm 1 + 4m$ and m an integer. Coming now to what actually happens, the remarkable thing is that only one harmonic is observable in the radiation field, that is, at infinite range. To put it concisely, it is the lowest harmonic (of the $\pm 1 + 4m$ series), which corresponds to an outward phase velocity along the arms at infinity. This means for $a > 0$ in $e^{a\phi}$, $e^{j\phi}$ excitation gives $e^{-3j\phi}$ in the radiation field, but $e^{-a\phi}$ gives $e^{j\phi}$. Generally speaking we can summarize the results this way. Let n_a = number of arms, n_e = the excitation in $\exp(\pm jn_e\phi)$, $n_a > n_e > 0$, $a > 0$. Then the radiation field is practically the pure harmonic $-(n_a - n_e)$ for the upper sign and $-n_e$ for the lower; that is, for $a > 0$ the lowest *negative* harmonic is obtained. On the other hand, in the immediate vicinity of the input, the observed field conforms closely to the lowest harmonic of all negative and positive, and, if this is not negative, a mixture of harmonics is observable in the transition region.

The purity of the single harmonic in the radiation field goes with the purity of circular polarization, for essentially the same reasons as given in Section 4.1. Similarly, the sense of polarization is the expanding sense for the spiral.

These results have an obvious but significant by-product: the $2N$-element spiral provides a pure $\exp(\pm jN\phi)$ mode *independent of frequency* (by putting equal and opposite currents into adjacent arms). This is amazing when we consider that to do it at a single frequency by conventional techniques is extremely difficult for high N, and simply impractical over a frequency range. One of the many applications where this kind of phasing is of fundamental importance is in radio direction finding.

REFERENCES

1. Dyson, J. D., Ph.D. thesis, Univ. Illinois, Urbana, Illinois, 1957.
2. Dyson, J. D., *IRE Trans.* **AP-7**, 181–187 (1959).
3. Dyson, J. D., *IRE Trans.* **AP-7**, 329–334 (1959).
4. Dyson, J. D., *Trans. IEEE* **AP-13**, 488–498 (1965).
5. Dyson, J. D., and P. E. Mayes, *IRE Trans.* **AP-9**, 334–341 (1961).
6. Sivan-Sussman, R., *Trans. IEEE* **AP-11**, 533–539 (1963).

5

LOG-PERIODIC ANTENNAS

5.1 Some General Aspects

The first successful log-periodic antennas were discovered by DuHamel and Isbell[6] only after a great deal of experimenting with divers designs. The unsuccessful attempts were log-periodic to be sure, but the variation of pattern and impedance over a period was too much for all usual applications. In other words, the problem in the beginning was to find designs that gave nearly constant performance over one period. It seemed then that this requirement made the dimensions very critical, and for some years after the secret of successful designs was a mystery.

There was, however, one certain way to eliminate the periodic variation of impedance—to make the shape self-complementary, as described in Chapter 3. This only applies to planar-sheet antennas and so explains why the first experiments took this particular direction. It appeared that the self-complementary condition was also required to get a good pattern, but later it was found to be desirable rather than necessary.

After a few years Isbell[11] made a successful log-periodic dipole array, and it seemed that the secret of this success after many earlier failures was the switching of phase from one dipole to the next, the earlier attempts having been unswitched. This explanation also failed to stand the test of time, for subsequently many successful unswitched designs were invented.

Now there is a common feature in the principles behind the self-complementary shape and the switched dipole array. It is illustrated in Figs. 5.1 and 5.2, which, for the sake of clarity, are drawn for the uniformly periodic case, that is, infinitely slow rate of expansion. If we

take the image of half the dipole array in the central plane (parallel to the dipoles and to their connecting line), we see that it is the same as the other half of the array shifted through half a period. This is also

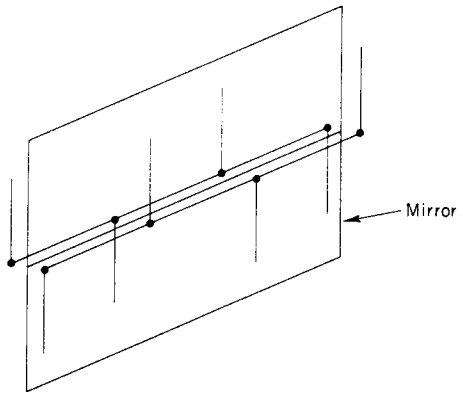

FIG. 5.1. Symmetry properties of the switched dipole array.

true for a self-complementary shape, as Fig. 5.2 shows (it represents a portion of a structure such as the one in Fig. 3.5).

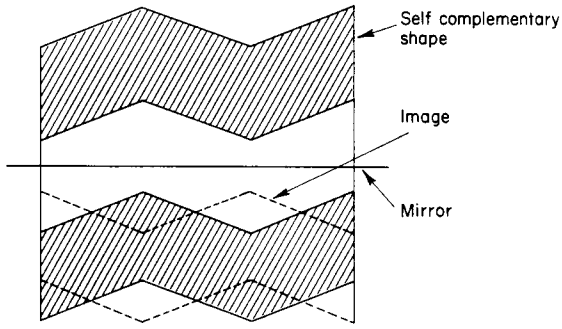

FIG. 5.2. Symmetry properties of a self-complementary structure.

We have seen that it is necessary to specify one characteristic length as well as various angles to determine completely any particular log-periodic structure. However, if the performance is frequency-independent, that is, if the variation over a period is negligible, this characteristic length evidently does not matter. Consequently, it is sufficient to

specify only angles for the structures described in the rest of this chapter, because only the frequency-independent versions are of interest. (The expansion parameter $1/f = \tau$ is in effect an angle, being the ratio of two lengths.)

The characteristic length does matter as far as the phase of the radiated field is concerned, as, for example, when the fields of two antennas are to be combined. The question is illustrated in Fig. 5.3,

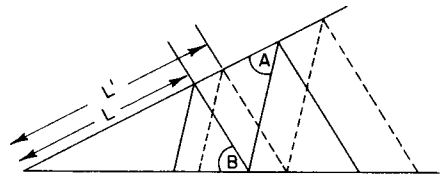

FIG. 5.3. Definition of characteristic length L.

which shows two structures differing only in their characteristic lengths L and L'. If each is fed at the apex by the same source, what is the phase difference in radiated fields? We can get a clue to this from the spiral antenna. In that case we know that an expansion of L'/L is equivalent to a rotation, which, in turn, is equivalent to a phase shift equal to the angle of rotation. It was discovered by DuHamel and Berry[5] that this is practically what happens for log-periodic antennas also (at least for the frequency-independent types). Shifting L to L' causes a phase shift of about $2\pi \log (L'/L)/\log \tau$. Clearly, this is exact when $L = \tau L'$, that is, when there is a shift of one period. If the cell is symmetrical, that is, $A = B$, a shift of half a period is equivalent to turning over the structure and therefore must give a phase shift of π. This also agrees with the formula on putting $L = (\tau L')^{1/2}$. For other cases the formula is empirically valid within about 20°. One of the most useful cases is a shift of a quarter of a period, to give a 90° phase shift independent of frequency. Thus, if two linearly polarized antennas L' and L are oriented at right angles and fed from a common apex, the resulting polarization is approximately circular at all frequencies if $L = \tau^{1/4} L'$. It may be of interest to note that the same principle has been found to apply to nonradiating log-periodic elements. Thus we have a way of designing for any fixed phase shift nearly independent of frequency. It will be appreciated that this is a most valuable by-product of frequency-independent-antenna research.

5.2 Planar-Sheet Structures

The form of the first successful log-periodic antennas is shown in Fig. 5.4. The terminals were connected to a fine coaxial line whose outer conductor was embedded in one sheet, the inner conductor being

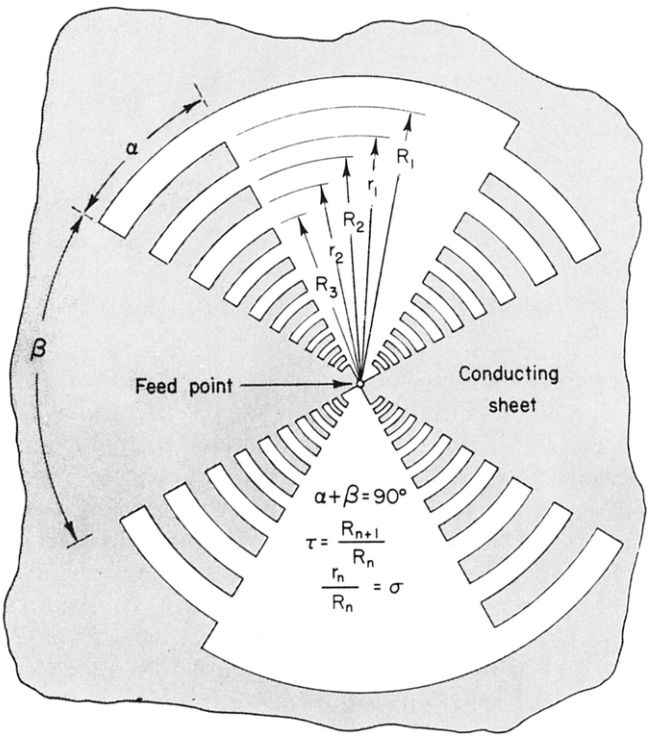

FIG. 5.4. Self-complementary planar antenna [after Ref. 6].

connected across a small gap to the other sheet. The self-complementary condition means that $\alpha + \beta = 90°$. In addition, all tests were made with $\sigma = (\tau)^{1/2}$, thus equalizing the widths of the teeth and the gaps between them. As an indication of the imperfections of the models, we might note that the measured impedance, which should have been 189 Ω independent of frequency, in fact varied over a 5:1 range! The measurements were made from 400 to 1600 Mc/s for an antenna of diameter 20 inches with $\alpha = 45°$. This diameter is too small to expect good correlation at 400 Mc/s (or 30-inch wavelength), but that did not explain

the large discrepancy, which clearly illustrates the difficulty of making meaningful measurements.

Values of 20, 45, and 60° for α were tried and it was fairly clear that $\alpha = 45°$ gave the best patterns: Typical results are shown in Fig. 5.5. Note that the pattern very nearly does go to zero in the plane of the

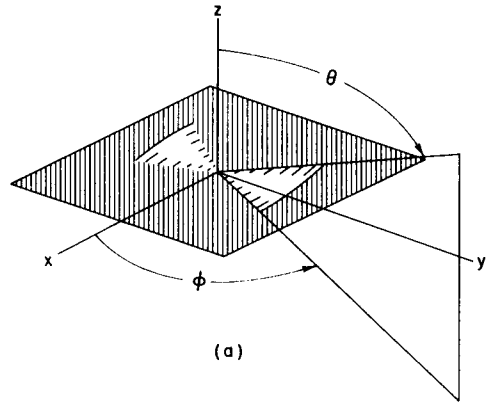

(a)

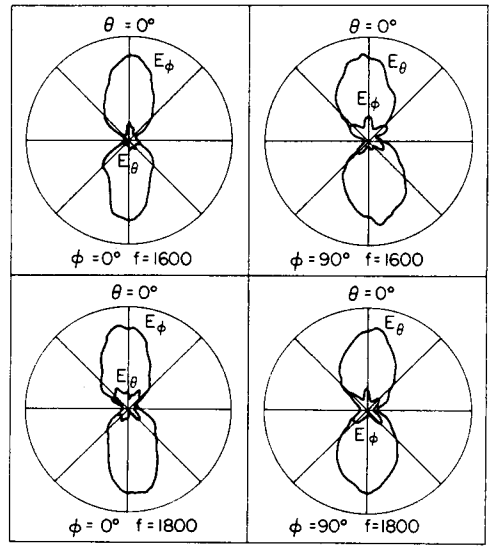

(b)

FIG. 5.5.a,b. Radiation patterns for $\alpha = \beta = 45°$, $\tau = 0.5$ [after Ref. 6].

antenna, as we know it must to be frequency-independent. Only two frequencies are shown, because it had been found by working over a 10:1 band that the patterns were indeed practically independent of frequency. By measuring in other ϕ planes, it was found that the distribution of radiated power was practically uniform in ϕ. This is another surprising result and evidently corresponds to the same effect observed on spiral antennas. In the latter case the polarization was circular: both $| E_\phi |$ and $| E_\theta |$ were constant with ϕ but now only $| E_\phi |^2 + | E_\theta |^2$ is constant. We saw that these two effects were different symptoms of a common cause—that the distribution in ϕ is expressed by a Fourier series with only one term. In the present case the polarization is linear, and evidently this must follow from the superposition of the two single-term Fourier series, which represent right- and left-handed circular polarizations. Thus if

$$E_{+\theta} = jE_{+\phi} = jE_0 e^{j\phi}$$

and

$$E_{-\theta} = -jE_{-\phi} = -jE_0 e^{-j\phi}$$

$$E_\phi = E_{+\phi} + E_{-\phi} = 2E_0 \cos\phi$$

and

$$E_\theta = E_{+\theta} + E_{-\theta} = -2E_0 \sin\phi$$

It will be seen that this agrees reasonably well with Fig. 5.5 for $\phi = 0$ and $\phi = 90°$. It predicts a simple law for rotation of polarization with ϕ, which could very easily be checked by measurement. But this was not realized at the time, so definite confirmation is not available. We can say, however, that if the radiated power is uniformly distributed in ϕ and the antenna is self-complementary, the polarization must be linear everywhere if it is linear anywhere and must rotate as the formula indicates.

The direction of polarization observed is highly significant. It is perpendicular to what it would be with no teeth, that is, to the biconical case represented by $\alpha = 0$. This shows that the component of current that flows in the direction of the teeth dominates the radial component. Thus the frequency-independent operation depends on a highly selective resonance of the transverse component of current!

Good patterns for $\tau = 0.8$, 0.7, 0.5, and 0.25 were obtained, and gave an unexpected control of beamwidth: the beamwidths between half power points were, respectively, 73, 70, 55, and 38°. A model with

$\alpha = 45°$ and $\beta = 75°$ illustrated the effect of departing from the self-complementary shape. The patterns were not significantly different but the variation of impedance was noticeably worse.

5.3 Inclined Plane-Sheet Structures

Shortly after the first discovery of frequency-independent performance from logarithmically periodic structures, an important step forward was made by Isbell. He tried two sheet metal elements whose planes were inclined at an angle ψ as in Figs. 5.6 and 5.7. Thus $\psi = 180°$

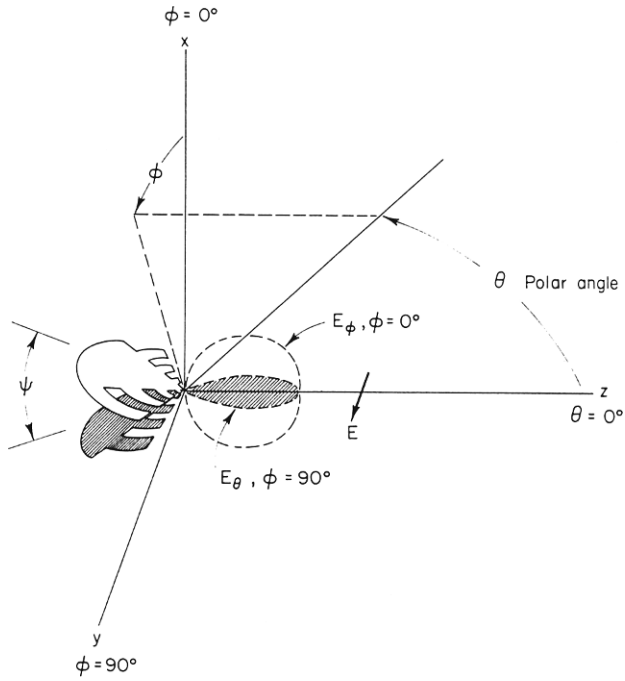

FIG. 5.6. Radiation-pattern coordinate system [after Ref. 11].

represents the original planar case discussed in the previous section, and $\psi \neq 180°$ evidently gives more radiation on one side than the other. In this way Isbell was able to find designs that gave good unidirectional patterns. Typical measured results are shown in Fig. 5.8. The patterns

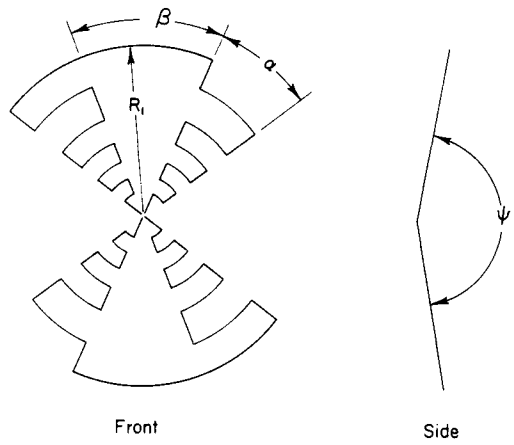

FIG. 5.7. Experimental-model configuration [after Ref. 11].

taken in the range 1000–3000 Mc/s evidently come close to the pure frequency-independent mode. Much the same results were obtained for $60° > \psi > 30°$.

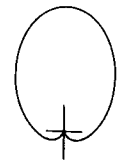

FIG. 5.8. Typical measured $E_\theta(\theta)$ for $\tau = 0.7$, $\psi = 40°$, $\alpha = 60°$, $\beta = 30°$.

The polarization proved to be a significant indicator, as it was in Section 5.2 and also in the case of spiral antennas. In this case the undesired or "cross-polarized" component is what would be radiated by the biconical mode, or radial component of current. The measurements strongly suggested that reduction of this cross-polarized component goes with improvement of the frequency-independent operation. Typically the averaged cross-polarized component was about 18 db below the field at $\theta = 0$.

As might be expected, the input impedance is lowered by decreasing ψ. Since all the designs tried by Isbell were self-complementary, the impedance for $\psi = 180°$ should have been 189 Ω: it was roughly 165 Ω. It decreased to about 70 Ω for $\psi = 30°$.

It was observed that the variation of impedance over a period increased as ψ decreased: for example, the variation for $\psi = 60°$ was about 3:1 with respect to the geometric mean. DuHamel and Ore[7] investigated a similar design, except that the teeth were straight instead of circular. The patterns were much the same, but there was considerable improvement of the impedance for small ψ, for example, a variation about the mean of 1.6:1 for $\psi = 60°$.

5.4 Wire Structures

The sheet-metal antennas described in previous sections are convenient at centimeter wavelengths, but they become impractical at longer wavelengths. This led DuHamel, and Ore[7] to see if the sheet could be simulated by a thin wire shaped to follow the outline of the sheet. It turned out that it could, and such antennas proved to be of great practical importance. The diameter of the wire should of course be proportional to the distance from the center, but in most tests and most applications a constant diameter was used. Usually this made very little difference to the pattern, but a much better impedance often resulted from using the properly scaled wire diameter.

A typical wire antenna is illustrated in Fig. 5.9. It consists of two wires in an expanding rectangular wave form and two "booms" lying along their center lines. The input terminals are therefore at the junction of the booms, so that the antenna can be fed by passing a coaxial cable through one boom, which forms the outer conductor, and connecting the inner conductor to the other boom. This is one reason for having the booms. The other is to give structural support. The infinite structure is characterized by the angles α and ψ and the expansion factor τ. As we shall see shortly, the radiation effectively comes only from currents parallel to the x axis. This explains why the lower element is shifted half a period with respect to the upper, for this puts these currents in phase at equal distances from the terminals (see Fig. 5.9). If the lower element were turned over, thus making it identical to the upper, the pattern would go to zero in the plane of symmetry: it would be the same as the upper element fed against a ground plane.

Typical patterns are shown in Fig. 5.10. Note that the E_ϕ pattern in the YZ plane does go close to zero in the directions that would be occupied by the infinite antenna. The fact that E_θ is comparatively high over these directions indicates that the E_θ measurement is not

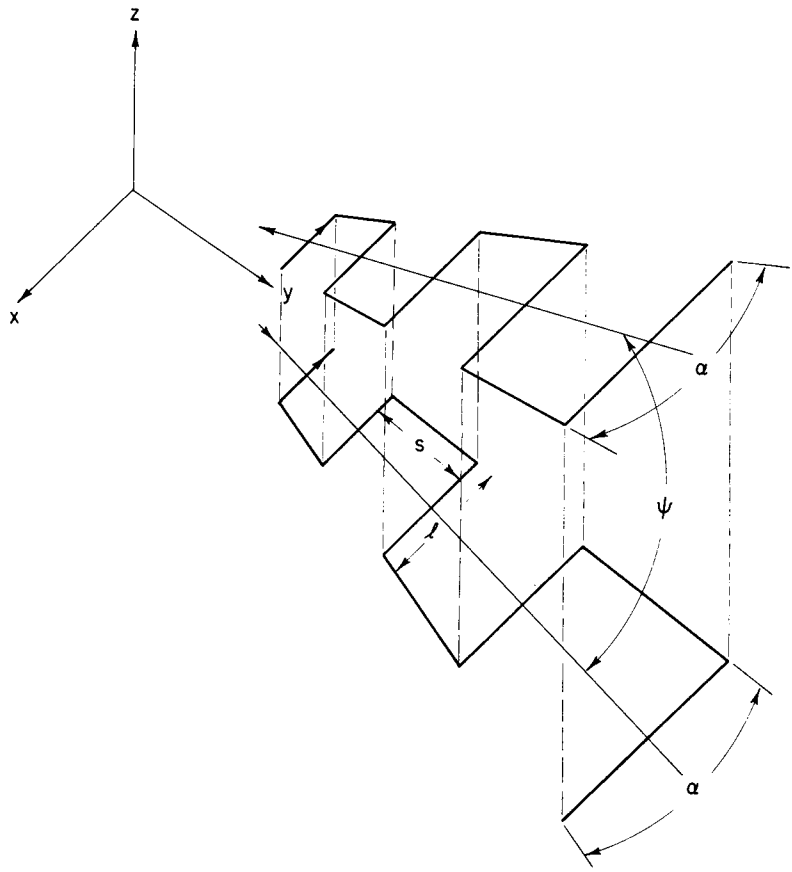

FIG. 5.9. Trapezoidal wire antenna showing direction of current for excitation at the apex.

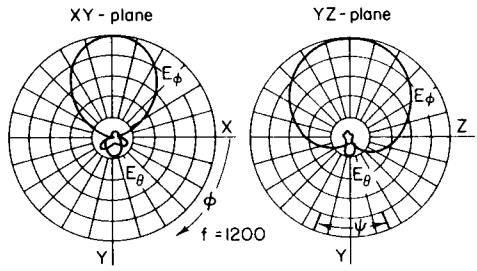

FIG. 5.10. Patterns for trapezoidal wire antenna. $\alpha = 75°$, $\tau = 0.5$, $\beta = 0°$, $\psi = 45°$.

characteristic of the infinite structure. The performance of various successful designs is given in Table I. The variations in beamwidth

TABLE I

Pattern Characteristics for Various Wire Structures

Ant	α	τ	ψ	XY beam	YZ beam	Gain (db)	Side lobes (db)
1	75	0.4	30	74	155	3.5	12.4
2	75	0.4	45	72	125	4.5	11.4
3	75	0.4	60	73	103	5.3	8.6
4	60	0.4	30	85	153	3.0	12.0
5	60	0.4	45	86	112	4.2	8.6
6	60	0.4	60	87	87	5.3	7.0
8	75	0.5	30	66	126	4.9	17.0
9	75	0.5	45	67	106	5.6	14.9
10	75	0.5	60	68	93	6.1	12.75
11	60	0.5	30	70	118	4.9	17.7
12	60	0.5	45	71	95	5.8	14.0
13	60	0.5	60	71	77	6.7	9.9
14	60	0.6	45	67	85	6.5	15.8
15	60	0.707	45	64	79	7.0	15.8
16	45	0.707	45	66	66	7.7	12.3
17	14.5	0.85	29	59	38	10	7

over a period were less than 10 %, for the 17 cases quoted. However, the pattern deteriorated (see Fig. 5.9) if

$$s > 0.3l$$

The high-gain design (No. 17) was checked for operation with a ground plane at $z = 0$ by turning over one element. Except for the zero produced in $z = 0$, this had practically no other effect on the performance. For a typical case the impedance varied from about 120 Ω at $\psi = 60°$ to 105 Ω at $\psi = 30°$, with a variation of about 2:1 over a period. For the last case, No. 17, the impedance was about 80 Ω, with very slight variation over a period.[5]

Structures with triangular instead of rectangular waveform gave slightly better patterns but were essentially similar in performance.[8] A detailed description of the current distribution on this type is given in Section 5.5.

5.5 Current-Distribution Measurements

A first-rate delineation of the near field of a typical log-periodic antenna was done by Bell, Elfving, and Franks.[1] They used an antenna like the one described in Section 5.4, but having a symmetric sawtooth waveform with $\tau = 0.85$, $\alpha = 28°$, and $\psi = 32°$ (see Fig. 5.9). Their results could be pictured as the combination of a "radiating" wave emanating from the "active" region and a "transmission line" wave emanating from the apex. When seen along the y axis, the transmission-line E

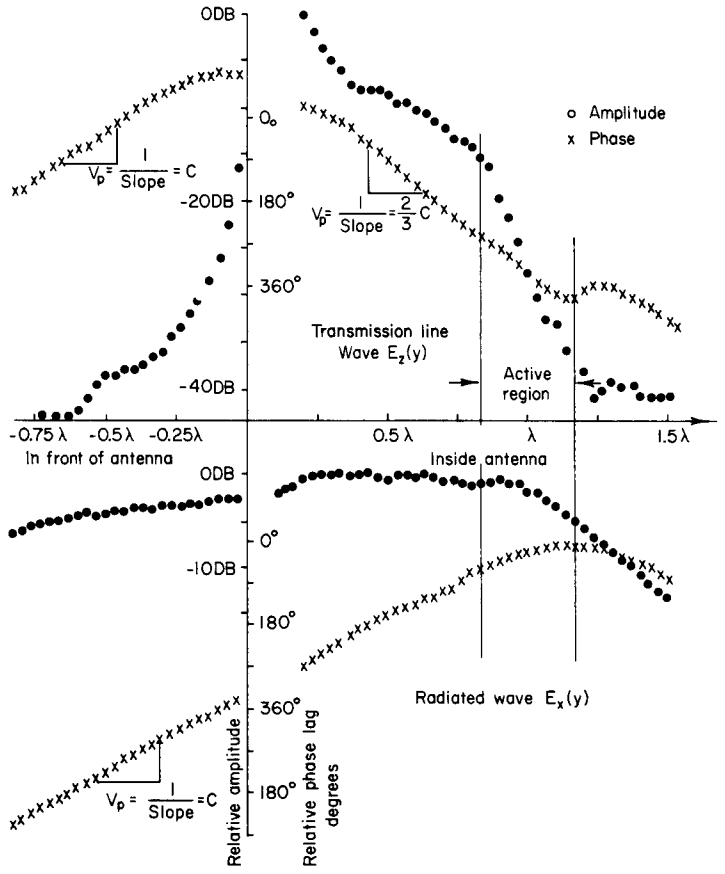

FIG. 5.11. Phases and amplitudes of the two waves measured along the central axis [after Ref. 1].

wave is polarized along the z axis and the radiating wave is polarized along the x axis. They can thus be separated by measuring the two polarizations along the y axis, which is the center line. The results are shown in Fig. 5.11. First, we note that the slopes of the phase curves clearly show where the two waves originate. Second, we see that the radiating wave hardly diminishes as it travels past the apex to the open space in front of the antenna. Third, the transmission-line wave diminishes rapidly beyond the active region—indeed, this is what defines the active region. As we saw in the discussion of the biconical antenna, the transmission-line mode normally decreases as $1/r$. Figure 5.12 shows

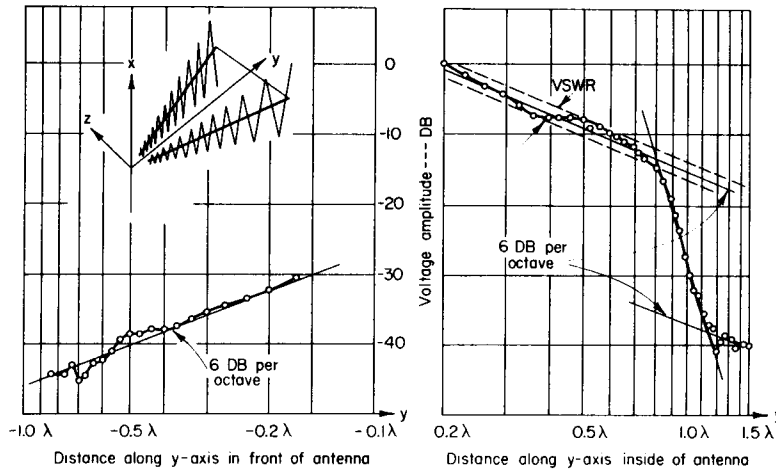

FIG. 5.12. Amplitude of the transmission line wave measured along the y axis [after Ref. 1].

the comparison with the $1/r$ law. A good picture of the two waves is given by the amplitude and phase contours taken in the central XY plane (Fig. 5.13). Here we see that the phase velocity of the transmission wave increases from about $2c/3$ (c = the free-space velocity) along the y axis to greater than c along the x axis. It looks as though the phase contours would become nearly straight and perpendicular to the y axis if the antenna expanded more gradually. This may be recognized as being characteristic of a slow-wave transmission line.

The current distribution was measured along the sawtooth path (but not along the boom, where it may be assumed to conform to the transmission-line wave). The amplitude in the active region is shown

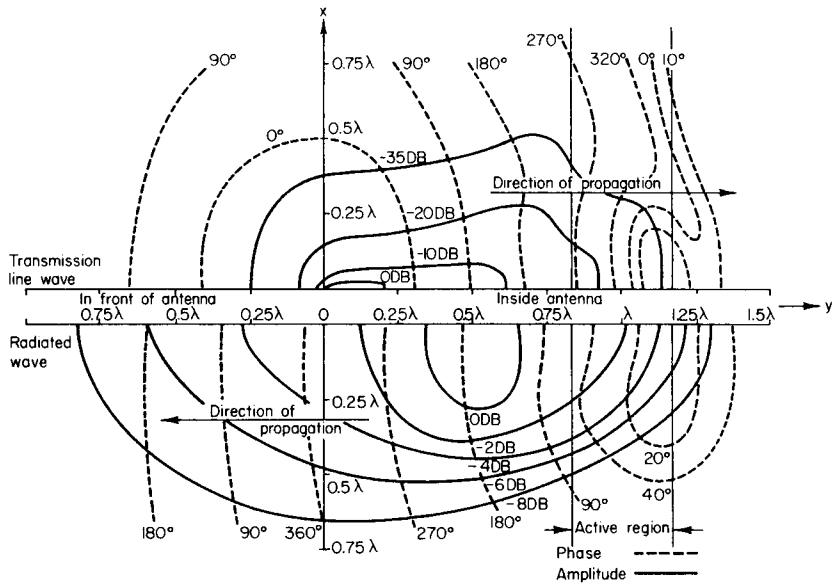

FIG. 5.13. Contours for the transmission line and radiated waves [after Ref. 1].

in Fig. 5.14(a). It is nearly zero at the peaks of the teeth and rises to a maximum at the boom, where it is much higher than the amplitude near the input. Outside the active region, the amplitude is much more nearly uniform. Note also that attenuation resulting from the active region shows up strongly in the current measurements. It is significant, but not surprising, that the height of the tooth in the center of the active region was very close to $\lambda/4$. In this connection we should note the thickness of the elements: The sawtooth elements were about $\lambda/100$ in diameter and the boom was a square bar about three times as thick. The picture we get from the amplitude measurements, then, is this. The region from the terminals to the active region functions as a transmission line. The active region consists of three or four cells in marked resonance, with currents much higher than the transmission-line current. There is negligible current beyond the active region.

Coming now to the phase of the current distribution, first note the importance of the coordinate system. For example, in conventional spherical coordinates $r\theta\phi$, if E_θ does not vanish at $\theta = 0$, its phase will show a jump of 180° as θ passes through zero, although its "physical" phase must be continuous, of course. (It would not have to be continuous

if $E_\theta = 0$ at $\theta = 0$.) The jump disappears if we measure the same component of E but refer the measurements to a rectangular coordinate system, for example. For these reasons it is a good idea to express the present case in terms of three coordinate systems, shown in Fig. 5.14(b), (c), and (d). They differ only by 180° either at the boom or the peaks, as indicated by the arrows. System (b) is essentially the radial component, (d) the transverse component, and (c) is like the θ component with $\theta = 0$ at the boom: it is the natural system for the transmission line wave and (d) is the natural system for the radiation wave. From the

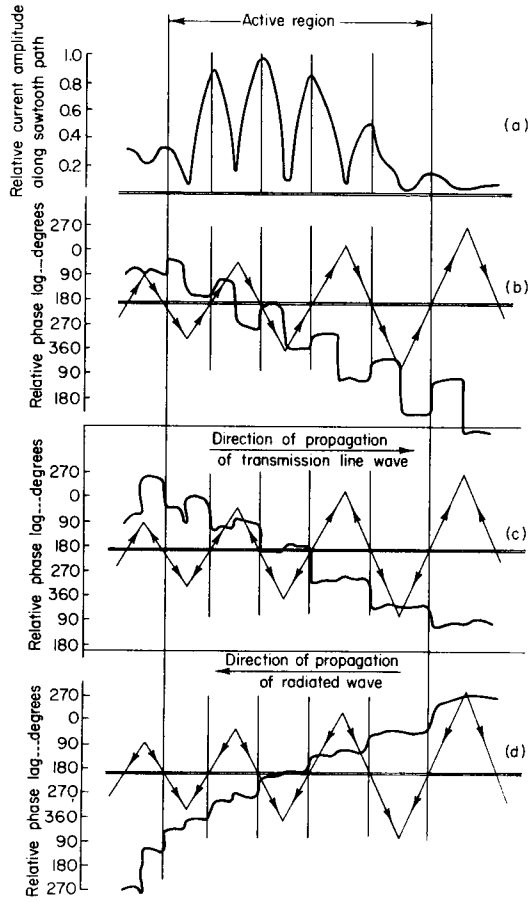

FIG. 5.14a–d. Phase distribution of currents in the teeth [after Ref. 1].

point of view of continuity of current, (b) shows a reversal at each peak, corresponding to the vanishing of the amplitude: before the active region there is no such reversal. Both (b) and (c) show an outward-traveling wave with a phase shift very close to 180° per cell in the active region. Note also a phase shift of approximately 90° in crossing the boom. From the point of view of the radiated field, (d) shows an inward-traveling wave also with 180° per cell. We shall see in Chapter 6 that these results are typical of the stop band in a periodic structure.

In these measurements the two halves of the antenna were oriented to give maximum radiation along the central line; that is, one is shifted by half a cell relative to the other. This puts the two radiated waves exactly in phase (at the central plane). It is interesting to ask what would happen if one half were turned over, thus making the two halves identical. The two radiated waves would then oppose each other, but the transmission-line wave would not be so affected. In fact, the resulting field may take quite a different form from what we have seen in these measurements. Unfortunately, this simple test was not thought of at the time. It would help a great deal in understanding why reversing one half of the structure makes such a difference to the frequency dependence.

5.6 Dipole Arrays

As soon as DuHamel and Isbell had their first success with planar structures, a log-periodic array of dipoles shunted across a transmission line was naturally tried. But the results were disappointing, because the pattern varied greatly over a period. Some years later Isbell gave it another try, this time successfully.[12] The difference from the earlier attempts was simply that an extra phase shift of 180° per dipole was introduced by switching the connections, as in Fig. 5.15. The idea was

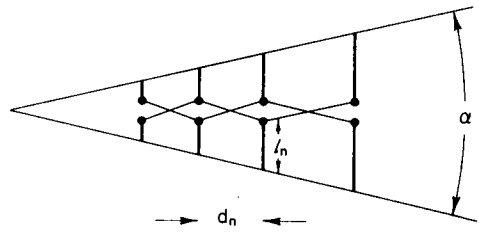

FIG. 5.15. Switched dipole carray.

this. The dipoles near the input, being nearly out of phase and close together, nearly cancel. As the spacing d_n expands, there comes a point where the phase delay in the transmission line combined with the 180° switch gives a total of 360° $(1 - d_n/\lambda)$. This puts the radiated fields from the two dipoles d_n apart in phase in the backward direction, that is, back toward the input. Moving further out increases the phase delay, and so the in-phase direction moves from backward through broadside to forward. (This is discussed at length in Chapter 6, but the elementary ideas are all we need here.) Therefore, a good beam coming off the apex should result if the dipoles are resonant where the total phase delay from one dipole to the next is about 360° $(1 - d_n/\lambda)$. The idea is to exhaust the power in the transmission line before the phasing changes greatly from this condition. The behavior of the active region described in Section 5.5 suggests how this might come about.

The antenna was fed as shown in Fig. 5.16, by running a coaxial

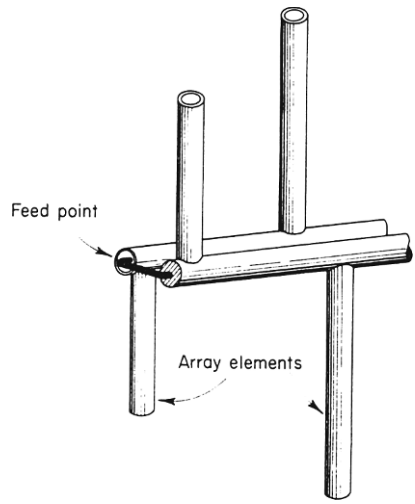

FIG. 5.16. Connection of elements to biaxial line [after Ref. 12].

line inside one side of the transmission line and connecting its inner conductor to the other side at the input. The shortest dipole was about a quarter the length l_1 of the longest and the transmission line was shorted at $l_1/2$ beyond the longest. The input impedance was approximately resistive. Its mean value R_0 is shown in Figs. 5.17–5.19, with the maximum VSWR over a period with respect to R_0. Typical patterns

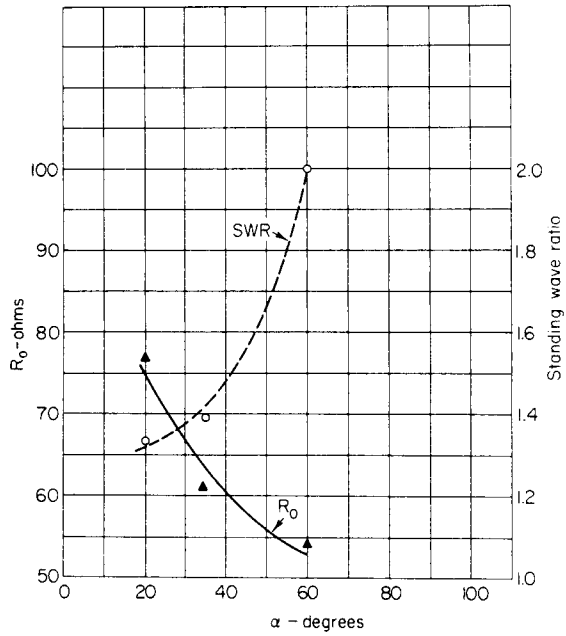

FIG. 5.17. Input impedance $\tau = 0.95$ [after Ref. 12].

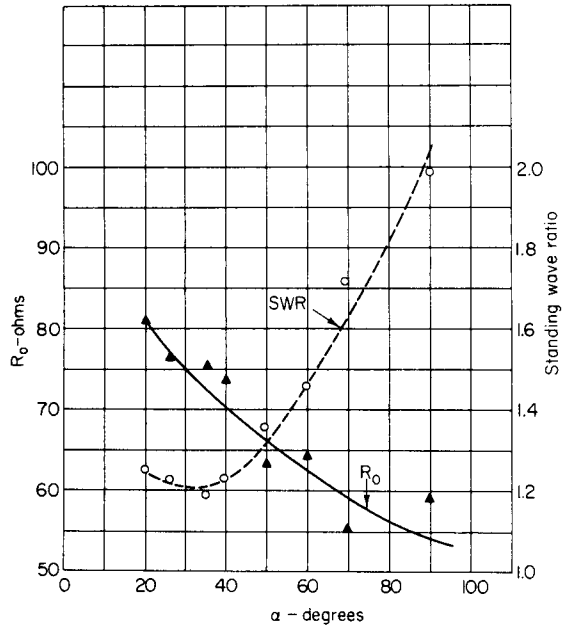

FIG. 5.18. Input impedance $\tau = 0.89$ [after Ref. 12].

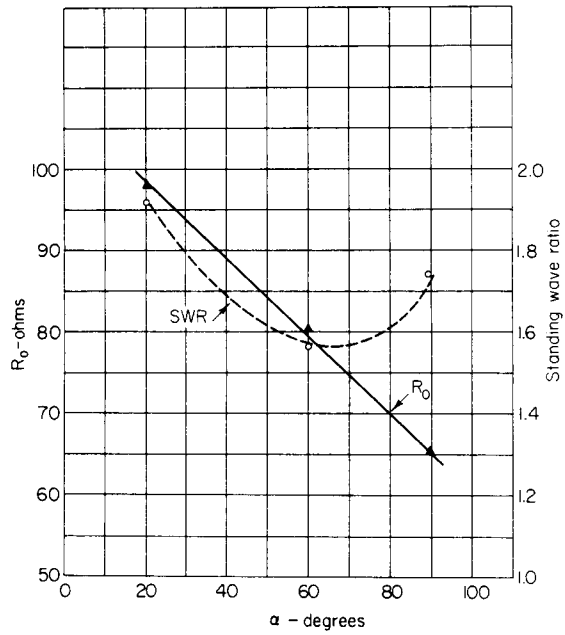

FIG. 5.19. Input impedance $\tau = 0.81$ [after Ref. 12].

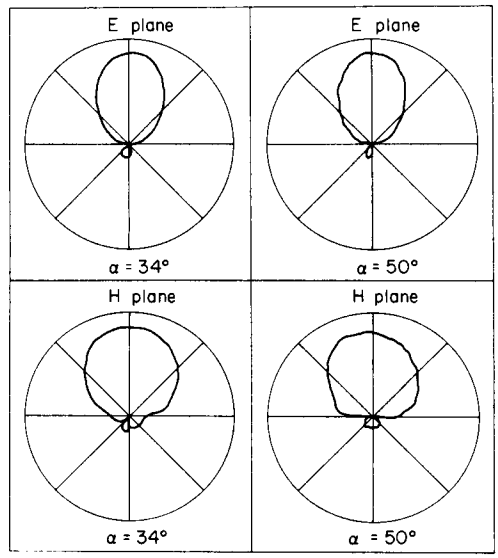

FIG. 5.20. Typical patterns for $\tau = 0.95$ [after Ref. 12].

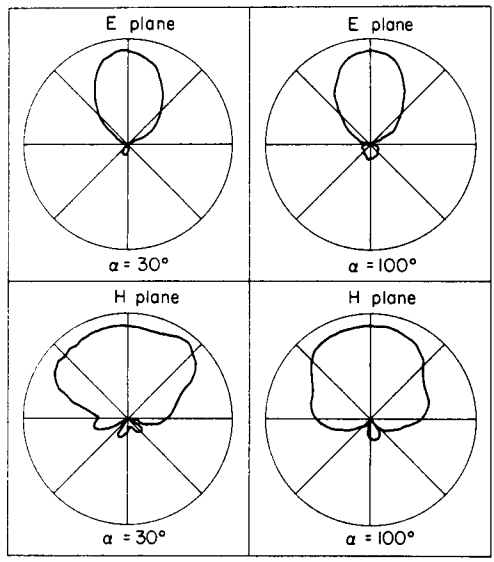

FIG. 5.21. Typical patterns for $\tau = 0.81$ [after Ref. 12].

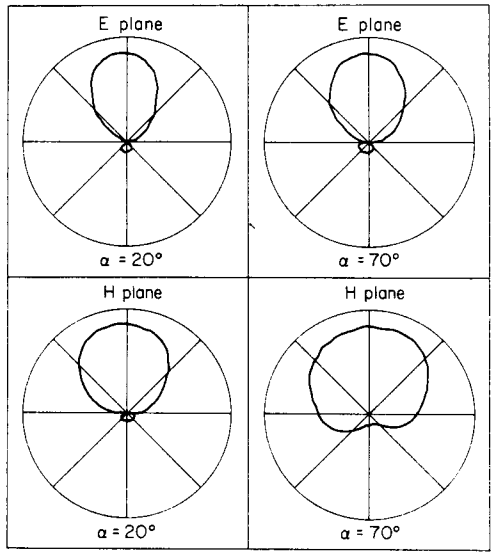

FIG. 5.22. Typical patterns for $\tau = 0.89$ [after Ref. 12].

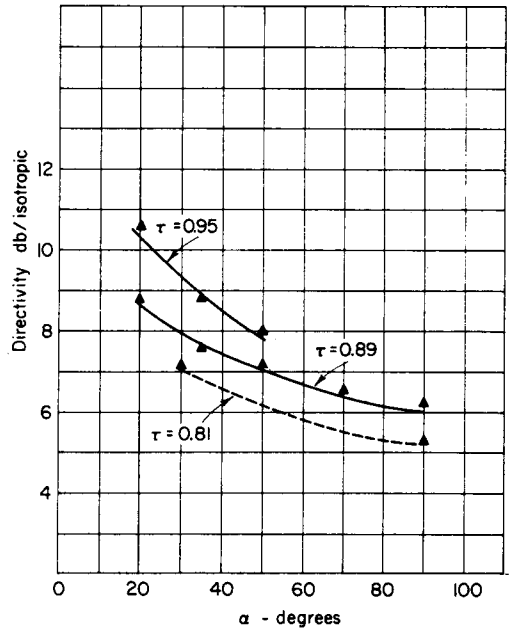

FIG. 5.23. Directivity versus τ and α [after Ref. 12].

are shown in Figs. 5.20–5.23. The variation of pattern over a period was practically insignificant.

At this point it may be worthwhile to discuss a variation of the angle principle which is implied in the present case. As we have seen, all dimensions should be scaled in proportion to distance from the origin, which means the transmission line should be biconical. In this case we are using two parallel wires instead of two cones. However, either forms a uniform transmission line for the TEM mode and so they are equivalent, provided this is the only mode present. Evidently, then, the parallel-wire line is equivalent to a biconical line if the spacing of the wires is negligible compared to the shortest wavelength of operation, and if the spacing of the bases of the cones also fits this requirement.

A thorough analysis of this antenna was worked out by Carrel,[4] for an array of eight dipoles. Dipole self and mutual impedances were calculated by the induced-emf method assuming a sinusoidal distribution of dipole current. Although not exact, this is more accurate than most measurements for the range of thicknesses represented by $50a_n < l_n < 10{,}000a_n$, where a_n is the radius. The theory is therefore essentially

exact for eight elements. Moreover the results show that this gives a very good estimate of the performance for the infinite case.

Patterns were calculated for eight frequencies in geometric progression corresponding to the expansion factor τ, the lowest being the resonance frequency for the longest dipole. The patterns for the lowest and highest frequencies did show some aberration, but the other six showed perfect agreement; certainly any difference was 10 times smaller than the best of measurement errors. This shows conclusively that the eight dipoles behave as if they were in an infinite structure. The frequency-independent nature of the pattern was also established most convincingly by calculating patterns at f, $(\tau^{1/4}f)$, $(\tau^{1/2}f)$, and $(\tau^{3/4}f)$. Again the agreement was certainly within 1% of the maximum for any direction or frequency. The phase principle mentioned in Section 5.1 was also checked, but oddly this did show a significant departure from the idealized formula: the maximum departure was nearly 20°. Directivity contours are shown in Fig. 5.24: high gain requires very slow expansion. The directivity is very slightly affected by dipole thickness. It increases by about 0.2 db when the thickness is doubled in the range $50a < l < 10{,}000a$.

The calculated mean impedance R_0 is linearly proportional to the

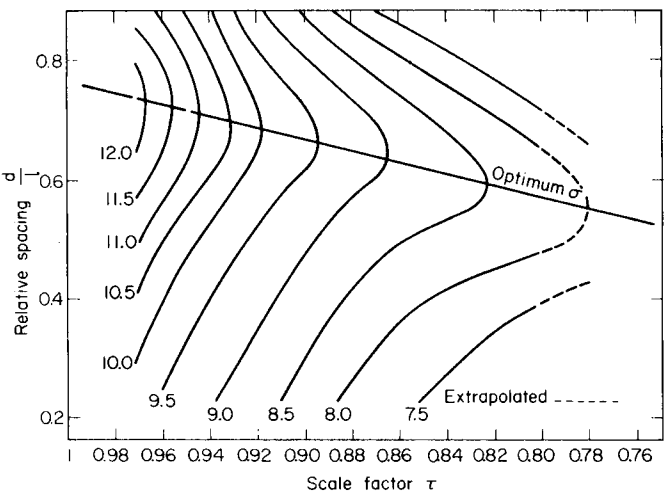

FIG. 5.24. Constant directivity contours in decibels versus τ and σ. $Z_0 = 100$, $l/a = 125$. Optimum σ indicates maximum directivity for a given value of τ [after Ref. 12].

characteristic impedance Z_0 of the transmission line, all other parameters being constant: R_0 varies from 42 to 93 as Z_0 varies from 50 to 150. The max VSWR with respect to R_0 over a period varies linearly from 1.1 to 1.2 over this range. This is much less than measured values and shows again how difficult it is to make meaningful impedance measurements. The variation of R_0 with α and τ is shown in Fig. 5.25.

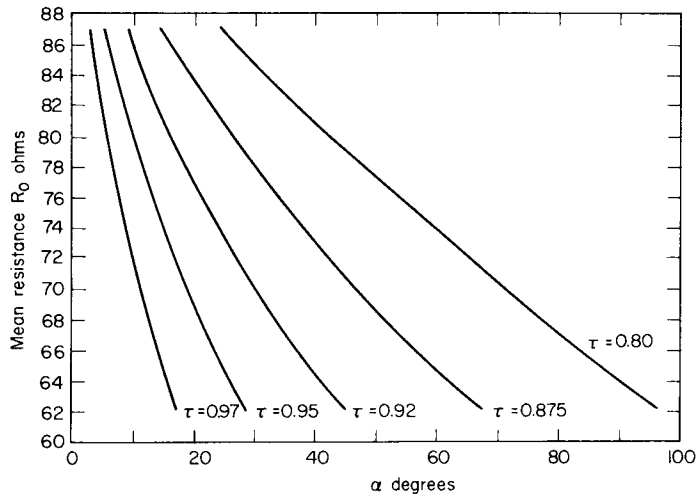

FIG. 5.25. Mean resistance level R_0 versus α and τ for $Z_0 = 100$, $l/a = 125$ [after Ref. 12].

The phase and amplitude distributions of dipole input currents are shown in Fig. 5.26. Note how similar they are to the distributions in the active region for the sawtooth structure of Section 5.5. For the purpose of comparison, note that one cell of this structure corresponds to an expansion of τ^2 (using τ to mean l_n/l_{n-1}). If we used only τ, all cells would not be identical, because of the switching of the transmission line. Thus the active region, taken as that between the 10-db points of the amplitude curve, covers about two cells and the phase shift is about 180° per cell.

It will be noted that this type of array gives rather low directive gain. To get higher gain over a specific band of frequencies, Mayes and Carrel tried higher mode operation of an array in which the longest dipole was three or four times longer than the shortest.[14] The low-frequency limit then occurs when the longest dipole is a little over $\lambda/2$ long.

As frequency is raised, the active region moves from the large to the small end. When it gets there, the longest dipoles are about $3\lambda/2$ long, so the active region tends to reappear in the $3\lambda/2$ mode at the large end as it disappears in the $\lambda/2$ mode at the small end. The λ mode is hardly excited, because of its high impedance. The process is then repeated

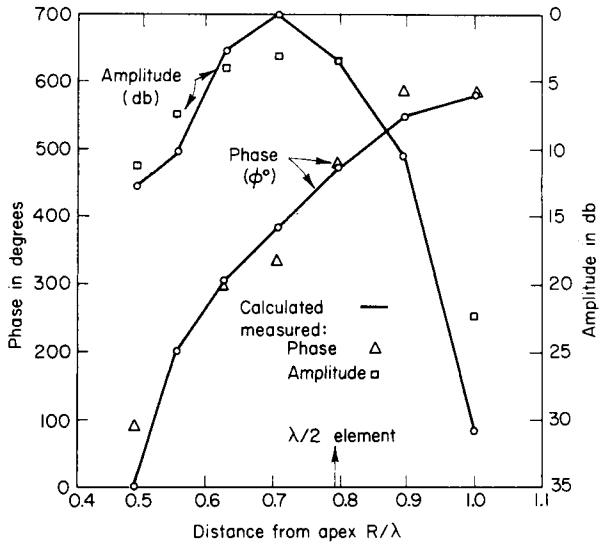

FIG. 5.26. Relative magnitude and phase of element base current vs R/λ, $\tau = 0.88$, $d/l = 0.36$, $\alpha = 17.5°$, $N = 8$, $Z_0 = 100\Omega$, $l/a = 125$ with short-circuit termination $0.128\ \lambda$ behind longest element [after Ref. 4].

until the $5\lambda/2$ mode appears. Evidently, this does not go on indefinitely because the spacing of the modes becomes more and more mismatched to the ratio of largest to smallest dipole. There was also some deterioration in shifting from one mode to the next. The dipole pattern itself is undesirable in the higher modes but this was put right by inclining the dipoles toward the apex through an angle of 45–65°. In summary, good performance was obtained over a 12:1 band by operating in the $\lambda/2$, $3\lambda/2$, $5\lambda/2$, and $7\lambda/2$ modes. Note that this approach does not give a frequency-independent pattern, because the gain increases with the mode order. The highest gain was about 17 db.

5.7 Antennas over a Ground Plane

The key to the success of the dipole arrays was, as we have seen, the switching of the connections to give an extra 180° phase shift per dipole. In this section we consider a few examples, which give nearly frequency-independent operation yet do not use this switched excitation. This allows a "ground" plane to be inserted at the plane of symmetry, and

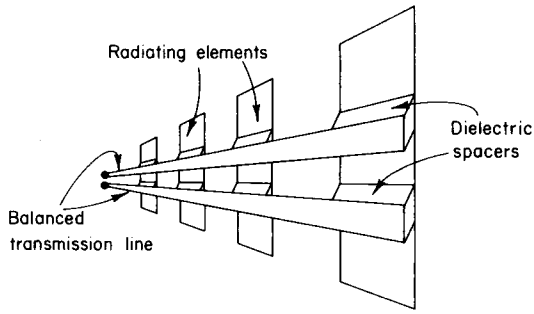

FIG. 5.27. Tapered ladden antenna.

so has an important advantage which the switched feed rules out. We have already come across one example in Section 5.4 that can be used over a ground plane. Other early examples were proved by Wickersham

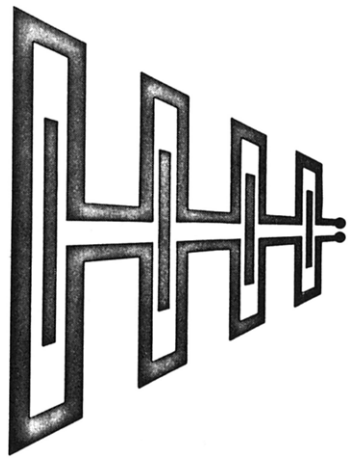

FIG. 5.28. Folded dipole array.

et al.[16,17]; one of these is illustrated in Fig. 5.27. It consists of a balanced line, made of two coplanar strips, which is capacitively coupled to transverse radiating strips. Examples of later designs are shown in Fig. 6.20[10] and Fig. 5.28.[9] The latter is entirely in one plane and therefore can also be used in the complementary form. It consists of a balanced line with folded dipoles directly coupled in series. In addition, a transverse element is placed inside the folded dipole to bring about the right phasing from one dipole to the next. The theory of unswitched designs is discussed in Chapter 6, but briefly it can be stated here that the basic principle is to make the phase shift per cell near the input much greater than it would be for free-space propagation. (*Very* near the input, this does not matter, because the elements are so small that radiation is negligible.) In other words, unswitched structures do not work unless they produce a very slow wave. One obvious way of accomplishing this is to coil the transmission line; this is the case in Fig. 6.20. The other examples can be thought of as delaying the wave by means of reactive loading in various forms.

The example chosen for discussion is shown in Fig. 5.29. It consists

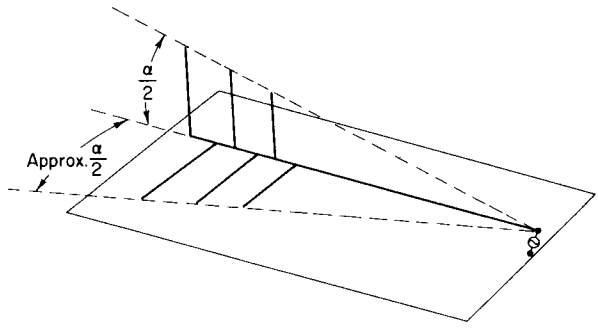

FIG. 5.29. Monopole array over a ground plane.

of vertical monopoles connected to a horizontal wire above a ground plane.[2] The requisite phase delay is provided by the horizontal stubs, which, being open at the end, act as capacitive loading at low frequency, that is, near the input. Where they are $\lambda/4$ long, the transmission line is short-circuited. This seems to leave no doubt that the structure can be truncated, yet the argument is not incontrovertible. That is why this particular example has been chosen for discussion, even though the design is reported to be more critical than some of the others men-

tioned. (On the other hand, there seems to be no reason why it should inherently be more critical.)

To bring out the point of interest we can argue as follows. Since the line is shorted where the stubs are $\lambda/4$ long, the active region must come before that. Now, in a voltage-standing-wave pattern the phase shifts by 180° on passing through a voltage zero and then stays constant until we come to the next zero. Hence the phase shift per cell in the shorted region is evidently 180°. Therefore, it must be less than 180° in the active region, and there the spacing between dipoles is less than $\lambda/10$. On working out the combination of contributions from two adjacent dipoles, it will be found that the direction of maximum radiation must be forward along the transmission line, whereas in fact it is backward. (Indeed the pattern is very much the same for all switched designs.) Moreover, frequency-independent operation is inconsistent with a forward beam, because the pattern must go to zero in all directions that would be occupied by the infinite structure. So the argument based on simple transmission-line theory must be false. The explanation is that radiation coupling between dipoles transmits power past the shorting stubs. As we shall see in Chapter 6, radiation coupling has the effect of making the loaded transmission line behave as a waveguide: the transmission-line mode is but one of an infinite number of modes which make up the current and voltage distributions on the loaded transmission line. It can be seen, then, that radiation coupling is an essential ingredient in all unswitched designs.

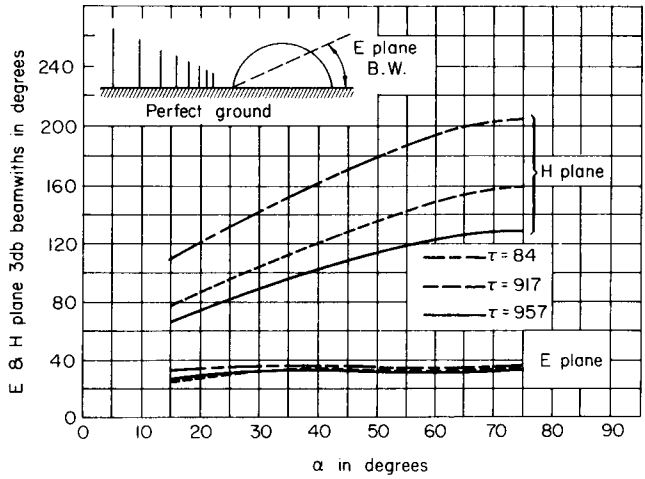

FIG. 5.30. Variation of beamwidth [after Ref. 2].

The patterns are similar to those of Section 5.6 for small α and for τ near unity, but for more rapidly expanding designs the directivity is significantly lower. Figure 5.30 shows the variation of directivity. The impedance characteristics are also similar to those of Section 5.6. The mean for the half-structure can be controlled between 20 Ω and 80 Ω by varying the characteristic impedance of the stubs. Apparently this does not greatly affect the patterns.

5.8 Directive Arrays

Arrays have been used to produce directive gain since the earliest days of antennas. The principle is simply to excite the elements of the array so that all radiate in phase in the desired direction. DuHamel and Berry[5] pioneered the extension of this principle to frequency-independent antennas. They used as elements the antennas described in Fig. 5.9, disposed in the *xy* plane as illustrated in Fig. 5.31, or with

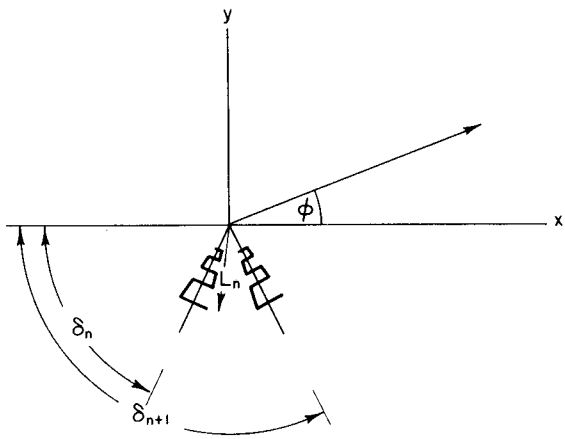

FIG. 5.31. Layout of array elements.

the plane of an element perpendicular to the *xy* plane. The elements are identical except for a variation of the characteristic length L_n, which is used to control the phase of the radiation from the nth element. Note that the positions of the elements are specified by the angles δ_n.

To illustrate the method of design, consider the pattern in the *xy* plane. It can be formulated as follows. Let e_n represent the radiated E

when all input currents I_n are zero except $I_n = 1$. Then the pattern of the array must be

$$E(\phi) = \sum_n I_n e_n(\phi) \tag{5.1}$$

For identical elements it is usually assumed that the "element patterns" e_n are identical, although this is at best an approximation.[13] So, approximately, identical elements give

$$e_n(\phi) = e_0(\phi - \delta_n + \delta_0) \tag{5.2}$$

However, the elements are not identical—the L_n's differ. As we saw in Section 5.1, this affects the phase. We can express the result like this. When the direction ϕ is within 30° of the axis of any element, the phase ψ_n of e_n approximately fits the formula

$$\psi_n(\phi) = \gamma_n + \psi_0(\phi - \delta_n + \delta_0) \tag{5.3}$$

where

$$\gamma_n = 2\pi \frac{\ln L_n - \ln L_0}{\ln \tau} \tag{5.4}$$

Finally, we see from Fig. 5.31 that

$$\psi_0(\phi) = -\frac{2\pi d_0}{\lambda} \cos(\phi - \delta_0) \tag{5.5}$$

where d_0 is the distance from the origin to the effective phase center of the element $n = 0$. The resulting formula for the pattern is then

$$E(\phi) = \sum I_n \mid e_0(\phi - \delta_n + \delta_0) \mid \exp\{j[\gamma_n - (2\pi d_0/\lambda)\cos(\phi - \delta_n)]\} \tag{5.6}$$

The method of feeding is constrained by the fact that all elements must terminate at the origin. There they must be connected in a way that provides a pair of input terminals. For optimum directive gain, it is further required that all I_n's be approximately equal. Thus for n even, half the elements can be connected to one terminal and the other half to the other terminal. The fact that this puts half the input I_n's out of phase with the other half can be counteracted simply by turning over half the elements. With this arrangement the direction of maximum gain is obviously along the line of symmetry, and therefore the L_n's (or γ_n's) are adjusted to make all elements radiate in phase along this line.

The basis for the phase rule (5.4) and the phase center is, of course, empirical. It was established by measuring the radiation from a single element fed against a rod which is aligned normal to the plane of the element. Thus the coaxial feed line runs down the central boom, as described in Section 5.4, and its inner conductor is connected to the center of the rod, which is about half a wavelength long. The radiation from the element alone can then be measured directly, because it is polarized perpendicular to that from the rod. In this way it was found that there was a reasonably well-defined phase center; that is, equiphase contours were approximately spherical, for observations over a 60° sector. Similarly, (5.4) was justified within 20°.

Many interesting arrays were developed in this way by DuHamel and Berry.[5] As a typical illustration we take an array of six elements disposed as in Fig. 5.31 but polarized orthogonal to the xy plane. The parameters were as given in Table II. The results are shown in Fig. 5.32 for two frequencies differing by the factor $\sqrt{\tau}$. The directivity is estimated to be between 16 and 17 db.

A different approach to array design is shown in Figs. 5.33 and 5.34.[15] The crosses represent dipole positions, which are fed with a transmission-

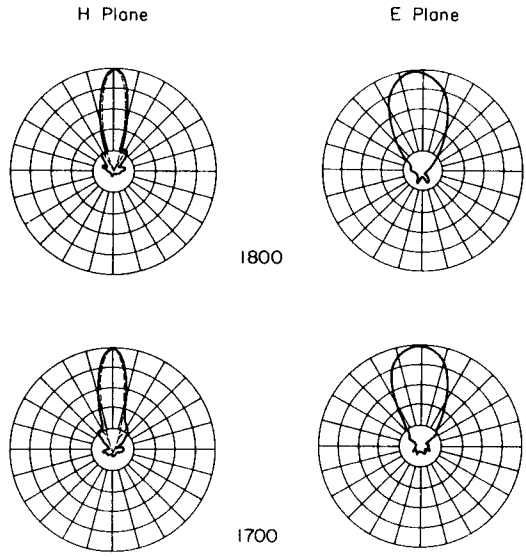

FIG. 5.32. Predicted (dashed line) and measured (solid line) patterns of six-element phased array [after Ref. 5].

TABLE II[a]

n	δ_n (deg)	γ_n (deg)
1	48	−184
2	64	−80
3	82	0
4	98	0
5	114	−80
6	132	−184

[a] $\tau = 0.885$, $\alpha = 9.5°$, $d = 1.95\ \lambda$, approx.

line structure which puts all four dipoles in one horizontal row approximately in phase. Thus one row by itself will produce the typical broadside-array pattern. The entire structure is evidently like the simple arrays

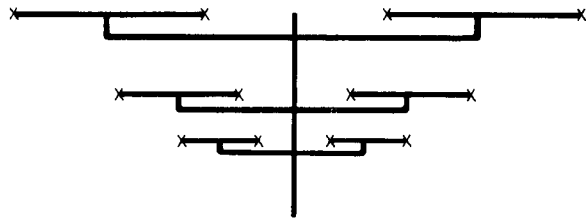

FIG. 5.33. Branched feed for broadside array.

of Sections 5.6 and 5.7, but with the broadside combination in place of a single dipole. Experiments on this approach have been carried out by using a ground plane as one conductor of the transmission line. The structures were fabricated from a 10-mil Teflon sheet coated on both sides with thin copper foil. One side formed the ground plane, and the transmission-line configuration was etched on the other side.

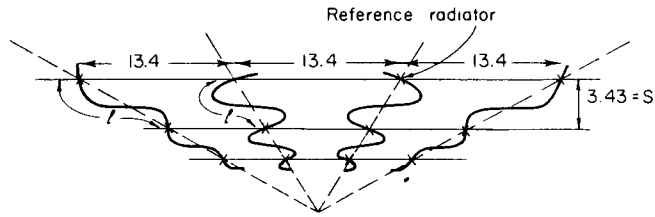

FIG. 5.34. Snake feed for broadside array.

The monopoles (half-dipoles) were soldered perpendicular to the sheet. Tests over many periods in the microwave range showed excellent frequency-independent operation. The snake form appeared to be less sensitive to errors of construction and proved to be the simpler to fabricate. Otherwise, the performance appeared to be the same. The pattern in the plane of the figure was typical of four elements spaced about one wavelength apart, except that the side lobes were at least 17 db down. In the orthogonal plane, the pattern is much like those for the corresponding structures in Sections 5.6 and 5.7. The specifications of a typical design for the snake type are: $-70\ \Omega$ characteristic impedance for all lines, length of reference radiator 3.35, diameter 0.18, spacing as in Fig. 5.34, with a geometric slowness factor l/s of about 1.9. Tests with other slowness factors show that good patterns are obtained when the spacing s for the quarter-wave elements is approximately $0.8\ \lambda\tau(1 + \tau)^{-1}$.

The advantage of this approach is, of course, that it gives excellent directional patterns from a simple design principle. The number of elements in a broadside combination is obviously not limited to four, but presumably there is a limit. When this number is very high, it will be seen that the slowness factor l/s has to be very high, because the outermost elements lie on a line which is almost perpendicular to the center line. Hence the limit.

REFERENCES

1. Bell, R. L., C. T. Elfving, and R. E. Franks, *IRE Trans.* **AP-8**, 559–566 (1960).
2. Berry, D. G., and F. R. Ore, *IRE Intern. Conv. Record* **1961**, Pt. I, 76–85.
3. Carr, J. W., *IRE Trans.* **AP-9**, 229 (1961).
4. Carrel, R. L., *IRE Intern. Conv. Record* **1961**, Pt. I, 61–75; also Ph.D. thesis, Univ. Illinois, Urbana, Illinois, 1961.
5. DuHamel, R. H., and D. G. Berry, *IRE Wescon Conv. Record* **1958**, Pt. 1, 161–174.
6. DuHamel, R. H., and D. E. Isbell, *IRE Intern. Conv. Record* **1957**, Pt. I, 119–128.
7. DuHamel, R. H., and F. R. Ore, *IRE Intern. Conv. Record* **1958**, Pt. I, 139–151.
8. Elfving, C. T., *IRE Wescon Conv. Record* **1961**, Pt. I.
9. Greiser, J. W., *Proc. IEEE*, **52**, 617–618 (1964).
10. Greiser, J. W., and P. E. Mayes, *Trans. IEEE* **AP-12**, 281–290 (1964).
11. Isbell, D. E., *Univ. Illinois Antenna Lab. Rept.* 30, Urbana, Illinois, 1958.
12. Isbell, D. E., *IRE Trans.* **AP-8**, 260–267 (1960).
13. Hines, J. N., V. H. Rumsey, and T. E. Tice, *Proc. IRE* **42**, 1262–1267 (1954).
14. Mayes, P. E., and R. L. Carrel, *IRE Wescon Conv. Record* **1961**, Pt. I.
15. Mei, K. K., M. Moberg, V. H. Rumsey, and Y. S. Yeh, *Trans. IEEE* **AP-13**, 807–809 (1965).
16. Wickersham, A. E., *Proc. IRE* **48**, 794–795 (1960).
17. Wickersham, A. F., R. E. Franks, and R. L. Bell, *Proc. IRE* **49**, 378 (1961).

6

THE PERIODIC STRUCTURE APPROACH

6.1 Log-Periodic Structures as Gradually Expanding Periodic Structures

Although the geometric principle governing log-periodic antennas is very simple, no simple theory for the fields which they radiate has yet been found. Even the problem of a log-periodic transmission line has proved to be quite difficult, and this is but the first step toward a solution of the field-theory problem. So we are led to consider the log-periodic structure as if it were locally part of a periodic structure. Obviously this is not a valid approximation unless the expansion parameter τ is very near unity. However, this approach has proved to be more successful than might consequently be expected. Not only does it admit the application of periodic structure theory, which has been highly developed, but it suggests practical log-periodic antennas on the basis of established periodic designs.[2,4,5,7,11,12]

To illustrate the approach, consider an array of dipoles connected at constant spacing along a uniform transmission line. In view of the perfect periodicity of the structure, there will evidently exist traveling-wave solutions, that is, solutions with constant phase shift β and attenuation α per period or cell. Thus we may speak of the modes of the periodic waveguide. Now if there were no coupling by radiation between the dipoles, there would be only one mode (or more precisely one forward and one backward). Of course, there is radiation coupling between dipoles, but still, for a single mode, all dipoles have the same effective inpedance. Note, however, that this impedance changes with the mode;

that is, it now depends on α and β. As we shall see in Section 6.2, this means that many modes are now possible. The analysis is then immensely more complicated, just as waveguide theory is more complicated than transmission-line theory. For example, it is very difficult to estimate how much of each mode will be generated in the tapered structure just as it is for a tapered waveguide section. The situation is not quite as bad as in the waveguide case, because radiation coupling between distant dipoles can be ignored, thus reducing the problem to a finite number of modes. Even so, the rigorous formulation of radiating periodic structure theory is barely practical. Consequently, much of this chapter will be limited to single-mode theory.

6.2 Circuit-Theory Approach to Periodically Loaded Transmission Lines

We begin with a specific example to make clear the physical effects which need to be taken into account, namely, a uniform transmission line periodically loaded with dipole antennas in shunt (see Fig. 6.1).

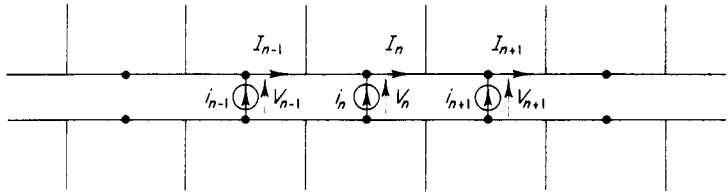

FIG. 6.1. Experiment for formulating propagation factor.

This kind of periodic structure is essentially different from that which is commonly treated, because of the coupling by radiation between dipoles. A network-theory approach taking radiation coupling into account has been worked out by Carrel[1] (for the log-periodic case) and by Mittra and Jones[6] (for the uniformly periodic case); for our present purposes a somewhat different approach will be used.

The notation is defined in Fig. 6.1. The transmission-line current and voltage are represented by I_n and V_n at the input to the nth cell or period. The terminals of a cell can be positioned wherever convenient; they are shown midway between dipoles only to make the figure clear. The structure is excited by the shunt current sources i_n. They would

be zero when the structure is fed from one end (except for that end). The reason for introducing them is that we can write a system of equations for every n of the form

$$i_n = A_0V_n + A_1V_{n+1} + A_{-1}V_{n-1} + A_2V_{n+2} + A_{-2}V_{n-2} + \cdots \quad (6.1)$$

The coefficients A_1, A_1, A_{-1}, ..., are the same for all n because the structure is periodic. Their physical significance is illustrated in Fig. 6.2,

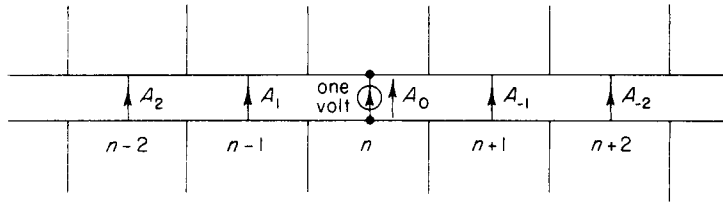

FIG. 6.2. Physical significance of admittance coefficients A_n.

which is constructed directly from the definition (6.1). For example, putting all $V_j = 0$ except V_n shows that A_0 is the input admittance with all except the nth terminals shorted, and, for the same case, (6.1) applied to i_{n+1} shows that A_{-1} is the short-circuit current at $n + 1$ for a 1-volt input at n, as shown in Fig. 6.2. Now, by the reciprocity theorem, if we interchange the unit voltage source at n with the short circuit at $n + 1$, the resulting short-circuit current at n is A_{-1}. But such a shift of the source by one period must simply reproduce Fig. 6.2 with all currents shifted up one period, which puts A_1 through the short circuit at n. Hence $A_{-1} = A_1$ if the system is reciprocal, and so $A_{-n} = A_n$:

$$i_n = A_0V_n + A_1(V_{n+1} + V_{n-1}) = A_2(V_{n+2} + V_{n-2}) + \cdots \quad (6.2)$$

We see from Fig. 6.2 that A_2 would be zero unless power is transmitted past the short circuits at $n - 1$ and $n + 1$. This shows what a difference radiation coupling makes. Without it all $A_i = 0$, except A_0 and A_1. Note also the practical example of transmission past a short circuit which we came across in Section 5.7.

A mode of the structure is defined for all $i_n = 0$ by the condition that the voltage (or current) distribution over all periods be the same apart from a constant.

Thus

$$V_n = fV_{n+1} \tag{6.3}$$

for all n with f fixed. Substitution in (6.2) gives

$$0 = A_0 + A_1(f + f^{-1}) + A_2(f^2 + f^{-2}) + \cdots \tag{6.4}$$

If there is no radiation coupling, we have a simple quadratic for f:

$$0 = A_0 f + A_1(f^2 + 1) \tag{6.5}$$

In either case we see that if f is a root, so is f^{-1}. Now, if we put

$$f = e^{\gamma} = e^{\alpha + j\beta} \tag{6.6}$$

we can call α and β the attenuation and phase shift per cell. Then we see that if f represents a forward wave, f^{-1} represents the corresponding backward wave, having the same propagation factor. Thus counting both solutions $\pm\gamma$ as one mode, without radiation coupling only one mode exists, but with it an infinite number exist.

Considering the experiment illustrated by Fig. 6.2, we see that as n becomes large it is reasonable to assume that the A_n's will conform to a traveling wave; that is,

$$A_{n+1} = RA_n \tag{6.7}$$

with R fixed. If we apply this to $n > i$, (6.4) becomes

$$0 = A_0 + \sum_{l=1}^{i+1} A_l(f^l + f^{-l}) + RA_{i+1}[f^{i+1}(1 - Rf)^{-1} + f^{-i-1}(1 - Rf^{-1})^{-1}] \tag{6.8}$$

assuming $|Rf| < |$ and $|Rf^{-1}| < |$ (which is evidently justified on physical grounds because we cannot have a growing wave). This gives a finite number of modes, $L + 1$. Judging from experience with traveling-wave structures, it looks as though $L = 2$ or 3 would be a reasonable approximation, in which case comparatively few modes would suffice. We have already seen, however, that the problem is to decide how much of each mode would be present.

For an individual mode we can define forward- and backward-looking characteristic impedances Z_{0+} and Z_{0-} by the standard formula $V_+ = Z_{0+}I_+$, V_+ and I_+ being the voltage and current at the input of a cell when there is a pure forward wave. Again we must be careful about the physical significance. For example, we shall not get Z_0 at

the input of an isolated cell whose output is terminated by Z_0, because isolation of the cell eliminates radiation coupling. We can, however, recover this familiar result by replacing the dipole with its equivalent impedance, as seen by the mode in question.

A simple formula for Z_0 can be derived by considering the experiment shown in Fig. 6.3. All cells are terminated with short circuits. Equal

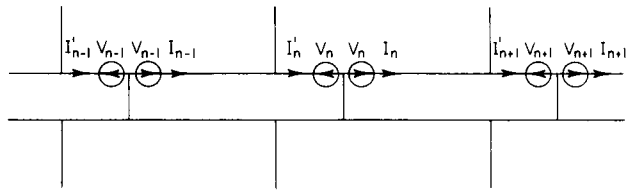

FIG. 6.3. Experiment for formulating characteristic impedance.

and opposite voltage sources V_n are put against the short circuits as shown. Clearly, this establishes continuity of voltage and reproduces the distribution of $\{V_n\}$ and $\{I_n\}$ shown in Fig. 6.1. In this case we write

$$I_n = C_0 V_n + C_1 V_{n+1} + C_{-1} V_{n-1} + \cdots \tag{6.9}$$

$$I_n' = C_0' V_n + C_1' V_{n+1} + C_{-1}' V_{n-1} + \cdots \tag{6.10}$$

The physical significance of the C_n's is shown in Fig. 6.4. We see that

$$C_n - C_n' = A_n \tag{6.11}$$

On putting (6.3) in (6.9), we get for the characteristic admittance

$$Y_{0\pm} = \sum_{n=-\infty}^{\infty} C_n f^{\pm n} \tag{6.12}$$

f having been found from (6.4), and the C_n's being found by solving

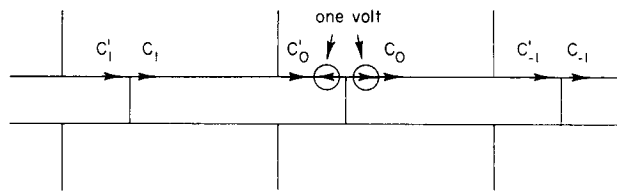

FIG. 6.4. Physical significance of admittance coefficients C_n.

the problem of Fig. 6.4. When there is no radiation coupling, this reduces to the simple form

$$Y_{0\pm} = C_0 + C_1 f^{\pm 1} \tag{6.13}$$

Note that the C_n are pure imaginary for a lossless system. Consequently, if f is real, Y_0 is pure imaginary.

The general formulas for the distribution of current and voltage can now be expressed in terms of the forward and backward modes at n as follows:

$$I_n = \sum_{\text{all modes } m} (I_{m+} + I_{m-}) = \sum_m (Y_{0m+} V_{m+} - Y_{0m-} V_{m-}) \tag{6.14}$$

$$V_n = \sum_m (V_{m+} + V_{m-}) = \sum_m (Z_{0m+} I_{m+} - Z_{0m-} I_{m-}) \tag{6.15}$$

$$I_{n+l} = \sum_m (f_m{}^l I_{m+} + f_m^{-l} I_{m-}) = \sum_m (Y_{0m+} f_m{}^l V_{m+} - Y_{0m-} f_m^{-l} V_{m-}) \tag{6.16}$$

$$V_{n+l} = \sum_m (f_m{}^l V_{m+} + f_m^{-l} V_{m-}) = \sum_m (Z_{0m+} f_m{}^l I_{m+} - Z_{0m-} f_m^{-l} I_{m-}) \tag{6.17}$$

The added subscript m is needed to distinguish the different roots of (6.4).

6.3 Conditions for Attenuation of the Current Distribution

As a simple illustration let us consider application of Section 6.2 to a transmission line loaded with an admittance Y every s meters. First we have to choose where to put the boundaries of a cell. Considering Fig. 6.2, it is clear that the evaluation of A_n is easiest if we take the cell boundaries right next to Y, as illustrated in Fig. 6.5. Note that the choice

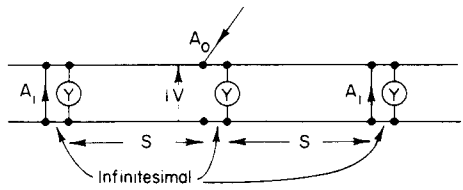

FIG. 6.5. Choice of position for cell boundary.

of cell boundary makes a considerable difference even for the present rudimentary case, which reduces to the circuit shown in Fig. 6.6. Putting

$$\theta = 2\pi s/\lambda \tag{6.18}$$

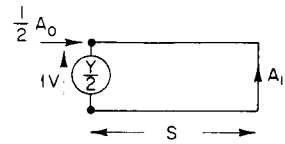

FIG. 6.6. Determination of A_0 and A_1.

and Y_{00} = characteristic admittance of transmission line, we have

$$A_0 = Y - 2jY_{00} \cot \theta \tag{6.19}$$

$$A_1 = jY_{00} \csc \theta \tag{6.20}$$

Thus (6.5) gives

$$\cosh \gamma = \cos \theta + \frac{jY \sin \theta}{2Y_{00}} \tag{6.21}$$

To take the simplest of all cases, suppose Y represents a capacitor. Then (6.21) becomes

$$\cosh \gamma = \cos \theta - C\theta \sin \theta \tag{6.22}$$

the real constant C being proportional to the capacity and θ being proportional to the size of the cell. Note that γ is pure imaginary if the right side of (6.22) is between ± 1, but pure real otherwise. Evidently, then, γ gives phase shift with no attenuation if the size (or frequency) θ is small enough, but above a certain size θ_c there is attenuation. This simple example is no doubt familiar in another connection as a low-pass filter: it has also an infinite series of pass bands at higher frequency. We see then that, above a certain size, the current distribution is attenuated, and so the structure can be truncated, even when it is perfectly lossless. For the log-periodic structure this means that the current will be attenuated beyond the point where $\theta = \theta_c$, as suggested in Fig. 6.7.

Note that as θ increases from 0 to θ_c, γ increases from $j0$ to $j\pi$ (see Eq. (6.22), for example). Thus at θ_c the phase shift per cell is π. Note that this is what we saw in Chapter 5 was characteristic of the active region for dipole arrays and zigzag wire structures, empirically and theoretically. Here, then, is another significant connection between periodic structure theory and log-periodic antennas.

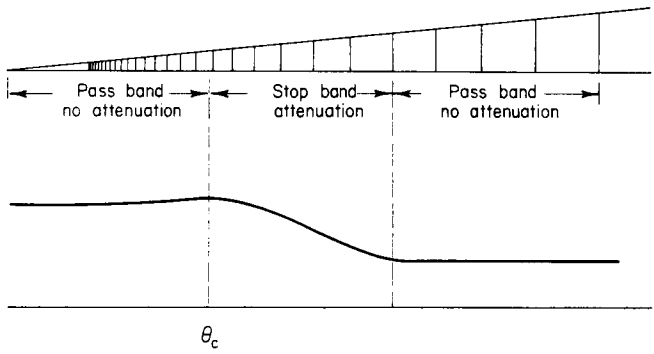

FIG. 6.7. Application of periodic structure theory to log-periodic case.

Extending this to the case of dipole loading, we have then complex Y and, consequently, complex γ. If the real part of Y/Y_{00} is small, it is plain that the essential features of the pass and stop bands still obtain; the effect of resistance is merely to smooth out the abrupt change from no attenuation to no phase shift. That is what we may expect, then, for a frequency-selective dipole below resonance. On resonance the resistive part may dominate, and then strong attenuation results from a quite different cause. Note, however, that because of radiation coupling, the resistance on resonance may be negligible; this is the case when the phase shift along the structure corresponds to a wave moving slower than the velocity of light. In summary then, the stop-band effect is an important factor in causing attenuation of the current distribution on log-periodic structures. If it were not for the multimode effect of radiation coupling, we could say that it ensures eventual attenuation. Even with multimode operation, each mode will have its stop bands, and so each must eventually be attenuated, unless the conversion (due to expansion) from one mode to another just happens to avoid all stop bands.

For the slowly expanding log-periodic structure, the impedance seen at the origin can be estimated from the characteristic impedance of the corresponding periodic structure. The formula for it is (6.12) or (6.13). For small θ (corresponding to conditions near the origin), we are in the pass band, f is complex, of unit magnitude, and so Y_0 is complex. Its value depends on the choice of reference point or cell boundary, whereas f does not. Farther away from the origin, where the structure is large enough to put it in the stop band, Y_0 could be pure imaginary if the effective dipole impedance were pure imaginary. Thus if the stop band

is significant and the preceding pass band is nearly lossless, the input impedance will be nearly all reactive. Obviously this is something to avoid. It will be avoided if significant radiation occurs before or in the stop band. We shall see shortly that the switched type of array (Fig. 5.15) tends to give strong radiation before the stop band, but not the unswitched. Consequently, it can be expected that it will be more difficult to find unswitched designs which give a good input impedance, although, once found, such designs are not necessarily more critical.

So far we have considered only shunt capacitive loading. As to other forms of loading, we can dismiss series capacitance and shunt inductance at low frequencies, because Z_0 is then an open or short circuit, respectively. Series impedance Z gives

$$\cosh \gamma = \cos \theta + \frac{jZ}{2Z_{00}} \sin \theta \tag{6.23}$$

rather than (6.21). When Z is an inductor L, this gives (6.22) again with L in place of C. Thus from the point of view of γ, there is no essential difference between series inductance and shunt capacitance. The difference with respect to Z_0 is evidently that Y affects Y_0 as Z affects Z_0. So if shunt capacity raises Y_0, series inductance raises Z_0 in the same relation.

Having found that capacitive and inductive loading are essentially the same in their effect on γ, let us use (6.22) to work out the effect of loading on phase velocity. Putting $\gamma = \alpha + j\beta$ for frequencies below θ_c, we have

$$\cos \beta = \cos \theta - C\theta \sin \theta \tag{6.24}$$

from which it is clear that $\beta > \theta$ if $\theta < \pi/2$; in fact, $\beta > \theta$ if $\theta < \theta_c$. The effect of loading is therefore to increase the phase shift per cell for small cells, specifically for $\theta < \theta_c$. In other words, the phase velocity (measured along the transmission line) is slower than when unloaded. Series capacitive and shunt inductive loading increase the phase velocity. As we have seen, such loading is impractical at low frequencies, but it does come into play at higher frequencies.

The types of log-periodic structure shown in Figs. 6.8 and 6.9 can be illustrated by the periodic structure whose typical cell is shown in Fig. 6.10. It can be analyzed in terms of the even and odd modes on the folded dipole. They are represented as shown by $(v_1 i_1)$ and $(v_2 i_2)$, respectively. The transmission-line voltages and currents are $V_1 I_1$ just to the left and $V_2 I_2$ just to the right of the folded dipole.

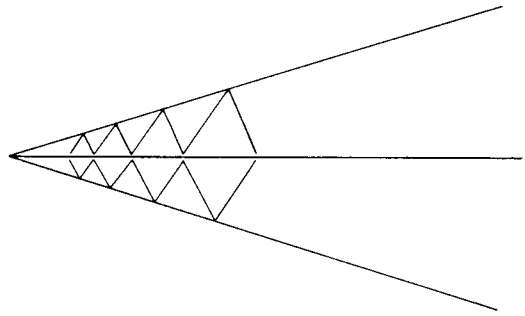

FIG. 6.8. Expanding zigzag structure.

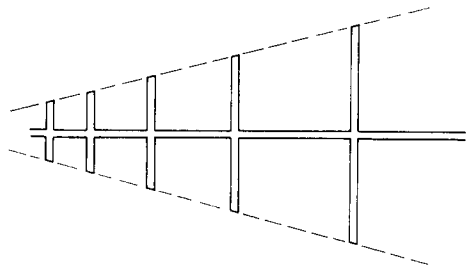

FIG. 6.9. Expanding folded-dipole structure.

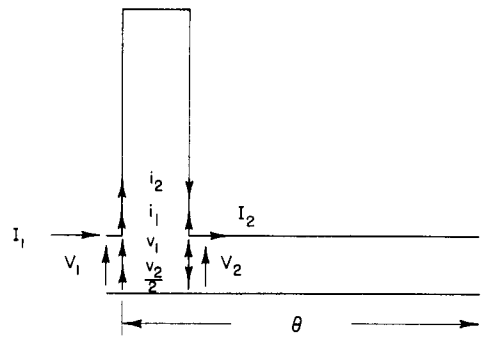

FIG. 6.10. Currents and voltages on folded-dipole structure.

Thus

$$I_1 = i_1 + i_2 \qquad V_1 = v_1 + \tfrac{1}{2}v_2 \tag{6.25}$$

$$I_2 = i_2 - i_1 \qquad V_2 = v_1 - \tfrac{1}{2}v_2 \tag{6.26}$$

We introduce the susceptance B of the odd mode:

$$jBv_2 = i_2 \tag{6.27}$$

and the dipole admittance Y of the even mode:

$$Yv_1 = 2i_1 \tag{6.28}$$

Using θ for the electrical length of the unloaded cell as before, we get

$$\cosh \gamma = \frac{(8jB + Y)\cos\theta + 2(2j - BY)\sin\theta}{8jB - Y} \tag{6.29}$$

with $Z_{00} = 1$, and Y the effective dipole admittance for the mode.

6.4 Connection with Radiation from Dipole Arrays

Figures 6.11 and 6.12 show two typical uniformly periodic dipole arrays. In the second, the phase of alternate dipoles is reversed. Suppose that they are excited so that only the forward wave I_+e^{γ} exists. Consider the radiation field produced in a direction making an angle ψ with the forward direction (the x axis). In the unswitched case, Fig. 6.11, the

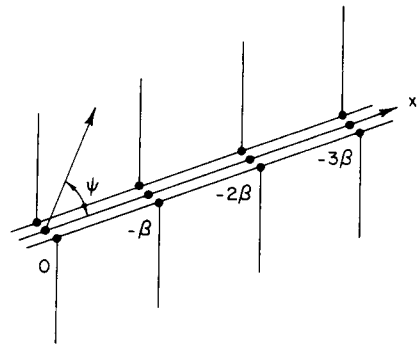

FIG. 6.11. Phasing for unswitched dipole array.

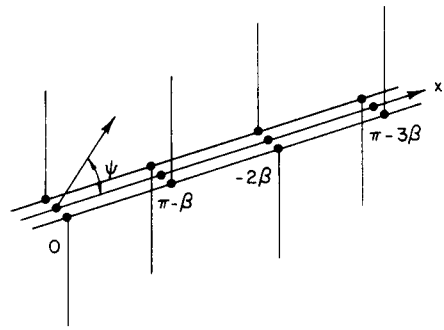

FIG. 6.12. Phasing for switched dipole array.

phase difference between adjacent dipole currents is β. Thus ψ_m is the direction of maximum radiation if

$$\beta = K \cos \psi_m \tag{6.30}$$

$K = 2\pi d/\lambda$ and d being the spacing in radians and in meters, respectively. For the switched case (Fig. 6.12), the relation is

$$K \cos \psi_m = \beta - \pi \tag{6.31}$$

Now K is what the phase shift per cell would be for free-space propagation. Thus $K \leqslant \theta$ (defined in 6.18), for $\theta < \theta_c$ and $\theta < \beta$. So

$$K < \beta \tag{6.32}$$

This means that ψ_m is pure imaginary in (6.30) but (6.31) can be solved by real ψ_m if

$$\beta < K + \pi \tag{6.33}$$

To understand this result, we first work out the pattern of $n + 1$ elements of the unswitched dipole array. The pattern is expressed as the product of the dipole pattern and the array factor, whose magnitude is

$$\frac{\sin (n/2)(\beta - K \cos \psi)}{\sin (1/2)(\beta - K \cos \psi)} \tag{6.34}$$

If β were K, the maximum would occur at $\psi = 0$ and its value would be n. If β is slightly greater than K, the maximum still occurs at $\psi = 0$,

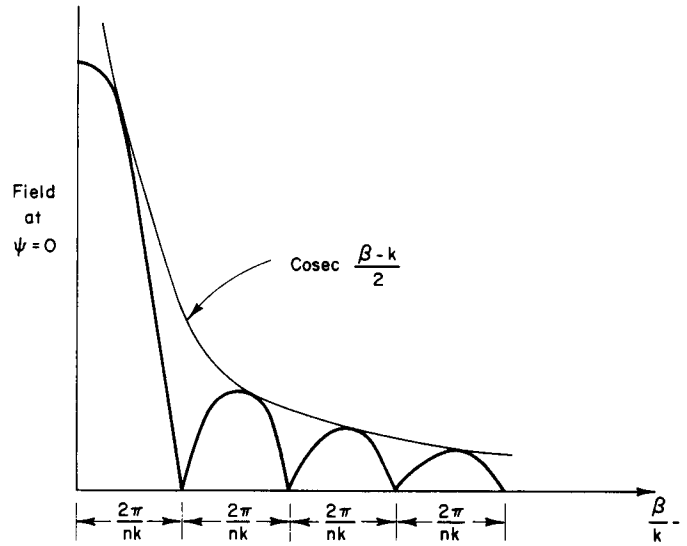

Fig. 6.13. Field radiated in direction of axis for various phase velocities K/β.

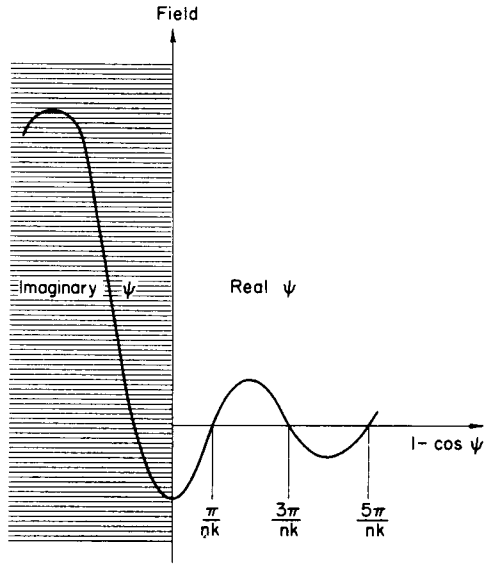

FIG. 6.14. Pattern of uniform n-element array with $\beta = K + 3\pi/n$.

but its value is less than n. The field at $\psi = 0$ for various phase velocities K/β is illustrated in Fig. 6.13. A typical pattern is illustrated in Fig. 6.14 for the case $\beta = K + 3\pi/n$. Thus the fact that (6.30) gives imaginary ψ_m does not mean there is no radiation. It means the radiation is less than it would be for real ψ_m, and there is no well-defined direction of maximum radiation. As we can see from Fig. 6.14, the maximum radiation occurs near $\psi = 0$, but its magnitude is nearly the same as succeeding maxima. It is about one-fifth of what it would be for $\beta \leqslant K$ and its beamwidth is about half that for $\beta = K$. When n and β become very large, we do approach the condition of no radiation. But for the application to log-periodic structures, n is not large unless the rate of expansion is impractically slow.

Turning now to the switched case represented by (6.33) in place of (6.34) we have, for the array factor,

$$\frac{\cos nu}{\cos u} \qquad \text{if } n \text{ is odd} \tag{6.35}$$

$$\frac{\sin nu}{\cos u} \qquad \text{if } n \text{ is even} \tag{6.36}$$

with

$$u = \tfrac{1}{2}(\beta - K\cos\psi) \tag{6.37}$$

The distribution with respect to u about the maximum is not much different from (6.34); there are some minor differences in beamwidth and in the ratio of first to second maximum. In short Fig. 6.13 gives a fair idea of the distribution in this case also, with the maximum at $u = \pi/2$. The big difference is in the variation with frequency, or spacing of the dipoles, both of which are represented by K. Suppose that $K = \theta$ and that K is small. Then (6.22) gives

$$\beta \simeq \theta(1 + 2C)^{1/2} \tag{6.38}$$

On putting this in (6.31) we find that ψ_m is imaginary unless

$$K_2 = \frac{\pi}{(1 + 2C)^{1/2} - 1} \geqslant K \geqslant \frac{\pi}{(1 + 2C)^{1/2} + 1} = K_1 \tag{6.39}$$

Thus for sizes smaller than K_1 the radiation is comparatively low and dispersed among many nearly equal maxima. At $K = K_1$ it is strong and beamed in the backward direction $\psi = \pi$. As K is increased from K_1 to K_2 the radiation remains equally strong and the direction of the

beam turns toward the forward direction $\psi = 0$. However at $\psi = \pi/2$, $\cos\psi = 0$. Therefore, $\beta = \pi$ and $K = \theta = \theta_C = K_C$. So the stop band comes before K reaches K_2. If n were infinite, this would mean the beam would turn no further than the broadside direction $\psi = \pi/2$. So for a finite array we can expect a well-defined beam turning from backward ($\psi = \pi$) to broadside ($\psi = \pi/2$) as K increases from K_1 to K_C, then changing to a poorly defined beam for $K > K_C$. This is of course only a rough estimate based on the postulate that loading due to radiation is negligible, and that the dipoles operate below resonance for all K involved. But still it comes close to explaining the actual behavior of practical designs.

A minor point remains to be cleared up—that addition of 2π to β makes no difference to the physical interpretation. Generally, we can subtract $2N\pi$ from β in (6.30) and (6.31), thus admitting many more solutions that are physically distinct. The result is that ψ is real in (6.30) if

$$2N\pi + K > \beta > 2N\pi - K \tag{6.40}$$

and in (6.31) if

$$(2N + 1)\pi + K > \beta > (2N + 1)\pi - K \tag{6.41}$$

It is not difficult to see that these require $\beta > K_C$, except for the case already considered when $N = -1$. So these solutions do not come into play in the range of small K.

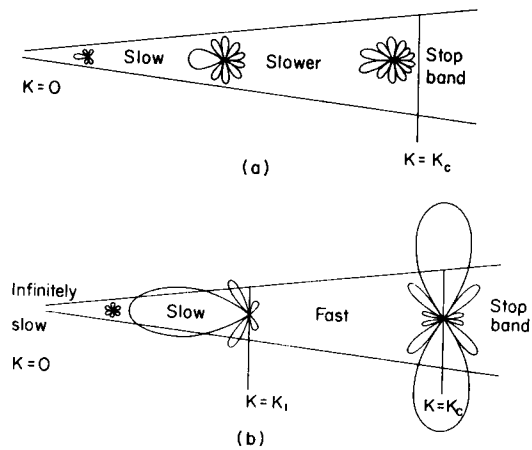

FIG. 6.15. Indication of radiation pattern for unswitched (a) and switched (b) structures with infinitesimal coupling.

The application of these results to log-periodic arrays is illustrated in Fig. 6.15. We see that the switched type can produce a reasonably well-formed beam in the backward direction if attenuation effectively exhausts the power in the transmission line while the phase velocity is still near the velocity of light, that is, while θ is near θ_1. The unswitched case, however, shows poor prospects of a well-formed beam unless power can be fed through the first stop band. This, no doubt, is why the first experiments with unswitched types were not successful. Once more it must be emphasized that this is only a rough indication of how log-periodic structures behave: for example, the idea of a stop band becomes untenable when a large amount of power is radiated per cell.

6.5 Dispersion Diagrams

The foregoing part of this chapter gives some idea of how frequency affects periodic structures and how they radiate. With this as background we can now turn to the interpretation of dispersion diagrams,[8–11] which are simply graphs of frequency K versus phase shift β per cell. As a start, let us examine the case of a uniform lossless transmission line periodically loaded with capacitors. To bring in radiation effects we can think of the capacitors as a first approximation to dipoles, as was done in Section 6.3. The formula in question is then

$$\cos \beta = \cos K - CK \sin K$$

It gives the diagram shown in Fig. 6.16, for a typical value of the loading capacitance C. The graph is periodic in β, so that the range $-\pi \leqslant \beta \leqslant \pi$ is sufficient. The first stop band, where $\gamma = \alpha + j\beta$ has the form $\alpha + j\pi$, is thus represented by the vertical line $\beta = \pi$ between $K = K_c$ and $K = \pi$.

Because we do not change the formula by reversing the sign of β, the graph is symmetric about $\beta = 0$. For a matched (or infinite) structure fed at one end, only one of the two possible β's for given K is physically correct, namely, that which corresponds to power flow away from the source. Usually this is given by the "group velocity" $d\omega/d\beta$, or $dK/d\beta$ in our case, which is a measure of the speed of a pulse of current traveling along the structure. Because the shape of the pulse changes as it travels along, the meaning of its speed is more or less arbitrary; for example, the speed of the point of maximum current is different from that of the

mean current. The distortion, or dispersion of different frequencies, is due to the fact that α and β depend on K. Consequently, the group velocity is not an infallible guide, especially in connection with periodic structures; the power flow is. In the present simple case the correct solution is the portion of the graph with positive slope, which is shown in Fig. 6.16 as a continuous line.

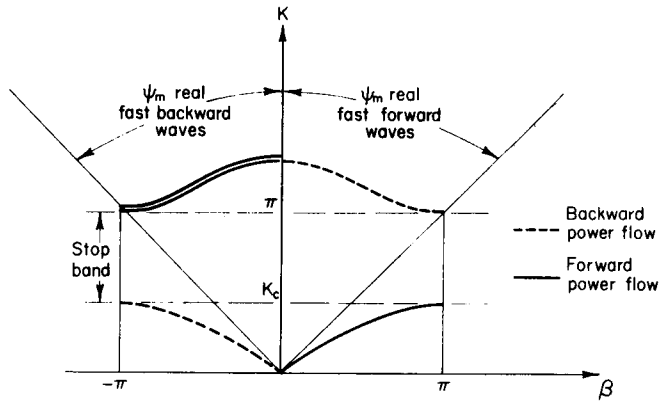

FIG. 6.16. Dispersion curve for capacitive loading.

The angle of maximum radiation ψ_m discussed in Section 6.4 is real when $K \geqslant |\beta|$. Thus ψ_m is real above the 45° lines in the $K\beta$ diagram, as shown in Fig. 6.16. According to the discussion in Section 6.4, this is then the region where good radiation patterns are expected. It is indicated by a double line in the figure, and it is not reached until we have passed through the first stop band.

The switched case is graphed in Fig. 6.17. It is essentially a repetition of Fig. 6.16 but shifted by half a period in β. In this case we take β to be the phase shift of dipole current in passing from one dipole to the next. Strictly speaking, this is not the phase shift in one cell but in half a cell, but then K is the length of half a cell, so the shape of the graph remains the same. It shows immediately that the switched structure gives a fast backward wave (real ψ_m) before the first stop band.

The example of capacitance loading is extremely idealized, of course, although it does give valuable indications. The first step toward a realistic case is the inclusion of radiation resistance. This gives complex γ at all frequencies, and under these circumstances a graph of only β gives a one-sided picture of what is happening to γ. A complete picture

is obtained by plotting the locus of a point which moves with K in the complex cosh γ plane. In this plane the lines $\alpha =$ constant are ellipses with foci at ± 1 and the lines $\beta =$ constant are the orthogonal hyperbolas. Thus one advantage of this plot is that an increase of 2π in β

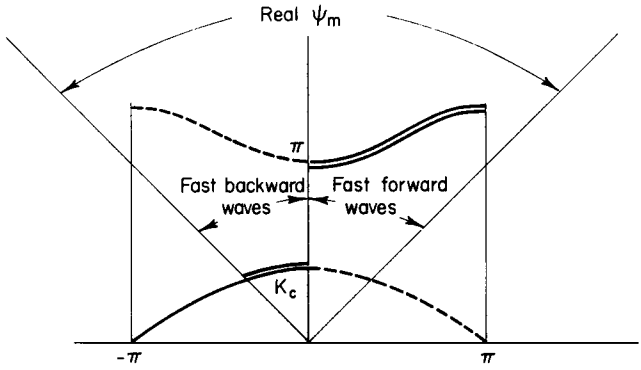

FIG. 6.17. Switched structure gives real ψ_m before the stop band.

automatically comes back to the same point. To illustrate how it works, the case for combined capacitance jKY_{00} and conductance $2Y_{00}$ has been plotted in Fig. 6.18. As the purely capacitive case is approached, the curve shrinks onto the real axis. Then the pass band is represented by

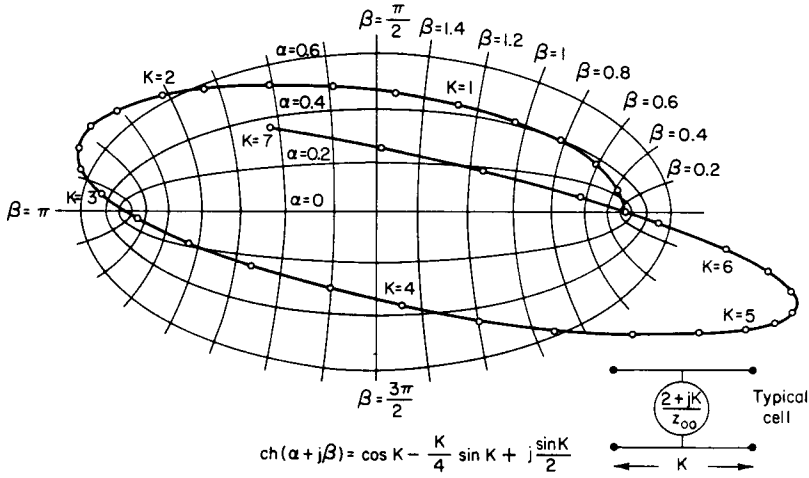

FIG. 6.18. Frequency characteristic for lossy capacitive loading.

the portion between the foci, and the stop band by what is outside. A typical plot for dipole loading (ignoring mutual impedance) is shown in Fig. 6.19. The fast-wave region is shown by a double line. It will be

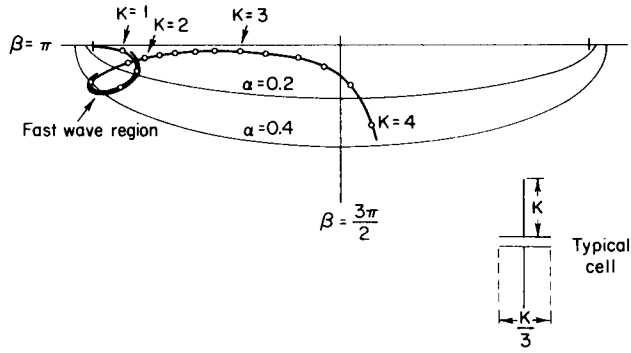

FIG. 6.19. Frequency characteristic for dipole-loaded 50-Ω switched line calculated without mutual.

seen that the attenuation increases rapidly and β changes slowly after the beginning of the fast-wave portion, which is the condition needed for a good frequency-independent pattern.

6.6 Bent Zigzag Antenna

The basic form of the antenna is shown in Fig. 6.20.[3] It consists of a continuous wire above a horizontal ground plane and is therefore an unswitched structure. It has been picked out for inclusion in this chapter because it is a good example of how periodic structure theory can be used to arrive at practical designs.

A cell consists of the combination of a radiating element and a delay line; the former lies in the vertical plane $y = 0$ and the latter lies in the plane $x = z \tan \xi$. The thickness of the wire should be in proportion to the distance from the origin, of course, thus ensuring among other things that the delay line has uniform characteristic impedance. This particular configuration was adopted to fit the requirements for construction in the HF band: it can easily be suspended above the earth on poles.

In this case it turns out that a good estimate of practical performance is obtained by assuming that the phase velocity along the wire is c. Although this ignores the periodic effect, it is in fact reliable for essentially all wire structures, and is surprisingly justified by some exact solutions of Maxwell's equations, as we shall see in Chapter 8. The dispersion curve is accordingly the straight line

$$\frac{\beta}{K} = \left[1 + \left(\frac{1+\sqrt{\tau}}{1-\sqrt{\tau}}\right)^2 \tan^2 \alpha\right]^{1/2} \tag{6.42}$$

taking the case $\alpha_E = \alpha_S = \alpha$ for simplicity. Typically this slowness factor is in the range 4 to 16.

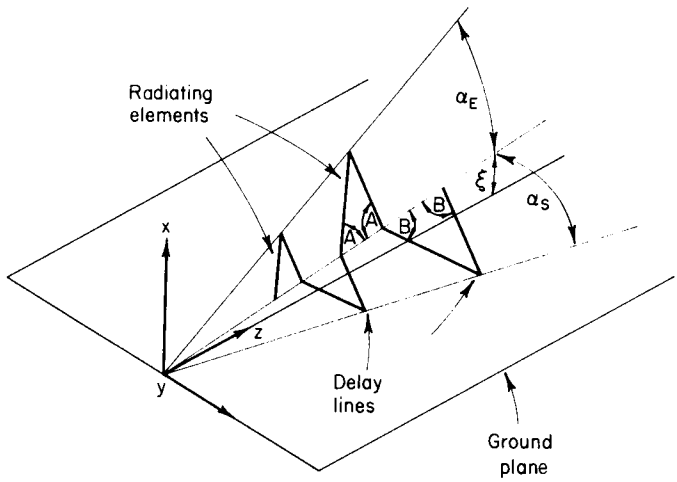

FIG. 6.20. Bent zigzag antenna.

As we saw in Fig. 6.5 we can associate with any region of a log-periodic structure the direction of maximum radiation represented by ψ_m. Near the origin ψ_m is imaginary, corresponding to a slow wave, at K_1 we have $\psi_m = \pi$ corresponding to a backward wave with the velocity of light, and at K_c we have $\psi_m = \pi/2$ corresponding to infinite phase velocity. For each cell we can calculate ψ_m from the formula

$$K \cos \psi_m = \beta + 2n\pi \tag{6.43}$$

But of course it would be absurd to conclude that each cell produces

its own individual beam in the direction ψ_m because the typical cell contains only one radiator. What we can say is that if β changes slowly with cell number, the group of cells in the vicinity of the jth cell will produce a beam approximately in the direction of ψ_m for the jth cell. For the purpose of definition, let j denote the cell which is nearest to $\lambda/4$ high. Roughly speaking, this is where we expect the strongest radiation and consequently the dominant ψ_m, provided ψ_m is real. Thus the design procedure would be to measure the pattern of a trial design constructed according to these rough ideas, analyze the results, and apply the same approximation to estimate what is needed to improve the design. Let us look at a specific example to see how this works.

First note that with the high values of slowness factor involved, first real values of ψ_m occur when $n = -1$ in (6.43). Having settled the value of n, (6.42) and (6.43) can be applied to calculate ψ_m for any cell. The cells are ordered so that the largest has the smallest index! (That is how they are ordered in the literature.) Now we can examine the pattern actually obtained in a practical case. It is shown in Fig. 6.21.

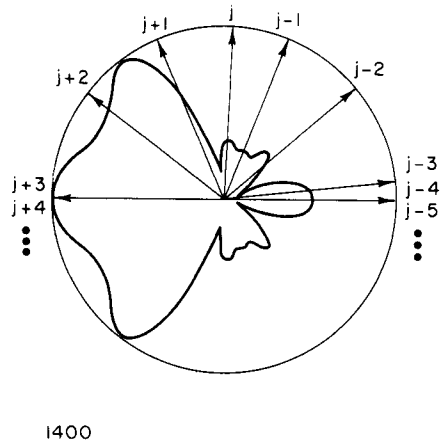

FIG. 6.21. Typical pattern before correction [after Ref. 12].

The directions ψ_m are also shown for the cells which give real ψ_m. In this case we see that the maxima actually measured do not fall along the directions ψ_m. It should also be stated that ψ_m for $j + 3$, $j + 4$, ... and $j - 4$, $j - 5$, ... are imaginary, although the effect of this, as we have seen earlier, is minor for the first couple of cells in the imaginary

region. Although these results give rather poor agreement with the crude theory, they do show that the slowness factor needs to be reduced, to put ψ_m for the jth cell in the backward direction, that is, to put $\psi_m = \pi$. This can be accomplished easily by the appropriate reduction in α_s; the effect of this simple redesign is indeed a remarkable improvement. To get a well-formed beam, we want to make sure that the power radiated by cells with ψ_m much less than π is negligible. This suggests that we should make $-\cos\psi_m$ for the jth cell somewhat greater than unity. Empirically it has been found that a value near -2 is a good starting point. The typical result is shown in Fig. 6.22.

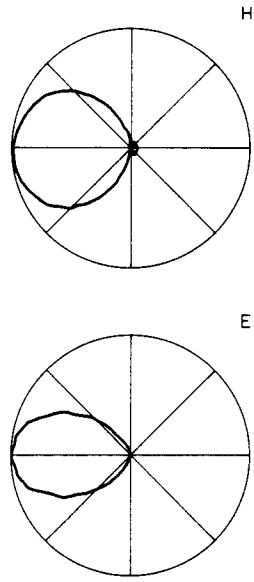

FIG. 6.22. Typical pattern after correction [after Ref. 12].

As a practical matter, other changes which give some improvement should be mentioned. They are (1) alternating the delay-line stubs along the positive and negative y axes, giving better symmetry; (2) terminating the large end of the antenna with a parasitic reflector 0.247 λ long at 0.1 λ beyond the end, λ being the longest operating wavelength; and (3) changing to a higher τ for the first quarter of the structure at the large end. (1) improves the pattern in the yz plane; (2) and (3) improve the back-to-front ratio.

Table III summarizes 15 successful designs.

TABLE III

τ	α_E (deg)	α_S (deg)	yz beam (deg)	xz beam (deg)	Gain over isotropic (db/iso.)
0.97	2.5	1.36	50	43	13
0.97	5.0	3.42	58	45	12
0.95	5.0	2.0	64	54	11
0.95	7.5	7.5	77	55	10
0.93	5.0	2.2	66	49	11
0.93	16	12	87	57	9
0.9025	10	10	84	49	10
0.90	25	20.5	106	69	8
0.87	10	4.37	90	56	9
0.87	16	8.6	93	59	9
0.87	25	17	101	56	9
0.85	13.7	7	89	54	9
0.85	20	14	111	56	8
0.83	30	15	100	61	8
0.82	25	18	113	57	8

The other point of interest is that power is evidently fed through the stop band before it gets to the first resonance element. The evidence for this is that $\beta = \pi$ at the first stop band, which means the length of wire in one cell is $\lambda/2$. Hence, taking $\alpha_E = \alpha_S$, the height of a radiating element is about $\lambda/8$ at the first stop band. Now a model was tested over a 10:1 frequency range, and the results were convincingly constant. If the stop-band effect were serious, it would obviously show up in the lower part of this frequency range. Of course, the effect must cause some attenuation, which would make the antenna impedance more mismatched to the Z_{00} of the delay line than a comparable switched design. Indeed the impedance was found to behave in a rather unusual way. It is described in the Table IV. The antennas referred to in this table were made in three ways, out of uniform wire, metal strip of the properly expanding width, or double wire following the outline of the proper metal strip. The third was practically like the second, as we saw in Chapter 5. The first gave poorer pattern and impedance, as might be expected, because it disagrees with the angle principle. The parameter γ in the "modifications" column when expressed in radians is the ratio of the width of the metal strip to its distance from the origin. For small ξ and γ, as in the

present case, Z_{00} varies as $60 \ln(\xi/\gamma)$. For the first two cases in the table, the wire diameter is the same but ξ differs by a factor of 4. So Z_{00} differs by about 83 Ω, but Z_0 differs in the opposite direction by about 40 Ω, as well as having a high reactive component.

TABLE IV

τ	α_E (deg)	α_S (deg)	ξ (deg)	Z_0	VSWR	Modifications
0.97	5.0	3.42	0.5	177-j60	1.5	Alt. stubs 0.039-in. wire
0.95	7.5	7.5	2.0	138-j62	1.4	0.039-in. wire
0.9025	10.0	10.0	2.0	153-j58	1.7	$\gamma = 0.102°$
0.87	16.0	8.6	1.5	144-j19	1.7	Alt. stubs 0.062-in. wire
0.87	25.0	17.0	3.0	154-j54	1.5	Alt. stubs $\gamma = 0.24°$
0.85	13.7	7.0	1.5	141-j41	1.5	0.039-in. wire

It is also significant that shifting the resonance cell into the imaginary backward region (the empirical condition for a good pattern) moves the resonance cell closer to the pass band.

REFERENCES

1. Carrel, R., *IRE Intern. Conv. Record* **1961**, Pt. I, 61–75.
2. DuHamel, R. H., *in* "Electromagnetic Theory and Antennas" (Proc. URSI Symp., Copenhagen, June 1962) (E. C. Jordan, ed.), pp. 1031–1050. Pergamon Press, New York, 1963.
3. Greiser, J. W., and P. E. Mayes, *Trans. IEEE* **AP-12**, 281–290 (1964).
4. Mayes, P. E., G. A. Deschamps, and W. T. Patton, *Proc. IRE* **49**, 962–963 (1961); also, *Univ. Illinois Antenna Lab. Rept. 60*, Urbana, Illinois, 1962.
5. Mittra, R., *Univ. Illinois Antenna Lab. Rept. 59*, Urbana, Illinois, 1962.
6. Mittra, R., and K. E. Jones, *Trans. IEEE* **AP-12**, 533–540 (1964).
7. Oliner, A. A., *in* "Electromagnetic Theory and Antennas" Proc. URSI Symp., Copenhagen, June 1962) (E. C. Jordan, ed.), pp. 837–856. Pergamon Press, New York, 1963.
8. Oliner, A. A., and A. Hessel, *Trans. IRE* **AP-7**, S201–S208 (1959).
9. Brillouin, S., "Wave Propagation in Periodic Structures," 2nd ed. Dover, New York, 1953.
10. Pierce, J. R., *J. Appl. Phys.* **25**, 179–183 (1954).
11. Watkins, D. A., "Topics in Electromagnetic Theory." Wiley, New York, 1958.
12. Wickersham, A. F., *Proc. IRE* **48**, 794–795 (1960).
13. Wickersham, A. F., R. E. Franks, and R. L. Bell, *Proc. IRE* **49** 378 (1961).

7

SOLUTION OF MAXWELL'S EQUATIONS FOR IDEALIZED SPIRAL STRUCTURES

7.1 Solution of Maxwell's Equations for a Sheet of Spiral Wires

In the previous chapter we saw that periodic structure theory provides a rough, though satisfactory, way of understanding the peculiarities of frequency independent antennas. Although successful, periodic structure theory is however only a crude approximation for two main reasons: (*1*) it applies strictly only in the limit of infinitely slow expansion, and (*2*) radiation coupling between periods gives many possible modes and so the result is an indeterminate combination of these modes. In this chapter we shall try to get a precise way of understanding our subject through a rigorous approach based on Maxwell's equations.

The planar equiangular spiral antenna is evidently the simplest type from the theoretical viewpoint, but even this has proved to be intractable. We are therefore forced to consider a simpler case which, while retaining the essential frequency-independent feature, is amenable to theoretical solution. The first theoretical solution we shall consider is such an idealization.[1] It can be described by taking a self-complementary antenna with many spiral elements, as in Fig. 7.1. We now suppose that the number of elements is infinite, so that the antenna takes the form of an anisotropic sheet which is perfectly conducting along the spiral direction, but perfectly transparent along the orthogonal spiral direction.

The boundary conditions can be expressed very simply by making use of the self-complementary feature. We saw in Chapter 3 that the space between the metal parts is equivalent to a magnetic conductor.

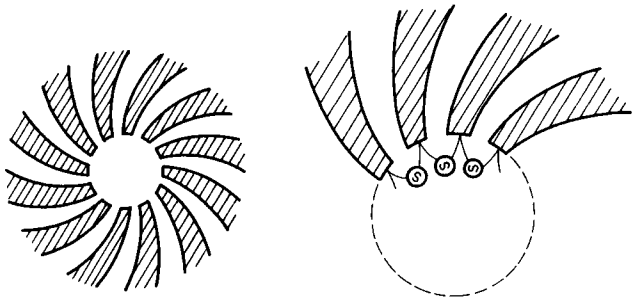

FIG. 7.1. Multielement spiral antenna [after Ref. 1].

Thus we can take the anisotropic plane as perfectly conducting in both the electric and magnetic senses along the spiral direction. The boundary conditions are therefore that E and H parallel to the spirals be zero. To complete the specification we have to add the conditions at the origin and at infinity. Thus if we excite the structure appropriately, we can get a solution in which E is the same as H, apart from a constant. Such solutions of Maxwell's equations are of considerable interest in themselves—they are another valuable byproduct of frequency-independent-antenna research.[7] We shall explore their main features in Section 7.2.

7.2 Circularly Polarized Solutions of Maxwell's Equations

The remarkable development of microwave technology in recent times depends to a great extent on a certain way of solving Maxwell's equations, namely the decomposition of the field into transverse electric (TE) and transverse magnetic (TM) parts. The importance of this technique rests on the fact that it is practically the only way of getting a complete set of solutions. In this section we shall work out an alternative way of solving Maxwell's equations which may be described roughly as a decomposition of the field into right-handed and left-handed circularly

polarized parts (it is a rough description because it is not literally true, but still serves as a meaningful name).

To understand how this compares with the TE, TM method, suppose we take the z axis as the reference, so that $E_z = 0$ for the TE part and $H_z = 0$ for the TM part. Thus the TM and TE parts can be considered to have been generated respectively by electric and magnetic dipoles which are parallel to the z axis. From this point of view the circularly polarized parts can be considered to have been generated by right- and left-handed circularly polarized dipoles parallel to the z axis, a circularly polarized dipole consisting of a certain combination of an electric and a magnetic dipole. Hence we can see in a rough way that the two methods are equivalent in generality. The choice between the two therefore depends on the nature of the problem at hand. It turns out that the circularly polarized method has the advantage in connection with problems involving propagation over sheets made of perfectly conducting filaments, so that, at any point on the sheet, the conductivity is infinite in one direction but zero in the direction at right angles. The simplest example is a sheet made of parallel copper wires extremely close together, but not touching, so that the sheet would be "invisible" to an electric field parallel to the sheet but perpendicular to the wires.

Let us begin with a statement of the classical technique (usually called the *Hertz potential method*). It says that Maxwell's equations, in the form

$$\nabla \times \mathbf{H} = j\omega\epsilon\mathbf{E} \qquad \nabla \times \mathbf{E} = -j\omega\mu\mathbf{H} \tag{7.1}$$

(assuming the $e^{j\omega t}$ time convention) are solved by putting

$$\mathbf{E} = \mathbf{E}_e + \mathbf{E}_m \qquad \text{and} \qquad \mathbf{H} = \mathbf{H}_e + \mathbf{H}_m \tag{7.2}$$

with

$$\mathbf{E}_e = \nabla \times \hat{\mathbf{z}}U \qquad \text{and} \qquad \mathbf{H}_m = \nabla \times \hat{\mathbf{z}}V \tag{7.3}$$

where $\hat{\mathbf{z}}$ is a unit vector parallel to the z axis and U and V satisfy the scalar wave equation

$$\nabla^2 f + k^2 f = 0 \qquad (k^2 = \omega^2\mu\epsilon) \tag{7.4}$$

It can be shown that if U and V are general solutions of (7.4), the Hertz potential method gives a general solution of (7.1).[6,7]

As an alternative, let us now consider solutions of (7.1) for which

$\mathbf{E} = C\mathbf{H}$, C being some scalar constant. Substitution in (7.1) shows that this is possible if

$$C = \pm jZ_0 \tag{7.5}$$

where

$$Z_0 = (\mu/\epsilon)^{1/2} \tag{7.6}$$

Thus we get two types of solution denoted by $\mathbf{E}_1$ and $\mathbf{E}_2$:

$$\mathbf{E}_1 = jZ_0\mathbf{H}_1 \quad \text{and} \quad \mathbf{E}_2 = -jZ_0\mathbf{H}_2 \tag{7.7}$$

Note that the Poynting vector is expressed by

$$\mathbf{P} = (\mathrm{Re}\,\mathbf{E}e^{j\omega t}) \times (\mathrm{Re}\,\mathbf{H}e^{j\omega t}) \tag{7.8}$$

which gives

$$\mathbf{P}_1 = Z_0\mathbf{H}_r \times \mathbf{H}_i \quad \text{and} \quad \mathbf{P}_2 = -Z_0\mathbf{H}_r \times \mathbf{H}_i \tag{7.9}$$

$\mathbf{H}_r$ and $\mathbf{H}_i$ being the real and imaginary parts of $\mathbf{H}_1$ (or $\mathbf{H}_2$), respectively. Thus the instantaneous Poynting vector is independent of time.

For a lossy medium with conductivity σ, we have

$$Z_0^2 = \frac{j\omega\mu}{j\omega\epsilon + \sigma} \tag{7.10}$$

$$\mathbf{P}_1 = \mathrm{Re}(Z_0)\mathbf{H}_r \times \mathbf{H}_i \quad \text{and} \quad \mathbf{P}_2 = -\mathrm{Re}(Z_0)\mathbf{H}_r \times \mathbf{H}_i \tag{7.11}$$

Although (7.4) immediately gives us $\mathbf{H}_1$ if we know $\mathbf{E}_1$, it does not tell us how the three components of $\mathbf{E}_1$ are related. Instead of working with the three scalar functions which constitute these three components, it is obviously much better to express the whole field by means of only one scalar function. This can be done by applying the Hertz potential technique to $\mathbf{E}_1$. The results are as follows:

$$\mathbf{E}_1 = \nabla \times \nabla \times \hat{\mathbf{z}}U_1 - k\nabla \times \hat{\mathbf{z}}U_1 \tag{7.12}$$

$$= \nabla\left(\frac{\partial U_1}{\partial z}\right) - k\nabla \times \hat{\mathbf{z}}U_1 + k^2\hat{\mathbf{z}}U_1 \tag{7.13}$$

the formulas for $\mathbf{E}_2$ being obtained by reversing the sign of k. The function U_1 from which $\mathbf{E}_1$ is derived is any solution of (7.4). Now let us put

$$\mathbf{E} = \mathbf{E}_1 + \mathbf{E}_2 \tag{7.14}$$

Then substitution for $\mathbf{E}_1$ and $\mathbf{E}_2$ from (7.12) gives

$$\mathbf{E} = \nabla \times \nabla \times \hat{\mathbf{z}}(U_1 + U_2) + k\nabla \times \hat{\mathbf{z}}(U_2 - U_1) \tag{7.15}$$

We see that $(U_1 + U_2)$ and $(U_2 - U_1)$ are the TM and TE Hertz potential functions for $\mathbf{E}$. Now it is evident that we can always find U_1 and U_2 to fit any such pair of Hertz potential functions and, therefore, in view of the generality of the Hertz potential method, we can represent any solution of (7.1) as a linear combination of solutions of types one and two. In short, the representation (7.14) is complete.

The orthogonality of the $\mathbf{E}_1$ and $\mathbf{E}_2$ types can be quickly demonstrated by means of the reaction integral.[6] We consider the reaction (or coupling) between a source **a**, which radiates a field of type $\mathbf{E}_1$, and a source **b**, which radiates a field of type $\mathbf{E}_2$. The reaction is expressed by

$$\oiint_S (\mathbf{E}_a \times \mathbf{H}_b - \mathbf{E}_b \times \mathbf{H}_a) \cdot \mathbf{n}\, dS \tag{7.16}$$

where S is any closed surface separating sources **a** and **b**, **n** pointing from **a** to **b**. The physical meaning of reaction is this. If source **a** is a unit current generator connected to an antenna which radiates a field of type $\mathbf{E}_1$, the reaction is the open-circuit voltage this antenna receives from source **b**. Thus vanishing of the reaction means that the antenna which radiates type $\mathbf{E}_1$ is "blind" to an incident field of type $\mathbf{E}_2$. On putting

$$\mathbf{E}_a = jZ_0\mathbf{H}_a \qquad \text{and} \qquad \mathbf{E}_b = -jZ_0\mathbf{H}_b \tag{7.17}$$

we see that the reaction is zero.

To derive the sources of these fields we use (7.12) in the form

$$\mathbf{H}_1 = \nabla \times \nabla \times \hat{\mathbf{z}}U_1 - k\nabla \times \hat{\mathbf{z}}U_1 \tag{7.18}$$

Now suppose that

$$U_1 = \frac{e^{-jkr}}{4\pi r} \tag{7.19}$$

which is the solution of the wave equation (7.4) for a unit point source. Then the second term of (7.18) will be recognized as the field of an electric dipole of current moment

$$\mathbf{I}l = -\hat{\mathbf{z}}k \tag{7.20}$$

and the first term represents a magnetic dipole of current moment

$$\mathbf{M}l = \hat{\mathbf{z}} j\omega\mu \tag{7.21}$$

Thus (7.18) represents the field of the combination of an electric and a magnetic dipole at the same point, aligned in the same direction, with

$$(\mathbf{M}l) = -jZ_0(\mathbf{I}l) \tag{7.22}$$

By working out (7.18) it will be found that such a combination gives a circularly polarized field at every point on the sphere at infinity; it may therefore be called a *circularly polarized dipole.* Note, however, that it does not give circular polarization in the near field, although the instantaneous Poynting vector is everywhere independent of time.

Now we can show that any field of type $\mathbf{E}_1$ must be due to a collection of these circularly polarized dipoles. To do this we write Maxwell's equations for the field of an electric-dipole density represented by $\mathbf{J}$ and a magnetic-dipole density represented by $\mathbf{K}$:

$$\nabla \times \mathbf{H} = \mathbf{J} + j\omega\epsilon\mathbf{E} \tag{7.23}$$

$$-\nabla \times \mathbf{E} = \mathbf{K} + j\omega\mu\mathbf{H} \tag{7.24}$$

Substitution from (7.4) immediately gives

$$\mathbf{K} = -jZ_0\mathbf{J} \tag{7.25}$$

which is precisely the condition (7.22) for a circularly polarized dipole.

7.3 Solution for a Sheet of Spiral Wires

We shall now use the method described in Section 7.2 to solve the idealized problem described in Section 7.1. The antenna consists of an infinite number of spiral wires lying in the plane $z = 0$. Because it is uniform with respect to ϕ (the usual angle measured about the z axis), we can assume a solution which varies as $e^{j\phi n}$. Let $\mathbf{E}_1$ and $\mathbf{E}_2$ be the fields above and below the sheet:

$$\mathbf{E}_1 = jZ_0\mathbf{H}_1 \qquad \text{for } z > 0 \tag{7.26}$$

$$\mathbf{E}_2 = -jZ_0\mathbf{H}_2 \qquad \text{for } z < 0 \tag{7.27}$$

Then the field above the sheet is represented by the scalar U_1 through (7.12). The form of U_1 is determined by the wave equation (7.4): the typical form in cylindrical coordinates $\rho\phi z$ is $e^{jn\phi}R(\rho)Z(z)$, where R is a solution of Bessel's equation and Z is a combination of positive and negative exponentials. To make the input current finite, R has to be the Bessel function $J_n(T\rho)$. To put the direction of power flow in the direction of increasing z, Z has to be $\exp[-z(T^2 - k^2)^{1/2}]$ if $T > k$ or $\exp[-jz(k^2 - T^2)^{1/2}]$ if $T < k$, T being real. The general solution subject to these limitations can be expressed as a combination of all the solutions corresponding to all real T. Such a combination is expressed by the Hankel transform (or Fourier Bessel integral)[4]:

$$U_1 = e^{jn\phi}\int_0^\infty g_1(T)J_n(T\rho)\exp[-jz(k^2 - T^2)]T\,dT \tag{7.28}$$

The function g_1 is at present arbitrary. Evidently it represents the spectrum of the combination. The point of using the Hankel transform is that if

$$f(\rho) = \int_0^\infty F(T)J_n(T\rho)T\,dT \tag{7.29}$$

for all ρ, then

$$F(T) = \int_0^\infty f(\rho)J_n(T\rho)\rho\,d\rho \tag{7.30}$$

One consequence is that if $f(\rho) = 0$ for all ρ, then $F(T) = 0$.

Similarly, for $z < 0$,

$$U_2 = e^{jn\phi}\int_0^\infty g_2(T)J_n(T\rho)\exp[jz(k^2 - T^2)]T\,dT \tag{7.31}$$

At $z = 0$ tangential $\mathbf{E}$ and $\mathbf{H}$ must be continuous. It is easily seen from (7.12) that this is ensured by setting

$$g_1(T) = g_2(T) = g(T) \tag{7.32}$$

The form of g is determined by the requirement that $\mathbf{E}$ and $\mathbf{H}$ parallel to the spiral wires be zero at $z = 0$. Taking the spiral as

$$\rho = e^{a\phi} \tag{7.33}$$

we have

$$aE_\rho + E_\phi = 0 \qquad \text{at } z = 0 \tag{7.34}$$

Substitution in (7.12) puts this in the form

$$a\left(\frac{k}{\rho}\frac{\partial U_1}{\partial \phi} - \frac{\partial^2 U_1}{\partial z\,\partial \rho}\right) = \frac{1}{\rho}\frac{\partial^2 U_1}{\partial \phi\,\partial z} + k\frac{\partial U_1}{\partial \rho} \qquad \text{at } z = 0 \tag{7.35}$$

Substitution of the integral for U_1 gives

$$\int_0^\infty \Big\{[n(k^2 - T^2)^{1/2} - jnka]\, T\frac{J_n(T\rho)}{\rho} + [k - ja(k^2 - T^2)]^{1/2}\, T^2 J_n'(T\rho)\Big\} g(T)\, dT = 0 \tag{7.36}$$

Integration by parts applied to the derivative J_n' gives

$$\int_0^\infty \Big\{[(k^2 - T^2)^{1/2} - jka]\, nTg - \frac{d}{dT}[k - ja(k^2 - T^2)^{1/2}]T^2 g\Big\}\frac{J_n}{\rho}\, dT + [k - ja(k^2 - T^2)^{1/2}]T^2 g\frac{J_n}{\rho}\Big|_{T=0}^{\infty} = 0 \tag{7.37}$$

At this point we assume that the latter term vanishes. It will turn out that this assumption is justified by the form of g obtained from it. Then the integral conforms to (7.29), so we can put the function of T represented by $\{\ \}$ equal to zero. This gives a straightforward differential equation for g whose solution is

$$g = C\left[\frac{1 - (1 - v)^{1/2}}{1 + (1 - v)^{1/2}}\right]^{n/2} \frac{1}{v[1 - ja(1 - v)^{1/2}]^{1 - jn/a}} \tag{7.38}$$

with

$$v = T^2/k^2 \tag{7.39}$$

If $n > 0$ it can be seen that g is such as to make the last term in (7.37) vanish at both limits as we have assumed. But if $n < 0$, then (7.37) cannot be used, because it diverges at $v = 0$, and so the original formula for U in (7.28) and (7.31) is ruled out. In the beginning we could have assumed a type 1 circularly polarized solution for $z < 0$ instead of for $z > 0$. Had we done so, we would have got the opposite sign for the exponential variation in z; that is, the sign of the square root in (7.28) would have been reversed. So (7.38) would have turned out with all square roots reversed in sign, and this gives finite g for $n < 0$. Hence

for $-m = n < 0$ the solution is expressed by (7.12) with $\mathbf{E}_1 = jZ_0\mathbf{H}_1$ for $z < 0$ and

$$U_1 = e^{-jm\phi} \int_0^\infty g J_m \exp[jz(k^2 - T^2)^{1/2}] T \, dT \qquad m > 0 \tag{7.40}$$

$$g = C \left[\frac{1 - (1 - v)^{1/2}}{1 + (1 - v)^{1/2}}\right]^{m/2} \frac{1}{v[1 + ja(1 - v)^{1/2}]^{1+jm/a}} \tag{7.41}$$

Thus the solution for negative n and z is obtained by reversing the sign of a.

This completes the formal solution but leaves the physical meaning rather obscure, because the integral for U_1 cannot be worked out for all ρ and z. There are two special cases which can be worked out, however. One represents the field near the origin and the other the field at infinity. The next two sections will therefore be concerned with these two cases.

Note that when $v > 1$, $j(1 - v)^{1/2}$ is replaced by $(v - 1)^{1/2}$ as explained in the first paragraph. Therefore (7.38) gives infinity when $v = 1 + a^{-2}$ if $a > 0$, but remains finite if $a < 0$. Consequently, some parts of the following sections are restricted to the case $a/n < 0$. The infinity in (7.38) can be dealt with by considering the case where k is complex, corresponding to a lossy medium. This gives v a positive imaginary part, thus avoiding the infinity and giving a well-defined integral in (7.28). For a lossless medium the correct form of (7.28) is evidently the limit obtained as the loss tends to zero, and this limit is finite. This peculiar difference between the cases $n/a > 0$ and $n/a < 0$ was overlooked in the original work. It was uncovered in connection with a different problem,[8] and remains unexplored.

7.4 Input Conditions for the Idealized Spiral Sheet

We recall the formula (7.12) for the field:

$$jZ_0\mathbf{H}_1 = \mathbf{E}_1 = k\hat{\mathbf{z}} \times \nabla U_1 + \nabla(\partial U_1/\partial z) + k^2\hat{\mathbf{z}}U_1$$

For finite input current or voltage $\mathbf{E}$ and $\mathbf{H}$ must tend to infinity as we approach the origin. It follows that in the limit the differential coefficient of highest order, $\nabla(\partial U_1/\partial z)$, dominates the rest:

$$\mathbf{E}_1 \to \nabla(\partial U_1/\partial z) \tag{7.42}$$

Evidently, then, $\partial U_1/\partial z$ must tend to the static potential function. The classical static solution in spherical coordinates is written in terms of the Legendre function as $r^m P_m{}^n(\cos\theta)\, e^{jn\phi}$. If we put $m = -jn/a$, this becomes

$$(re^{-a\phi})^{-jn/a} P^n_{-jn/a}(\cos\theta) \tag{7.43}$$

Evidently, this is constant where $re^{-a\phi}$ and θ are constant, that is, along the spiral lines $r \sim e^{a\phi}$ on cones $\theta =$ constant. So it is the static solution for our problem.

Turning now to (7.42), from (7.28) and (7.38), we have for $n > 0$,

$$\frac{\partial U_1}{\partial z} = Ce^{jn\phi} \int_0^\infty g[-j(1-v)^{1/2}] \exp[-j(1-v)^{1/2} kr\cos\theta] J_n(krv^{1/2}\sin\theta)\frac{dv}{2} \tag{7.44}$$

Now $J_n(x) \to x^n$ as $x \to 0$, so the J_n factor in the integrand varies as $r^n v^{n/2}$ as $r \to 0$. On working out the limit it will be found from (7.38) that g varies as $v^{(n/2)-1}$ as $v \to 0$, and g is finite for finite v. Consequently, if r is infinitesimal, the integrand is negligible unless $v^{1/2}$ is of the order of r^{-1}. We can therefore replace all except J_n by the approximation obtained from assuming v large. Hence

$$\frac{\partial U_1}{\partial z} \to C(-a)^{-1+jn/a} e^{jn\phi} \int_0^\infty v^{-1+jn/2a} \exp[-krv^{1/2}\cos\theta] J_n(krv^{1/2}\sin\theta)\, dv \tag{7.45}$$

This integral is a standard form for the Legendre function.[3] The classical result expressed in terms of gamma functions is

$$\frac{\partial U_1}{\partial z} \to \frac{C\Gamma[n+(jn/a)]\Gamma[1-n-(jn/a)]\, e^{jn\phi}(kr)^{-jn/a} P^n_{-jn/a}(\cos\theta)(-)^{-n/2}(-a)^{-1+jn/a}}{\Gamma[1+n-(jn/a)]} \tag{7.46}$$

which agrees with (7.43). This shows that the input voltage is finite, because it conforms to the static solution.

The source of this solution can be pictured as a system of current sources connected radially between the origin and the ends of the spiral wires at infinitesimal radius, and phased according to the $e^{jn\phi}$ factor. Now the radial current I per unit of angle ϕ at the origin is $-2rH_\phi$, H_ϕ being the tangential component just above the sheet of spirals. Since $E_{1\phi} = jZ_0 H_{1\phi}$, we then have

$$I = -2rH_\phi = -\frac{2rE_\phi}{jZ_0} = -\frac{2jV}{Z_0}$$

where V is the voltage increment per unit of angle ϕ. Since we have shown V to be finite, this shows that I is finite also.

The ratio of V to I, which is seen to be pure imaginary, is only indirectly connected with the idea of input impedance. A precise analysis of the input-impedance question was worked out in Section 3.3. There the symbol n represents number of elements, which is infinite here; m there represents n here; and the discrete variable $2\pi k/n$ there represents ϕ here. In the terms of (3.12), the combined current in an infinitesimal sector $\Delta\phi$ containing many elements is $\Delta\phi\, nI_0 e^{jm\phi}/2\pi$, which is our present $I\,\Delta\phi$. The voltage difference in $\Delta\phi$ is $V_0[e^{jm(\phi+\Delta\phi)} - e^{jm\phi}] = jm\,\Delta\phi\, V_0 e^{jm\phi}$, which is our present $V\,\Delta\phi$. Thus the ratio V/I is $jm2\pi V_0/nI_0$. On substituting for V_0/I_0 from (3.16) and taking the limit as $n \to \infty$ we get the same result as here.

7.5 Radiation Patterns

When seen from infinity, we know that the antenna must look like a point source. Therefore, as $r \to \infty$ U_1 must take the form $f(\theta)(e^{-jkr}/r)$. When this is put in (7.12) we find that $\mathbf{E}_1 \sim (\hat{\boldsymbol{\theta}} - j\hat{\boldsymbol{\phi}})\, U \sin\theta$, so $U_1 \sin\theta$ represents the pattern. From (7.28) and (7.39),

$$U_1 \sim \int_0^\infty g J_n(v^{1/2}kr \sin\theta) \exp[-jkr(1 - v)^{1/2} \cos\theta]\, dv \qquad (r \to \infty) \qquad (7.47)$$

Since $g \sim v^{(n/2)-1}$ as $v \to 0$ and $n \geqslant 1$, we can replace J_n by its value for large argument; that is,

$$J_n(x) \simeq \left(\frac{1}{2\pi x}\right)^{1/2} \left(\exp\left\{j\left[x - (n + \tfrac{1}{2})\frac{\pi}{2}\right]\right\} + \exp\left\{-j\left[x - (n + \tfrac{1}{2})\frac{\pi}{2}\right]\right\}\right)$$
$$(x \to \infty) \qquad (7.48)$$

When $r \to \infty$ the variation of g with v is negligible compared to that of J_n and the exponential in (7.47). The latter two oscillate rapidly about zero and so give negligible contribution to the integral except where they oscillate in step, for then their product has a nonzero average over many periods. The mathematical expression of this effect is known as the *method of stationary phase*. It says that, if $p \to \infty$ and $f(t)$ and $h(t)$ are two real functions,

$$\int_a^b f(t)e^{jph(t)}dt \simeq (1 + j)\left(\frac{\pi}{p|\,h''(\tau)|}\right)^{1/2} f(\tau)e^{jph(\tau)} \qquad (7.49)$$

where τ is the stationary-phase point, that is, $h'(\tau) = 0$, and the plus or minus sign is to be taken according to whether the stationary point is a minimum or maximum.[2] In the present case,

$$h(v) = \pm(v)^{1/2} \sin\theta - (1 - v)^{1/2} \cos\theta \tag{7.50}$$

the upper and lower signs coming from the first and second terms of (7.48). The only stationary-phase point therefore comes at $v^{1/2} = \sin\theta$. Application of (7.49) gives

$$U_1 \sim \frac{\cos\theta(\tan[\theta/2])^n e^{j(n\phi - kr)}}{r \sin^2\theta(1 - ja\cos\theta)^{1 - jn/a}} \qquad (n > 0) \tag{7.51}$$

Therefore,

$$|E| \sim \frac{\cot\theta(\tan[\theta/2])^{|n|} \exp[|n|a^{-1}\tan^{-1}(a\cos\theta)]}{(1 + a^2\cos^2\theta)^{1/2}} \qquad (\text{any } n \neq 0) \tag{7.52}$$

and

$$\text{phase } \mathbf{E} = \tan^{-1}(a\cos\theta) + \frac{n}{2a}\ln(1 + a^2\cos^2\theta) + n\phi - kr \qquad (n/a < 0)$$

$$= -\tan^{-1}(a\cos\theta) - \frac{n}{2a}\ln(1 + a^2\cos^2\theta) - n\phi - kr \quad (n/a > 0) \tag{7.53}$$

Patterns of $|\mathbf{E}|$ are plotted in Figs. 7.2 and 7.3 for various harmonics n and expansion factors a. Note that even $a = 1$ corresponds to an

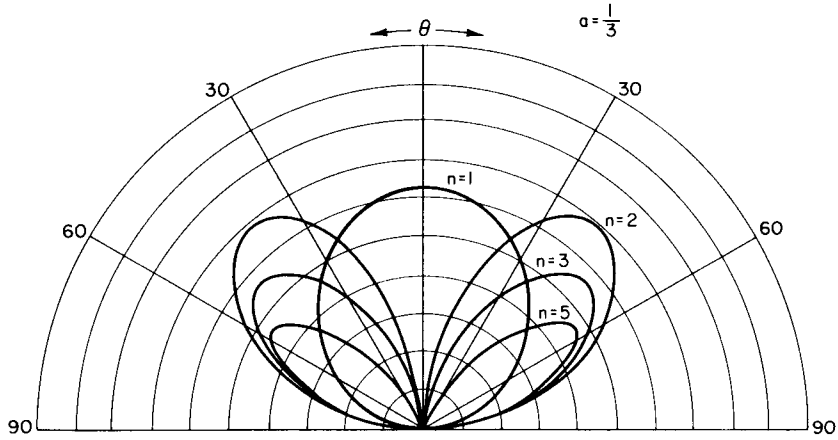

FIG. 7.2. Patterns of the spiral sheet for various harmonics n [after Ref. 1].

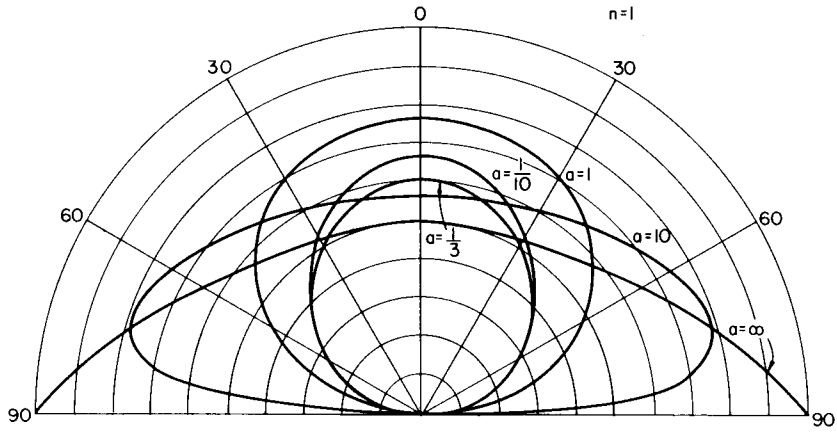

FIG. 7.3. Patterns for various rates of expansion with $n = 1$ [after Ref. 1].

expansion of over 500 per turn and $a = 10$ to the tenth power of that. Yet $a = 10$ is essentially different from the straight case, denoted by $a = \infty$. On the other hand, there is very little difference between the patterns for $a = 1$ and $a = \frac{1}{10}$. These patterns are remarkably close to those measured on two-element self-complementary spiral antennas. In fact, we saw in Chapter 4 that, if the measured pattern has amplitude independent of ϕ, it has to be circularly polarized everywhere and must consist of a single harmonic in ϕ. Both conditions are characteristic of the present idealized solution. Indeed, it was this solution that led to a more careful examination of the measurements to check whether the polarization might be circular everywhere. We are thus led to conclude that the idealized solution gives a very close approximation to the patterns of self-complementary spiral antennas.

In the idealized solution, positive and negative values of n are both allowed. The only difference is a reversal in the phase of $\mathbf{E}$, which consequently shows up in connection with the phase center. However, we can use the idea of a phase center only for a small range of θ in which the constant phase surface is approximately spherical. For example, if θ is near zero and the phase center is at a distance d behind the plane $z = 0$, the equiphase surface can be expressed as

$$R = r + d\left(1 - \frac{\theta^2}{2}\right) \tag{7.54}$$

where R is its radius.

On setting (7.53) constant and assuming $a \ll 1$, we have, for fixed ϕ,

$$k\left[r - \frac{a}{k}(n+1)\left(1 - \frac{\theta^2}{2}\right)\right] = \text{const} \qquad (n/a < 0) \tag{7.55}$$

giving for $a < 0$

$$d = \frac{a(n+1)\lambda}{2\pi} - \frac{\lambda a}{\pi} \qquad (n = 1) \tag{7.56}$$

and $d = 0$ for $n = -1$. For other values of n it is pointless to look near $\theta = 0$, because the field there is zero. Note the physical significance of d. It means that, apart from the $e^{jn\phi}$ variation, constant phase (and amplitude) would be observed at a fixed circularly polarized antenna when the idealized spiral antenna is pivoted about the phase center.

7.6 Current Distribution

The current I per unit of angle ϕ is $2\rho H_\phi$ at $z = 0$. By (7.12),

$$H_\phi \sim k\frac{\partial U}{\partial \rho} + \frac{jn}{\rho}\frac{\partial U}{\partial z} \qquad (\text{at } z = 0)$$

$$\sim \int_0^\infty g\left[k\, v^{1/2} J_n' + \frac{n}{\rho}(1-v)^{1/2} J_n\right] dv \qquad [\text{by (7.28)}]$$

On integrating by parts and substituting for g from (7.38), we have

$$I \sim \int_0^\infty \left[\frac{1-(1-v)^{1/2}}{1+(1-v)^{1/2}}\right]^{n/2} \left[n + \frac{1}{(1-v)^{1/2}}\right] \times [1 - ja(1-v)^{1/2}]^{-2-jn/a} J_n(k\rho v^{1/2})\, dv \qquad (a < 0) \tag{7.57}$$

It is possible to work out an explicit formula for this integral by a long series of operations on the assumption that $k\rho$ is large.[1] The result takes the form

$$I \sim \frac{e^{-jk\rho + jn\pi/2}}{k\rho}\left(j + \frac{n^2 - j5an + 6a^2}{2k\rho}\right) - \frac{1}{k^2\rho^2}\left(\frac{2}{\pi k\rho}\right)^{1/2}\left(\frac{n}{3} + 3n^2 - \frac{26a^2 n}{3} + 2ja + 6jan + \frac{2jn^2 a}{3} - 8ja^3\right) \times \cos\left(k\rho - \frac{n\pi}{2} - \frac{\pi}{4}\right) + \mathcal{O}(k\rho)^{-3} \tag{7.58}$$

As a check, the integral (7.57) has been evaluated by a computer for the case $n = 1$. The comparison with (7.58) is shown in Figs. 7.4 through 7.7. The case $a = \infty$ can be worked out exactly by a much simpler

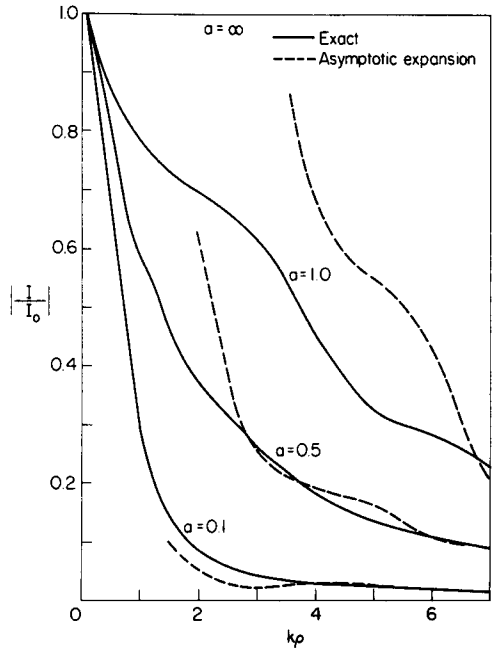

FIG. 7.4. Total current versus radial distance [after Ref. 1].

method.[5] It gives $I \sim e^{-jkr+jn\phi}$, which shows that the current is not attenuated. When a is not infinite, we see that the current is attenuated rapidly. Even for an expansion factor of 500 per turn, it is reduced by a factor of 2 in the first half-wavelength of ρ: for an expansion factor of 2, the current is halved in the first tenth of a wavelength (approximately). The asymptotic expansion (7.58) evidently improves with decreasing a; for the range of practical interest it appears to be good down to a radius of a half to one wavelength. When plotted versus distance along the spiral, the attenuation appears to change very little with a. It will be recalled that a similar insensitivity to the expansion factor was found in the radiation patterns. Of course, this holds only up to a point, because there is no attenuation when $a = \infty$ and the radiation pattern for $a = 10$ implies a considerable change in the current distribution.

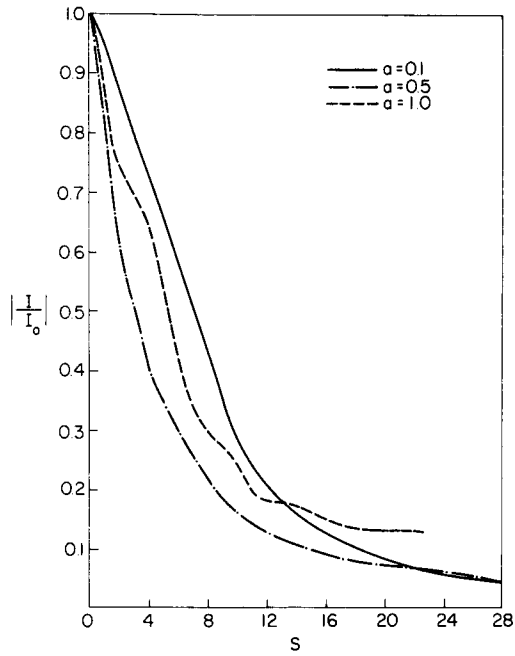

FIG. 7.5. Total current versus distance along spiral [after Ref. 1].

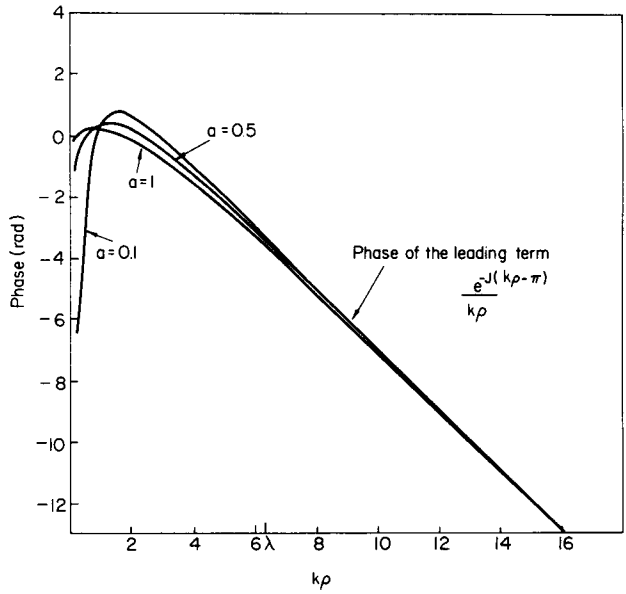

FIG. 7.6. Phase versus radial distance [after Ref. 1].

The phase characteristic is perhaps the most interesting feature of these results. For $n > 0$ it consists of an inward slow wave when r is very small, changing to a fast wave as r increases, which becomes infinitely fast at the point where the phase is a maximum in Fig. 7.6. Passing beyond this point, we find a fast outward wave which slows

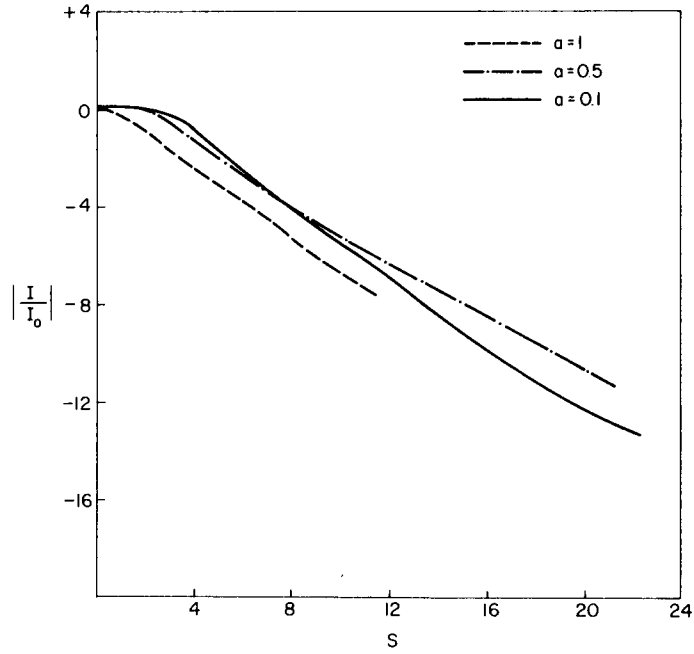

FIG. 7.7. Phase versus distance along spiral [after Ref. 1].

down to the velocity of light when $r \to \infty$. For small values of r the phase velocity is expressed by $r^{-jn/a} = \exp(-jna^{-1} \ln r)$ as in (7.43). We see that reversing the sign of n reverses the direction of radial phase velocity. For large values of r the effect of reversing n has to be dealt with as described in Section 7.3. Thus there is a marked difference in the radial phase variation of the two cases $\exp(\pm jn\phi)$.

This naturally led to an investigation of the effect of reversing n on practical structures. Of course, it is impossible to test this idealized case in practice, because it requires an infinite number of wires. The tests were therefore made on self-complementary spirals having many arms. Here another unsuspected effect was discovered. For although the

measurements did not at all confirm the surprising prediction of the theory, they did reveal an equally surprising principle for multielement spiral antennas, which has already been described in Section 4.4

REFERENCES

1. Cheo, B. R-S., V. H. Rumsey, and W. J. Welch, *IRE Trans.* **AP-9**, 527–534 (1961).
2. Erdelyi, A., "Asymptotic Expansions." Dover, New York, 1956.
3. Magnus, W., and F. Oberhettinger, "Formulas and Theorems for the Functions of Mathematical Physics." Chelsea, New York, 1954.
4. Morse, P. M., and H. Feshbach, "Methods of Theoretical Physics." McGraw-Hill, New York, 1953.
5. Rumsey, V. H., *IRE Trans.* **AP-7**, 461–465 (1961).
6. Rumsey, V. H., *Phys. Rev.* **94**, 1483 –1491 (1954).
7. Whittaker, E. T., *Proc. London Math. Soc.* **1**, 367–380 (1903).
8. Laxpati, S. J., Ph. D. Thesis, Univ. of Illinois, 1965.

8

SOLUTION OF MAXWELL'S EQUATIONS FOR IDEALIZED SINUSOIDAL STRUCTURES

8.1 Solution for a Sheet of Sinusoidal Wires

To represent a log-periodic antenna by the kind of idealization used in Chapter 7, we would make the plane $z = 0$ perfectly conducting along the curves

$$\phi + \phi_0 = A \sin(g \log r)$$

This problem has so far defied solution, so we are led to study the simply periodic case.[4] However, our approach will be essentially different from the periodic structure theory of Chapter 6, in that here we shall obtain an exact solution of Maxwell's equations.

The propagation of waves along periodic structures has been extensively worked out in connection with electronic-tube design (for example, Ref. 2 contains 295 references). There has also been a great deal of work on the related subject of surface waves, and here again the reader can get a good introduction through the "Proceedings of the URSI Symposium on Electromagnetic Theory" (Toronto, 1959), especially the paper by Oliner and Hessel.[3] Most of these papers are based on an impedance type of boundary condition; that is, it is assumed that tangential E is related to tangential H through a surface impedance which is some postulated function of position. What sort of physical structure corresponds to this postulate is left open to question, or indeed, the question of whether a physical counterpart exists. By

comparison, the solution we shall work out is based on the condition that E parallel to the wires is zero.

We consider a waveguide made of coplanar sinusoidal metal strips as illustrated in Fig. 8.1, the width of the strips being equal to the width

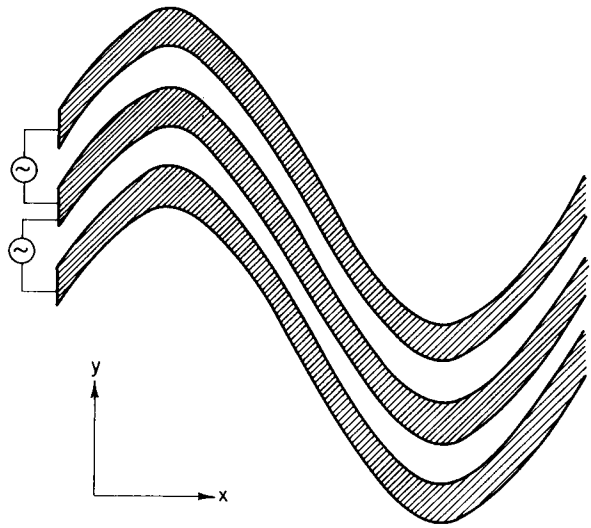

FIG. 8.1. Part of a sheet of sinusoidal wires [after Ref. 4].

of the space between them. When this common width tends to zero, the sheet becomes a continuous surface which is perfectly conducting in the direction of the sinusoids. Let us choose the coordinates XYZ so that the sheet is $Z = 0$ and the wires are parallel to the sinusoid

$$Y = a \sin pX \tag{8.1}$$

Then, at $Z = 0$,

$$E_x = -E_y ap \cos pX \tag{8.2}$$

Suppose that this waveguide is excited so that the field varies exponentially with Y as $\exp(-jYk \cos \theta)$. Thus as Y varies, the current amplitude stays constant and the phase varies linearly. Note that X and Y correspond to ρ and ϕ in the log-periodic case. When $\theta = \pi/2$ there is no variation with respect to Y, and consequently the wave travels over the surface in the X direction, or normal to the input X axis—hence "normal" excitation.

Since it is evident that we should use a Fourier series in X with the same period as the sinusoidal wires, it is convenient to introduce

$$x = pX \qquad y = pY \qquad z = pZ \tag{8.3}$$

Then as in Section 7.3 we can write

$$\begin{aligned} \mathbf{E} &= jZ_0\mathbf{H} && \text{for } z \geqslant 0 \\ &= -jZ_0\mathbf{H} && \text{for } z \leqslant 0 \end{aligned} \tag{8.4}$$

The Fourier series can be expressed compactly in terms of certain vectors $\mathbf{e}_n$, $\mathbf{F}_n$, and the position $\mathbf{r}$ as

$$\mathbf{E} = \sum_n \mathbf{e}_n \exp(-\mathbf{F}_n \cdot \mathbf{r}) \tag{8.5}$$

$\mathbf{e}_n$ and $\mathbf{F}_n$ being constant vectors. The y component of $\mathbf{F}_n$ must fit the prescribed excitation; it can be expressed as $-j(k/p)\cos\theta$. The x component involves an undetermined propagation factor jB, and it must fit the Fourier series: so it is $jB + jn$, with any integer for n. The z component $-\gamma_n$ is determined by the fact that each term must be a solution of Maxwell's equations. Thus

$$\gamma_n{}^2 = (B + n)^2 - F^2 \sin^2\theta \tag{8.6}$$

with

$$F = k/p \tag{8.7}$$

Hence

$$\mathbf{E} = \exp(jBx - jFy\cos\theta) \sum_{n=0\pm1\pm2\cdots} \mathbf{e}_n \exp(jnx - \gamma_n z) \tag{8.8}$$

Note that (8.4) gives

$$\mathbf{e}_n \times \mathbf{F}_n = -k\mathbf{e}_n \tag{8.9}$$

Thus if the components of $\mathbf{e}_n$ are a_n , b_n , and c_n ,

$$a_n : b_n : c_n = (B + n)\cos\theta - \gamma_n : F\sin^2\theta : j(\gamma_n \cos\theta - B - n) \tag{8.10}$$

Now (8.2) gives

$$a_n = -S(b_{n-1} + b_{n+1}) \tag{8.11}$$

where

$$S = \tfrac{1}{2}ap \qquad \text{(the slowness factor)} \tag{8.12}$$

Thus when (8.10) is substituted in (8.11), we have, on putting

$$d_n = \frac{\gamma_n - (B+n)\cos\theta}{SF\sin^2\theta} \tag{8.13}$$

$$\frac{b_{n-1}}{b_n} = d_n - \frac{1}{b_n/b_{n+1}} = d_n - \frac{1}{d_{n+1} - 1/(d_{n+2} - \cdots)}$$

or, alternatively,

$$\frac{1}{b_n/b_{n-1}} = \frac{1}{d_{n-1} - 1/(d_{n-2} - \cdots)} \tag{8.14}$$

Therefore,

$$d_n = \frac{1}{d_{n+1} - 1/(d_{n+2} - \cdots)} + \frac{1}{d_{n-1} - 1/(d_{n-2} - \cdots)} \tag{8.15}$$

This type of relation is familiar in the theory of periodic structures. It is, of course, valid for every n, but since it remains unchanged when n is replaced by $n+1$, it is entirely represented by putting $n = 0$. We see through (8.6) and (8.13) that it is an equation for B, all other quantities being given either by the form of the sinusoidal wires or the form of the excitation. Note that the proper sign of the square root γ_n is that which makes $\gamma_n < 0$ when γ_n is real. Thus the explicit form of (8.15) is

$$\begin{aligned}
&(B^2 - F^2\sin^2\theta)^{1/2} - B\cos\theta \\
&= S^2F^2\sin^4\theta\Big/[(B+1)^2 - F^2\sin^2\theta]^{1/2} - (B+1)\cos\theta \\
&\qquad - S^2F^2\sin^4\theta\Big/[(B+2)^2 - F^2\sin^2\theta]^{1/2} - (B+2)\cos\theta \\
&\qquad\qquad S^2F^2\sin^4\theta\Big/[(B+3)^2, \text{ etc.} \\
&+ S^2F^2\sin^4\theta\Big/[(B-1)^2 - F^2\sin^2\theta]^{1/2} - (B-1)\cos\theta \\
&\qquad - S^2F^2\sin^4\theta\Big/[(B-2)^2 - F^2\sin^2\theta]^{1/2} - (B-2)\cos\theta \\
&\qquad\qquad - S^2F^2\sin^4\theta\Big/[(B-3)^2, \text{ etc.}
\end{aligned} \tag{8.16}$$

Some typical results for real B, obtained by direct computation from (8.16) are shown in Figs. 8.2 and 8.3. Note that the plot is symmetric for normal excitations ($\theta = \pi/2$) but is skewed for oblique excitation.

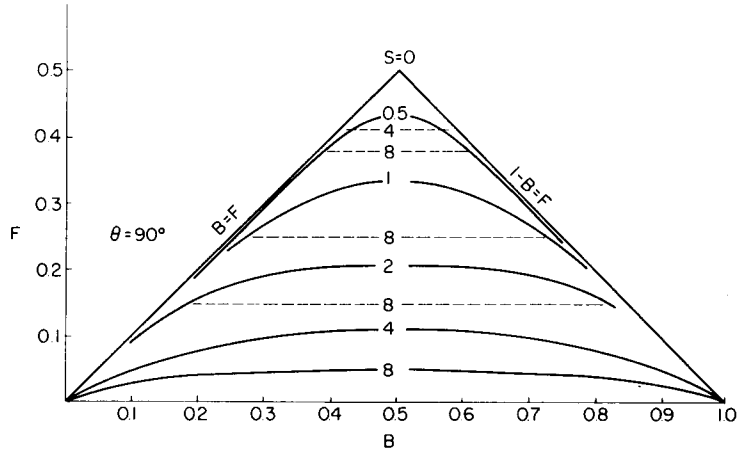

FIG. 8.2. Propagation constant B versus frequency F for various shapes of sinusoidal wires [after Ref. 4].

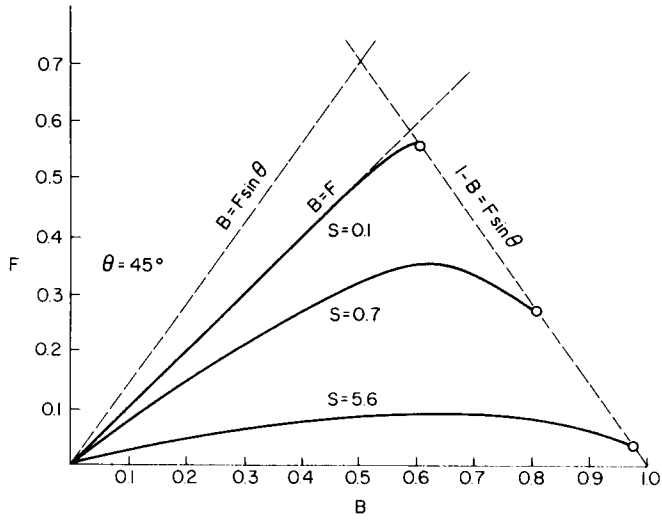

FIG. 8.3. For oblique excitation the graph stops abruptly at $1 - B = F \sin \theta$. [after Ref. 4].

Also note that the graph stops abruptly on the line $1 - B = F \sin\theta$ for oblique excitation, but continues down to $F = 0$, $B = 1$, for normal excitation. This seemingly inconsistent behavior can be understood if we think of the case $\theta = \pi/2$ as a degenerate combination of the cases $\theta_1 = \theta$ and $\theta_2 = \pi - \theta$ as $\theta \to \pi/2$. Using $B(\theta)$ to mean the value of B corresponding to the excitation θ, we find from (8.16) that

$$B(\theta) + B(\pi - \theta) = 1 \tag{8.17}$$

Thus the graph for $\pi - \theta$ is the image in $B = 0.5$ of that for θ. The dashed lines in Fig. 8.1 corresponding to $S = 4$ and $S = 8$ represent higher modes. These figures illustrate only a few of the infinite set of solutions of (8.16)—some of the real values of B corresponding to given F. When F and B are real, we can write $F = \Lambda_w/\lambda$ and $B = \Lambda_w/\lambda_g$, where

$$\Lambda_w = \frac{2\pi}{p}, \qquad \text{the wavelength of the wires}$$

$$\lambda_g = \text{guide wavelength measured in the } X \text{ direction}$$

The solutions of (8.16) do not represent a complete set but only those having $\mathbf{E} = jZ_0\mathbf{H}$ for $z \geqslant 0$ and $\mathbf{E} = -jZ_0H$ for $z \leqslant 0$. They may therefore be called the left-handed or L modes, because an individual term in the series for $z \geqslant 0$ represents a circularly polarized wave rotating about its direction of propagation $\mathbf{F}_n$ in the left-handed sense. The set is completed by adding the right-handed or R modes, as we saw in Section 7.2. These give a graph which is the image in the line $B = 0.5$ of that for the L modes. Thus, in effect, all the solutions are obtained by solving (8.16).

It has been pointed out by Borgiotti[1] that, as $n \to \infty$, b_n approaches the Bessel function J_n. Indeed, as $n \to \infty$,

$$d_n \to 2n/t \tag{8.18}$$

where

$$t = \frac{2SF\sin^2\theta}{1 - \cos\theta} \qquad \text{for } L \text{ modes} \tag{8.19}$$

or

$$t = \frac{2SF\sin^2\theta}{-1 - \cos\theta} \qquad \text{for } R \text{ modes} \tag{8.20}$$

Thus (8.14) takes the form

$$b_{n-1} + b_{n+1} = (2n/t)b_n \tag{8.21}$$

which coincides with the defining recurrence relation for $J_n(t)$. Now, as $n \to \infty$, it can be shown that

$$J_n(t) \to (t^n/2^n n!) \tag{8.22}$$

which shows that our series converges absolutely.

Note that complex values of B result from any frequency which gives fast waves and also from some frequencies which give slow waves. By a fast wave we mean that the phase velocity in the XY plane is greater than the velocity of light. It will be readily verified that any point outside of the triangle defined by $B = F \sin\theta$ and $1 - B = F \sin\theta$ in Figs. 8.2 and 8.3 represents a fast wave for either the $n = 0$ term or the $n = 1$ term in our Fourier series. That such points give complex B is apparent from (8.16), because at least one of the square roots is imaginary. Conversely, it will be found that a point inside the triangle represents slow waves for every term in the Fourier series. We can see that B may be complex in such cases by examining Fig. 8.2. For example, if $S = 8$ and $0.05 < F < 1.5$, there is no real value of B; this is a stop band such as we encountered in Chapter 6. Note also that $B = 0.5$ means the phase shift per cell is π, which, in Chapter 5, we saw was characteristic of the active region.

Although the continued fractions converge fairly quickly, the direct application of (8.16) is inadequate for the case when B is complex. This case is important because it gives an attenuated current distribution and hence permits truncation of the structure. We shall therefore investigate the mathematical characteristics of (8.16) for two typical cases: the case where the wires are nearly straight (S small) and the case where they are extremely curved (S large).

8.2 Slightly Curved Wires

When S is small enough, we can assume that

$$S^2F^2 \sin^4\theta \ll 1 \tag{8.23}$$

Reference to (8.16) shows that this gives $B = F$ as a first approximation.

Therefore, we assume that

$$B = F(1 + \delta) \tag{8.24}$$

where $\delta \ll 1$. Then (8.16) gives

$$\delta = S^2F \sin^2\theta \cos\theta \,(\{[(1+F)^2 - F^2\sin^2\theta]^{1/2} - (1+F)\cos\theta\}^{-1} - \{[(1-F)^2 - F^2\sin^2\theta]^{1/2} + (1-F)\cos\theta\}^{-1}) \qquad \text{for } \theta \neq \pi/2 \tag{8.25}$$

Therefore, δ is complex for

$$(1 + \sin\theta)^{-1} < F < (1 - \sin\theta)^{-1} \tag{8.26}$$

Of course, (8.25) applies only if the entire expression in parentheses remains of order unity, which it does for all positive F of order unity. Thus δ remains small over the range (8.26). A typical plot obtained from (8.25) is shown in Fig. 8.4. The attenuation constant $\alpha = \text{Im}\, B$ is

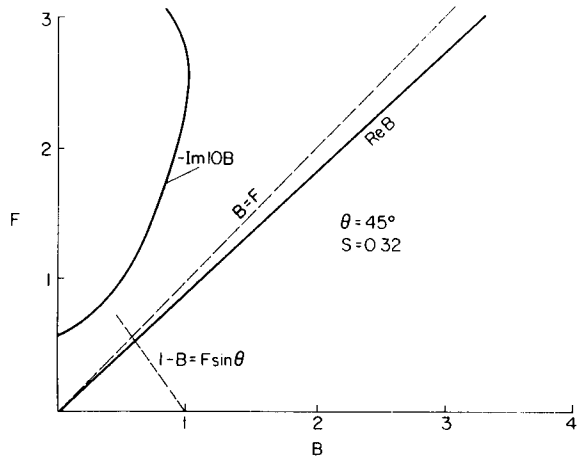

FIG. 8.4. Fast-wave solutions for slightly curved wires [after Ref. 4].

common to all terms in the Fourier series. In the present approximation $\alpha = 0$ for slow waves.

The case for normal excitation is distinctly different. Putting $\theta = \pi/2$ in (8.16), we find that we have

$$\delta = \frac{1 - 2F - \left\{(1-2F)^2 - \dfrac{S^4 4F^3(1-F)[(1+2F)^{1/2} + (1-2F)^{1/2}]^2}{1+2F}\right\}^{1/2}}{4F(1-F)} \qquad (F \leqslant 0.5) \tag{8.27}$$

or

$$\delta = \frac{1 - 2F - \{(1-2F)^2 - S^4 4F^3(1-F)[1 + j(2F-1)^{1/2}(2F+1)^{-1/2}]^2\}^{1/2}}{4F(1-F)} \qquad (F \geqslant 0.5) \qquad (8.28)$$

When $F^2S^4 \ll 1 - 1/4F \mid 1 - F \mid$, that is, F is not near 0.5,

$$\delta \simeq \frac{S^4F^2}{2(1-2F)}\left[1 + \left(\frac{1-2F}{1+2F}\right)^{1/2}\right]^2 \qquad (F < 0.5) \qquad (8.29)$$

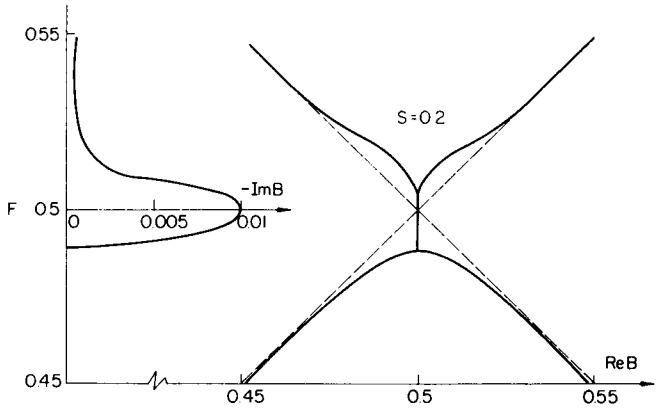

FIG. 8.5. Attenuation is a maximum in the slow-wave region [after Ref. 4].

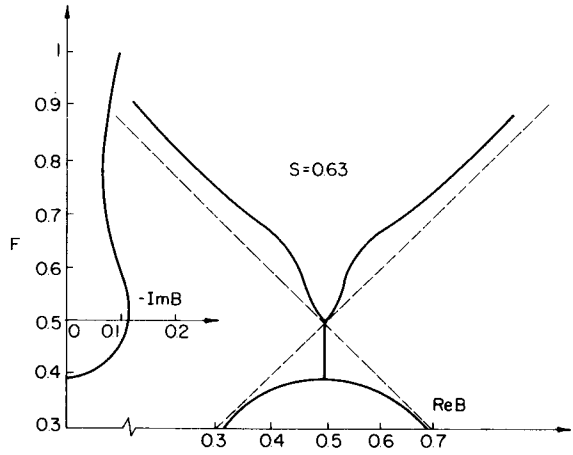

FIG. 8.6. The peak in attenuation is less marked for more curved wires [after Ref. 4].

or

$$\delta \simeq \frac{S^4F^2}{2(1-2F)}\left[1+j\left(\frac{2F-1}{2F+1}\right)^{1/2}\right]^2 \qquad (F > 0.5) \tag{8.30}$$

A typical plot of these results is shown in Figs. 8.5 and 8.6. A striking feature is illustrated by the curves for $S = 0.2$. Note that the attenuation constant $-\text{Im}\, B$ rises abruptly around $F = 0.49$ to a sharply defined maximum at $F \simeq 0.5$, whereas $\text{Re}\, B$, the phase constant, remains constant at 0.5. Since this part of the Re B graph lies inside the triangle, we have a slow-wave solution, yet the attenuation is much greater than it is for the fast-wave solutions obtained when $F > 0.5$. From the graph for $S = 0.63$, we see that this effect is less pronounced for larger values of S. However, $S = 0.63$ is near the limit of validity of the present approach, so let us turn to the next section to deal with the case $S > 1$.

8.3 Extremely Curved Wires

When S is large, we see from Figs. 8.2 and 8.3 that the lowest branch of the graph falls well below the lines $B = F\sin\theta$ and $1 - B = F\sin\theta$, except near $B = 0$ and $B = 1$. Therefore,

$$F^2\sin^2\theta \ll (B+n)^2 \qquad \text{for all } n \tag{8.31}$$

over most of the lowest branch. This condition greatly simplifies the characteristic equation (8.16), reducing it to the form

$$A_0 = \frac{T}{A_1 - T/(A_2 - \cdots)} + \frac{T}{B_1 - T/(B_2 - \cdots)} \tag{8.32}$$

where

$$T = S^2F^2\sin^4\theta \tag{8.33}$$

$$A_n = (n+B)(1-\cos\theta) \tag{8.34}$$

$$B_n = (n+B)(1+\cos\theta) \tag{8.35}$$

Thus B is now a function of the single variable T instead of the two variables F and S. In other words, provided S is large enough (larger than 4 or 5 as it turns out for the lowest branch), the guide wavelength λ_g remains unchanged when we increase the electric wavelength λ, if we

increase S by the same ratio, keeping the wire wavelength Λ_w constant. For large S the length of wire in one wavelength Λ_w is

$$4a = 4S\Lambda_w/\pi \tag{8.36}$$

It follows that the phase velocity along the wire (reckoned from the phase shift over Λ_w) is independent of the shape of the wire, provided S is large. This way of specifying phase velocity corresponds to the plot of Fig. 5.14(b), which shows the measured phase for a single expanding zigzag wire.

There are two ways of solving (8.32). The first way makes use of the fact that $T < 1$ even when S is large (for points on the lowest branch of the F/B graph). This results in a good approximation for T, given B, when (8.32) is solved by replacing "etc." with zero; the error is about 1%. Some typical results are shown in Fig. 8.7. The same approximation can also be used to calculate complex values of B, with the results shown in Fig. 8.7. Note that the attenuation constant $-\text{Im } B$ is remarkably high, exceeding the phase constant Re B over a consider-

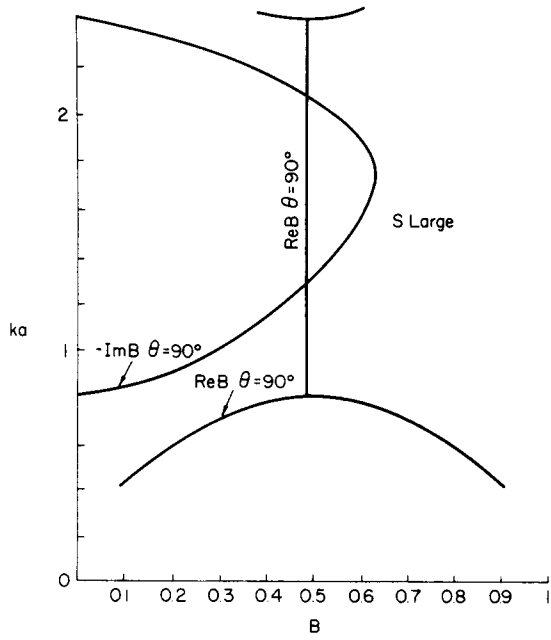

FIG. 8.7. Attenuated solutions for extremely curved wires [after Ref. 4].

able range of frequencies. For example, $-\text{Im } B = 0.6$ represents an attenuation of about 30 db per Λ_w or, for $S = 10$, about 430 db per electric wavelength λ.

The second way of solving (8.32) is based on the Bessel-function recurrence formula (8.20). Applying the procedure represented by (8.14) to this, we find that

$$\frac{J_n(u)}{J_{n-1}(u)} = \left\{n(2/u) - \left[1\Big/(n+1)(2/u) - \frac{1}{(n+2)(2/u) - 1, \text{ etc.}}\right]\right\}^{-1} \tag{8.37}$$

Fortunately, this is precisely the form of the continued fractions in (8.32), which can thus be expressed as

$$\frac{J_{B-1}(u_1)}{J_B(u_1)} = \frac{J_{1-B}(u_2)}{J_{-B}(u_2)} \qquad (0 < \text{Re } B < 1) \tag{8.38}$$

with

$$u_1 = 2SF(1 + \cos\theta) = ka(1 + \cos\theta) \tag{8.39}$$

$$u_2 = 2SF(1 - \cos\theta) = ka(1 - \cos\theta) \tag{8.40}$$

Unfortunately, (8.38), although providing an elegant expression for the characteristic equation, is not much use for calculating B. However, when $B = 0.5$ it simplifies drastically, giving

$$\cot u_1 = \tan u_2 \tag{8.41}$$

Hence, with $N = 0, 1, 2, \ldots$,

$$\pi(N + 0.5) = u_1 + u_2 = 2ka = 4\pi a\lambda^{-1} \tag{8.42}$$

Hence, for all θ, when $B = 0.5$,

$$a = 0.125\,\lambda, \quad 0.375\,\lambda, \quad 0.625\,\lambda, \quad \text{etc.} \tag{8.43}$$

The remarkable result of (8.43) is that the wave travels along the wires with the velocity of light. To see this we note that the length of wire in Λ_w is $4a$, and that $\lambda_g = 2\Lambda_w$. Thus λ_f, the electric wavelength measured along the wire, that is, the length of wire which gives a phase shift of 2π, is $8a$, which is exactly λ, $3\,\lambda$, $5\,\lambda$, etc., by (8.43). Therefore, at the lowest frequency which makes $B = 0.5$, the phase velocity along the wire is the velocity of light. Our proof of this applies only to $S \gg 1$, but by direct calculation (see Figs. 8.2 and 8.3) we find it to be true for smaller values of S also, and clearly it holds for sufficiently small S.

It therefore appears to hold generally. Here, then, is a surprising piece of evidence which supports the often used approximation that the wave travels with the velocity of light along the wire, at least in the active region.

8.4 Peculiarity of the Field in the Stop Band

We have seen in Figs. 8.4, 8.5, and 8.7, that for normal excitation

$$\operatorname{Re} B = 0.5 \tag{8.44}$$

in the stop band.

The surprising result of (8.44) is that it makes the Poynting vector zero at every instant, in every direction, and at every point. This follows from the fact that if $\mathbf{E}$ is of the L or R type, that is, $\mathbf{E} = \pm jZ_0\mathbf{H}$, the instantaneous Poynting vector vanishes when $\mathbf{E}$ is linearly polarized, as the reader may readily verify. Now (8.44) makes

$$\gamma_{-n-1} = \overset{*}{\gamma}_n \qquad \text{(the conjugate of } \gamma_n\text{)} \tag{8.45}$$

and by (8.10),

$$\mathbf{e}_{-n-1} = \overset{*}{\mathbf{e}}_n \tag{8.46}$$

On substitution in (8.6) we find that

$$\mathbf{E} = 2e^{-\alpha x} \operatorname{Re} \sum_{n=0,1,2} \mathbf{e}_n \exp[j(n + 0.5)x - \gamma_n z] \tag{8.47}$$

Since $\mathbf{E}$ is real, it must be linearly polarized and the instantaneous Poynting vector must vanish.

Although fields for which the average Poynting vector vanishes are common, the kind of field we have here is so uncommon that it may be worthwhile to quote a simple nontrivial example for which the details can be easily worked out.

$$\begin{aligned}\mathbf{E} &= e^{-\alpha z}[\hat{\mathbf{z}} \cos(ky + \alpha x) + \hat{\mathbf{x}} \sin(ky + \alpha x)] \\ &= jZ_0\mathbf{H}\end{aligned}$$

is such an example. It can represent the field on one side of a sheet of

straight wires in the xy plane and parallel to the y axis. Another peculiarity of (8.47) is exhibited by the variation with z. It has the form

$$\exp(-\alpha_n z)\cos\beta_n z$$

which is a standing wave, even though there is no reflection in the z direction. The distribution along the x axis also has this character.

8.5 Effects of Oblique Excitation

The essential difference between normal and oblique excitation is analogous to the difference between the coaxial and biaxial modes which we discussed in Chapter 1 in connection with a pair of parallel wires. For normal excitation the voltage between wires is zero. We have already encountered some of the theoretical aspects of this essential difference but for large S the transition from normal to oblique incidence is continuous. Because the difference we see in Fig. 8.3 arises on the boundary $1 - B = F\sin\theta$, to examine the transition we now apply the Bessel-function formula to (8.16), with $B = F\sin\theta$ or $1 - B = F\sin\theta$. The resulting formulas are, respectively,

$$(-\text{ or }+)\frac{\cot\theta}{S} = \frac{J_1[ka(1+\cos\theta)]}{J_0[ka(1+\cos\theta)]} + \frac{J_1[ka(1-\cos\theta)]}{J_0[ka(1-\cos\theta)]} \tag{8.48}$$

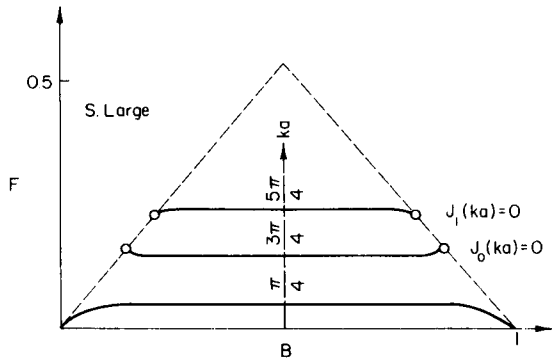

FIG. 8.8. Oblique excitation introduces a stop band which is absent for normal excitation [after Ref. 4].

When S is large and θ is near 90°, the left side vanishes, and it is clear that ka approximates the roots of J_0 and J_1 as shown in Fig. 8.8. The same results are obtained for normal incidence but by a different method.

When θ approaches zero, the height of the triangles tends to infinity, and the fast-wave region consequently disappears. Under these circumstances, (8.16) reduces to

$$J_{B-1}(2ka) = 0 \qquad (0 < B < 1) \tag{8.49}$$

and, provided S is finite, $B = 0$ and $B = 1$ at the same frequency, the root of

$$J_0(2ka) = 0 \tag{8.50}$$

However, if S is large and θ small so that $S\theta \simeq 1$, the values of ka are distinctly different, as illustrated in Fig. 8.9. [The second branch, which

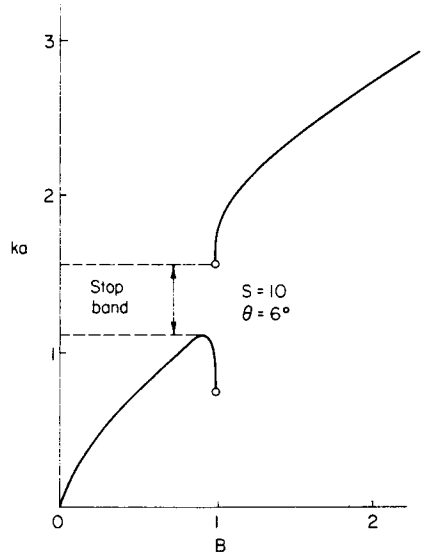

FIG. 8.9. Stop band for extremely oblique excitation [after Ref. 4].

previously has been shown in the range $0 \leqslant B \leqslant 1$, has been shifted to $1 \leqslant B \leqslant 2$ (where it is equally valid) for purposes of comparison

with the next figure.] We see that the stop band disappears at $\theta = 0$; at the same time all possibility of fast-wave solutions disappears.

Finally, we consider $\cos\theta > 1$, which means a slow-wave excitation along the y axis. When $\cos\theta$ is only a little greater than unity, we get a result much like the case $\theta \to 0$, except that B is real at all frequencies, as shown in Fig. 8.10. When $\cos\theta$ is much greater than unity, we can

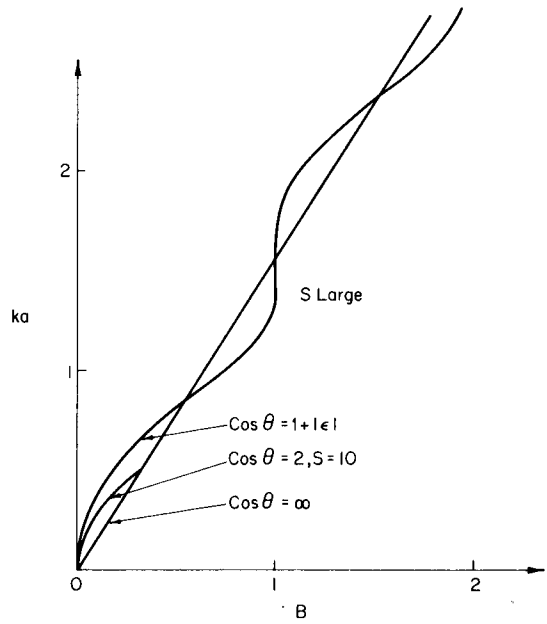

FIG. 8.10. There is no dispersion for extremely slow-wave excitation [after Ref. 4].

apply the asymptotic formulas for the Bessel functions in (8.38), which gives

$$2ka = \pi(m + B) \qquad (m = 0, \pm 1, \pm 2, \ldots) \tag{8.51}$$

This gives the straight line shown in Fig. 8.10. The physical interpretation of (8.51) is that the wave travels along the wires with the velocity of light at all frequencies, the velocity along the x axis being very slow because S is large. Thus the sheet of wires now gives very slow waves with no dispersion. Even for the comparatively small value of $\cos\theta = 2$ with $S = 10$, the graph is practically straight except for a deviation at the low-frequency end, as shown in Fig. 8.10.

8.6 Extrapolation of the Solution to a Log-Periodic Case

If we think of an idealized log-periodic antenna in the form of a sheet made of an infinite number of slowly expanding sinusoidal wires, the problem we have worked out represents a piece of this sheet over which the sinusoids are practically uniform. The physical significance of the solution is correlated with the radial and circumferential phase velocities of the current (which are represented by the symbols B and θ in the formulas of the preceding sections). The principal results can be described as follows.

The current is always attenuated where the radial phase velocity is faster than c, the velocity of light. This is a familiar result that could have been anticipated. What might not have been expected, however, is that such an open structure gives a highly effective stop band; that is, the current is attenuated at the rate of hundreds of decibels per wavelength when the wires are extremely curved, the radial phase velocity is slower than c, and the circumferential phase velocity faster than c. The fields in such regions of rapid attenuation are rather curious. They consist of exponentially damped standing waves in both the radial direction and the direction normal to the sheet.

Perhaps the most surprising result is that where the phase shift per cell is 180° (corresponding to $B = 0.5$), the phase velocity for the lowest mode is c when measured along the wire, for all degrees of curvature. Also, when the circumferential phase velocity is well above c, the region where the phase shift per cell is near 180° is also characterized by attenuation. Attenuation begins either just before or just after the phase shift per cell attains 180°, depending on the polarization of the mode. As we have seen in earlier chapters, these two results are typical of measurements on practical structures, although there is no evidence for two different modes of polarization.

There is no attenuation when the wavelength of the wires is much less than the free-space radio wavelength, or where the circumferential phase velocity is slower than c. The former is simply an indication that the solution conforms to the static solution in the limit as frequency approaches zero. The latter gives a precise check on the rough estimates of the effect of phase velocity which were first used in Chapter 4. Thus, for example, if the log-periodic structure is excited in the $e^{jn\phi}$ mode, attenuation cannot be expected until the circumference exceeds $n\lambda$. This also is typical of the measured results on multielement spiral structures.

REFERENCES

1. Borgiotti, G., M. S. thesis, Univ. California, Berkeley, California, 1961.
2. Harvey, A. F., *Trans. IRE PGMTT*, 30–61 (1960).
3. Oliner, A. A., and A. Hessel, *IRE Trans.* (Special Issue) **AP-7**, 201–208 (1959).
4. Rumsey, V. H., *in* "Electromagnetic Theory and Antennas" (Proc. URSI Symp., Copenhagen, June 1962), (E. C. Jordan, ed.), Pergamon Press, New York, 1963.

AUTHOR INDEX

Numbers in parentheses are reference numbers and indicate that an author's work is referred to although his name is not cited in the text. Numbers in italic show the page on which the complete reference is listed.

B

Bell, R. L., 66, 67(1), 68(1), 69(1), 80, *86*, *110*
Berry, D. G., 57, 80, 81(2), 82, 84, *86*
Booker, H. G., 27(1), *37*
Borgiotti, G., 134, *146*
Brillouin, S., 102(9), *110*

C

Carr, J. W., *86*
Carrel, R. L., 5(1), *12*, 28(2), 34(2), 35(2), 36(2), *37*, 75, 77, 78(4), *86*, 88, *110*
Cheo, B. R. S., 111(1), 112(1), 122(1), 123(1), 124(1), 125(1), 126(1), 127(1), *128*

D

Deschamps, G. A., 29, *37*, 87(4), *110*
Du Hamel, R. H., 16(1), *21*, 55, 57, 58(6), 59(6), 63, 82, 84, 86, 87(2), *110*
Duncan, J. W. 11(2), *12*
Dyson, J. D., 39, 42, 44(4), 45(4), 46(1, 3), 48(4), 50(5), 51(5), 52(5), *53*

E

Elfving, C. T., 65(8), 66, 67(1), 68(1), 69(1), *86*
Erdelyi, A., 122(2), *128*

F

Fesbach, H. 117(4), *128*
Franks, R. E., 66, 67(1), 68(1), 69(1), 80, *86*, *110*

G

Gans, M. J., 12(3), *12*
Greiser, J. W., 80(9, 10), *86*, 105(3), *110*

H

Harvey, A. F., 138(2), *146*
Hessel, A., 102(8), *110*, 129, *146*
Hines, J. N., 83(13), *86*

I

Isbell, D. E., 16(1), *21*, 55, 58(6), 59(6), 61, 62, 65(5), 70, 71, 72(12), 73(12), 74(12), 75(12), 76(12), 77(12), *86*

J

Jones, K. E., 88, *110*

K

Kajfez, D., 12(3), *12*

L

Laxpati, S. J., 119(8), *128*

M

Magnus, W., 120(3), *128*
Mayes, P. E., 50(5), 51(5), 52(5), *53*, 77, *86*, 87(4), 105(3), *110*
Mei, K. K., 84(15), *86*
Minerva, V. P., 11(2), *12*
Mittra, R., 87(5), 88, *110*
Moberg, M., 84(15), *86*
Morse, P. M., 117(4), *128*
Mushiake, Y., 27(4, 7), 30(7), 31(7), *37*

O

Oberhettinger, F., 120(3), *128*
Oliner, A. A., 87(7), 102(8), *110*, 129, *146*
Ore, F. R., 63, 80, 81(2), *86*

P

Patton, W. T., 87(4), *110*
Pierce, J. R., 102(10), *110*

R

Rumsey, V. H., 12(3), *12*, 19(2), 20(2), *21*, 83(13), 84(15), *86*, 111(1), 112(1), 113(6), 115(6), 122(1), 123(1), 124(1), 125(1), 125(5), 126(1), 127(1), *128*, 129(4), 130(4), 133(4), 136(4), 137(4), 139(4), 142(4), 143(4), 144(4), *146*

S

Schelkunoff, S. A., 4, *12*, 32(5), *37*
Sivan-Sussman, R., 52(6), *53*
Smythe, W. R., 34(6), *37*

T

Tice, T. E., 83(13), *86*

U

Uda, S., 27(7), 30(7), 31(7), *37*

W

Watkins, D. A., 87(11), 102(11), *110*
Welch, W.J., 111(1), 112(1), 122(1), 123(1), 124(1), 125(1), 126(1), 127(1), *128*
Weston, V. H., 20(3), *21*
Whittaker, E. T., 112(7), 113(7), *128*
Wickersham, A. E., 80, *86*, 87(12), 107(12), 108(12), *110*

Y

Yeh Y. S., 84(15), *86*

SUBJECT INDEX

A

"Active region," 66
Angle principle, 13
Antenna measurements, 6
Antennas over a ground plane, 79
Attenuation of current distribution on transmission line, 92

B

Balanced modes, 8
Balun, 10
Bent zig-zag antenna, 105
Biaxial line, 9
Biconical transmission lines, 4
Booker's relation, 27, 29
Broadside directive arrays, 84

C

Calculated performance of dipole arrays, 76
Characteristic impedance of antennas, 4
Characteristic impedance for flat cones, 32
Circularly polarized dipoles, 112, 116
Circularly polarized solutions of Maxwell's equations, 112
Circular polarization from spiral antennas, 41, 42
Coaxial line, 9
Complementary antennas, 25
Conical spiral, 42–49
Complex propagation factor, 104
Current distribution on antennas, 1
Current distribution measurements, 47, 66
Curvature effect on current, 19

D

Dipole antennas, 1
Dipole arrays, 56
  switched, 70
  switched and unswitched, 97
Directive arrays, 82
Directivity calculations, 76
Dispersion diagrams, 102
Dual solutions, 23

F

Flat sheet balun, 11
Folded log-periodic dipole, 80
Folded dipole loading of transmission line, 95

H

Hankel transform, 117
Hertz potential method, 113
Higher mode dipole arrays, 78

I

Impedance
  circuit theory definition, 6
  for a specific mode, 7
Inclined circular cones, 6
Inclined sheet structures, 61

L

Legendre function, 120
Linearly polarized sheet antennas, 60
Log-periodic structure, 15

M

Maxwell's equations, 2, 3, 111, 129
Modes of dipole loaded transmission line, 90
Multielement spiral antennas, 49–52
Multiterminal structures, 28
Mushiake's relation, 27, 29, 30

P

Pattern characteristics, 18
Periodic Structure Theory, 87, 129
Periodically loaded transmission line, 88
Phase distribution measurements, 66
Phase principle, 57
Planar spiral antennas, 40
Plane sheet antennas, 23
Plane sheet log, periodic antennas, 58
Polarization measurement, 7
Principal mode, 4

R

"Radiating" wave, 66
Radiation coupling effect, 81

S

Scaling principle, 2, 3
Self-complementary shapes, 56, 32, 27, 28
Shapes determined by angles, 16
Sheet metal antennas, 10
Sinusoidal wire sheet, 129
Slowness factor, 106
Spiral antennas, 14, 39
Spiral wire sheet, 111
Stationary phase method, 121
Stop-band effect on field, 143
Stop-band effect on patterns, 101
Symmetry properties of log-periodic structures, 56

T

Tapered ladder antenna, 80
Theoretical curves distribution on spiral, 124
Theoretical radiation patterns, 121
"Transmission line" wave, 66
Trapezoidal structures, 64
Truncation principle, 13

U

Unbalanced modes, 8

V

Voltage source in field theory, 24

W

Wire outline, structures, 63